The role of TBC1D1 in insulin secretion from mouse pancreatic islets

Inaugural-Dissertation

zur Erlangung des Doktorgrades
der Mathematisch-Naturwissenschaftlichen Fakultät
der Heinrich-Heine-Universität Düsseldorf

vorgelegt von

Torben Stermann
geb. Peter
aus Haan

Düsseldorf, November 2016

aus dem Institut für Klinische Biochemie und Pathobiochemie
des Deutschen Diabetes-Zentrums
Leibniz-Zentrum für Diabetesforschung
an der Heinrich-Heine-Universität Düsseldorf

Gedruckt mit der Genehmigung der
Mathematisch-Naturwissenschaftlichen Fakultät der
Heinrich-Heine-Universität Düsseldorf

Referent: Prof. Dr. Hadi Al-Hasani
Korreferent: Prof. Dr. Eckhard Lammert

Tag der mündlichen Prüfung: 28. November 2016

Ich versichere an Eides Statt, dass die Dissertation von mir selbständig und ohne unzulässige fremde Hilfe unter Beachtung der „Grundsätze zur Sicherung guter wissenschaftlicher Praxis an der Heinrich-Heine-Universität Düsseldorf“ erstellt und bei keiner anderen Fakultät vorgelegt worden ist.

Düsseldorf, den 28.11.2016 

TABLE OF CONTENTS

1 INTRODUCTION

1.1 Regulation of glucose homeostasis

1.1.1 Inter-organ crosstalk for the maintenance of whole-body glucose homeostasis

The blood glucose concentration of humans and mammals needs to be tightly regulated to ensure a healthy whole-body metabolism. Blood glucose has to be decreased in the post-prandial state, but it also needs to be increased or at least maintained during periods of starving. These processes involve several different organs and tissues, such as pancreas, skeletal muscle, white adipose tissue and liver. Each of those organs participates substantially in this inter-organ crosstalk to promote whole-body metabolism. The regulation of blood glucose and the relationships between the mentioned organs and tissues is demonstrated in Figure 1. Per definition, normoglycemia in humans is defined as a fasting plasma glucose concentration < 6.1 mmol/L (110 mg/dL) or a plasma glucose concentration < 7.8 mmol/L (140 mg/dL) two hours after glucose uptake in an oral glucose tolerance test (o. GTT) (Position statement: Screening for Type 2 Diabetes, Clinical Diabetes, Vol 18. No 2 Spring 2000, ADA).

Two different hormones, secreted from specialized endocrine cells (islets of Langerhans) in the pancreas, mainly regulate this essential balance between the hyper- and the hypoglycemic state.

Insulin is a peptide hormone of 51 amino acids [1, 2] and is produced exclusively in endocrine β-cells of the islets of Langerhans within the pancreas [3]. The main trigger for the secretion of insulin into the blood is an increased level of blood glucose [4]. In healthy individuals, the amount of secreted insulin strongly depends on the glucose concentration [5] according to the model of stimulus-secretion coupling of β-cells [6]. After secretion of insulin into the blood it facilitates the uptake of glucose into insulin-responsive tissues, such as skeletal muscle, liver and adipose tissue. This process in turn decreases blood glucose concentration, finally leading to a suppression of insulin secretion [5, 7]. To effectively sense glucose and react with insulin secretion, the islets of Langerhans are strongly vascularized by blood vessels [8].

The insulin-antagonist glucagon is also a peptide hormone of 29 amino acids [9] and is produced in endocrine α-cells of the islets of Langerhans. Secretion of glucagon, that is triggered by low blood glucose levels, amino acids, hormones and neurotransmitters [10], leads to an increase in blood glucose concentration due to elevated hepatic glucose production [11] that is attributed predominantly to breakdown of glycogen into glucose [12]. Glucagon

thereby binds to a special G-protein coupled receptor (glucagon receptor) in the plasma membrane [13] of its target cells.

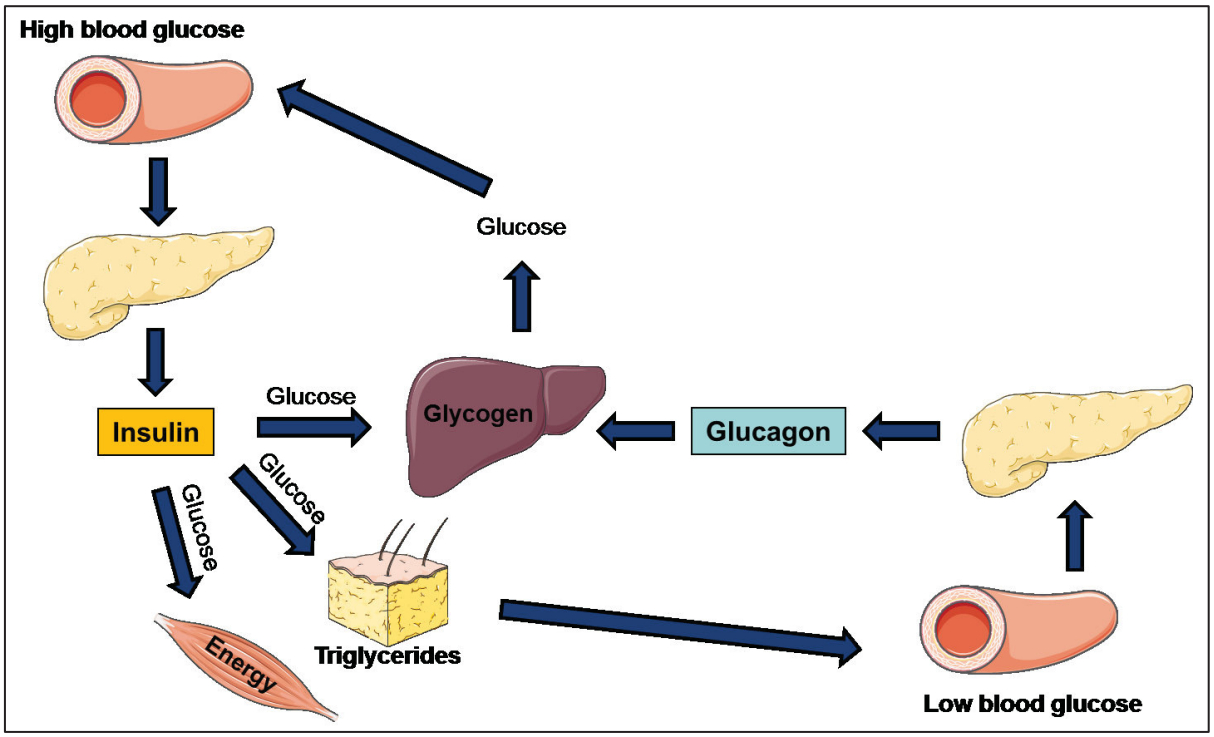

Figure 1: Schematic representation of blood glucose regulation with the mainly involved organs and tissues

Besides insulin and glucagon, the specialized cells of the pancreatic islets also produce somatostatin that regulates the secretion of insulin and glucagon [14] as well as pancreatic polypeptide [15] and ghrelin [16]. Table 1 summarizes the major cell types, the produced hormones and the approximate portion of the cells inside an islet.

Table 1: Cell types of islets of Langerhans and their features

Cell type	Produced hormone	Portion of the islet
α-cells	glucagon	15 %
β-cells	insulin	75-80 %
δ-cells	somatostatin	5 %
PP-cells (F-cells)	pancreatic polypeptide	few
ε-cells	ghrelin	few

1.2 Anatomy and physiology of the pancreas

1.2.1 Anatomic, morphologic and histologic properties of the pancreas

The pancreas is located in the upper left abdomen next to the stomach and the duodenum. It can be divided into three different parts. The so-called “head" lies between the stomach and the duodenum, the “tail” is attached to the spleen, and the “body” represents the part in between. As the pancreas is part of the gastrointestinal system it is also connected to the gall bladder and the liver by sharing a common duct system. At the head of the pancreas, the common bile duct (*Ductus choledochus*), that takes together the cystic duct (*Ductus cysticus*) and the hepatic duct (*Ductus hepaticus communis*), ends in the pancreatic duct (*Ductus pancreaticus*) to open out into the duodenum via the major papilla (*Papilla duodeni major* = ampulla of Vater) (Fig. 2). The pancreatic duct pervades the entire pancreas to branch in the single lobes of the exocrine acinar and tubular network. Histological examination after basic staining reveals distinct cell clusters within the pancreatic tissue, the islets of Langerhans. Thereby, the pancreas can be distinguished between the exocrine and the endocrine part of the pancreas. The exocrine part makes up more that 95 % of pancreatic cell mass and functionally consists of the acinar cells. They produce digestive enzymes and the pancreatic juice that is excreted into the duodenum via the pancreatic duct. The endocrine pancreas refers to the islets of Langerhans. They only make up 1-2 % of the pancreas mass and produce the previously mentioned hormones (Tab. 1), which are necessary for glucose homeostasis. The islets are dispersed throughout the pancreas but their distribution is heterogeneous. The highest islet concentration is found in the pancreatic tail compared to the other parts [17]. Pancreatic islets can be identified with hematoxylin staining by a paler cytoplasm compared to the surrounding exocrine tissue (Pancreapedia.org; Longnecker 2014, DOI: 10.3998/panc.2014.3).

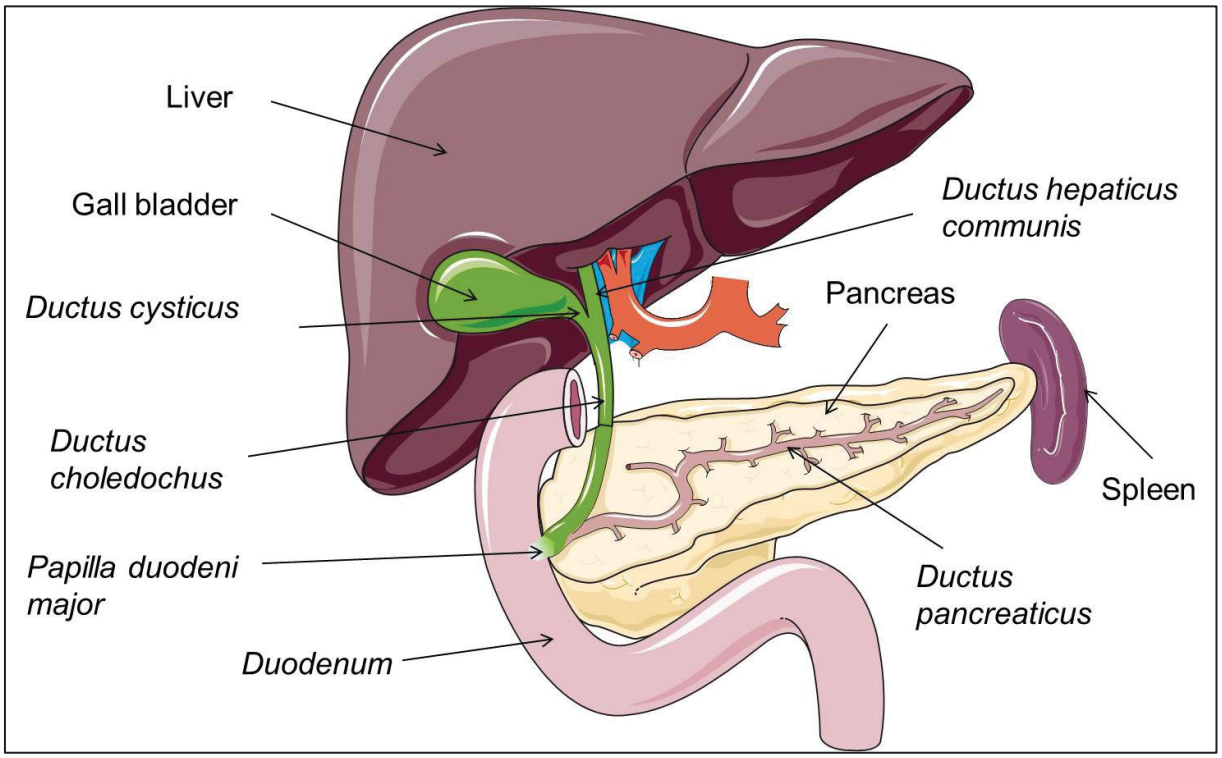

Figure 2: Anatomy of the pancreas and the adjacent organs in the upper abdomen.

1.2.2 Islets of Langerhans

The islets of Langerhans were first described in 1869 by Paul Langerhans. He reported about these “cell clusters” in his medical doctor thesis. Each islet is surrounded by a peri-insular basement membrane and is highly vascularized in order to secrete the produced hormones directly into the blood [8]. Therefore, the endothelial cells surrounding the vasculature are fenestrated ensuring the effective exchange of substances with the islet cells [18]. The islets show a diverse range of sizes and shapes within and between individuals and species. In humans, the average islet diameter is 100-150 µm [19]. The β-cells of rodents are clustered mainly in the islet center, whereas β-cells of humans do not show a distinct distribution within the islet ([20], Pancreapedia.org; Longnecker 2014, DOI: 10.3998/panc.2014.3). While the single cell distribution within the islet is independent of the islet size, the physiology may be not. It was reported that glucose-stimulated insulin secretion is much more profound in small islets (approx. 50 µm diameter) of rats compared to large islets (approx. 200 µm) [21].

1.3 Insulin secretion from pancreatic β-cells

1.3.1 Glucose-stimulated insulin secretion

The physiological need for increased insulin secretion from β-cells is given in the situation of increased blood glucose levels. The β-cells of rodents permanently sense the blood glucose concentration with the help of the facilitative glucose transporter 2 (GLUT2) [22], whereas in humans the predominant glucose transporter in β-cells is GLUT1 [23]. GLUT2 has a high capacity and a low affinity (high K_M ~ 15-20 mM) for glucose, which makes it a very efficient carrier for glucose [24]. Via GLUT2 glucose from the blood enters the pancreatic β-cells and becomes phosphorylated immediately by glucokinase [25]. This enzyme is a hexokinase isoenzyme (hexokinase 4) and its expression and activity is limited to only a few cell types, for instance in the liver, pancreas, gut and the brain [26]. Glucokinase exhibits special kinetic properties. It has a lower affinity for glucose compared to the other hexokinases and therefore its activity depends, at least under physiological conditions, on the glucose concentration [27]. The special feature of glucokinase is that it is not inhibited by its product glucose-6-phosphate [28], which makes this enzyme an obligatory player permanently triggering insulin release upon high glucose concentrations [29]. After phosphorylation, glucose is used in the glycolysis pathway to produce pyruvate. After the subsequent Krebs cycle and the oxidative phosphorylation inside the mitochondria, energy is produced equivalent as adenosine triphosphate (ATP). In β-cells, the rise in the ATP to ADP ratio mediates the closure of ATP-sensitive K^+ channels in the plasma membrane [30-33]. This K^+ channel in the β-cells is composed of two different subunits. $K_{ir}6.2$ is the major inward-rectifier potassium ion channel-forming subunit that builds an integral membrane protein. SUR1 (sulfonylurea receptor 1) is a regulatory subunit that associates with the $K_{ir}6.2$ subunit [34]. To form a functional receptor, four subunits of each type assemble in a special conformation to allow potassium flux. Upon closure of this channel, the cell membrane starts to depolarize due to the accumulation of positively charged ions inside the cell. This initial depolarization triggers a set of additional ion channels to open and to further increase membrane depolarization. These channels include transient receptor potential (TRP) channels, voltage-dependent T-type Ca^{2+} and Na^+ channels [35]. The rise in positively charged Na^+ and Ca^{2+} ions increases the depolarization to a threshold value upon which voltage-dependent L-type Ca^{2+}-channels (VDCC) open. The subsequent influx of Ca^{2+} ions into the β-cell mediates insulin exocytosis [36] by vesicle movement and actin reorganization [37]. The entry of Ca^{2+} ions from outside the cell through the VDCCs also activates the type 2 ryanodine receptor (RyR2) which functions as a calcium release channel in the membrane of the endoplasmic reticulum [38, 39]. This rapidly increases the cytosolic Ca^{2+} concentration to support the release of insulin.

Glucose-stimulated insulin secretion usually consists of two phases as a consequence of the depletion of different insulin granule pools [40-45]. First phase insulin secretion occurs in the first few minutes after the detection of the glucose rise in the blood stream. It is triggered mainly by the pathway mentioned above (Fig. 3). To rapidly secrete a substantial amount of insulin after a rise in glucose concentration, the β-cell holds a readily releasable pool (RRP) of insulin granules available that are pre-docked to the plasma membrane. These granules are preferably used to secrete insulin in the first phase [41, 46]. The second phase of insulin secretion is thought to be independent of the pathway that includes the ATP-sensitive K^+ channel. This phase is more supported by metabolic adaptations of the cell and uses the reserve pool of insulin granules and newly formed granules with freshly expressed insulin [45] that has to be translocated to the plasma membrane, presumably by the small G protein Rab27A [47]. The pathways leading to the second phase of insulin secretion are more complex and include different mediators, such as cyclic adenosine monophosphate (cAMP), free fatty acids, incretins and others [48].

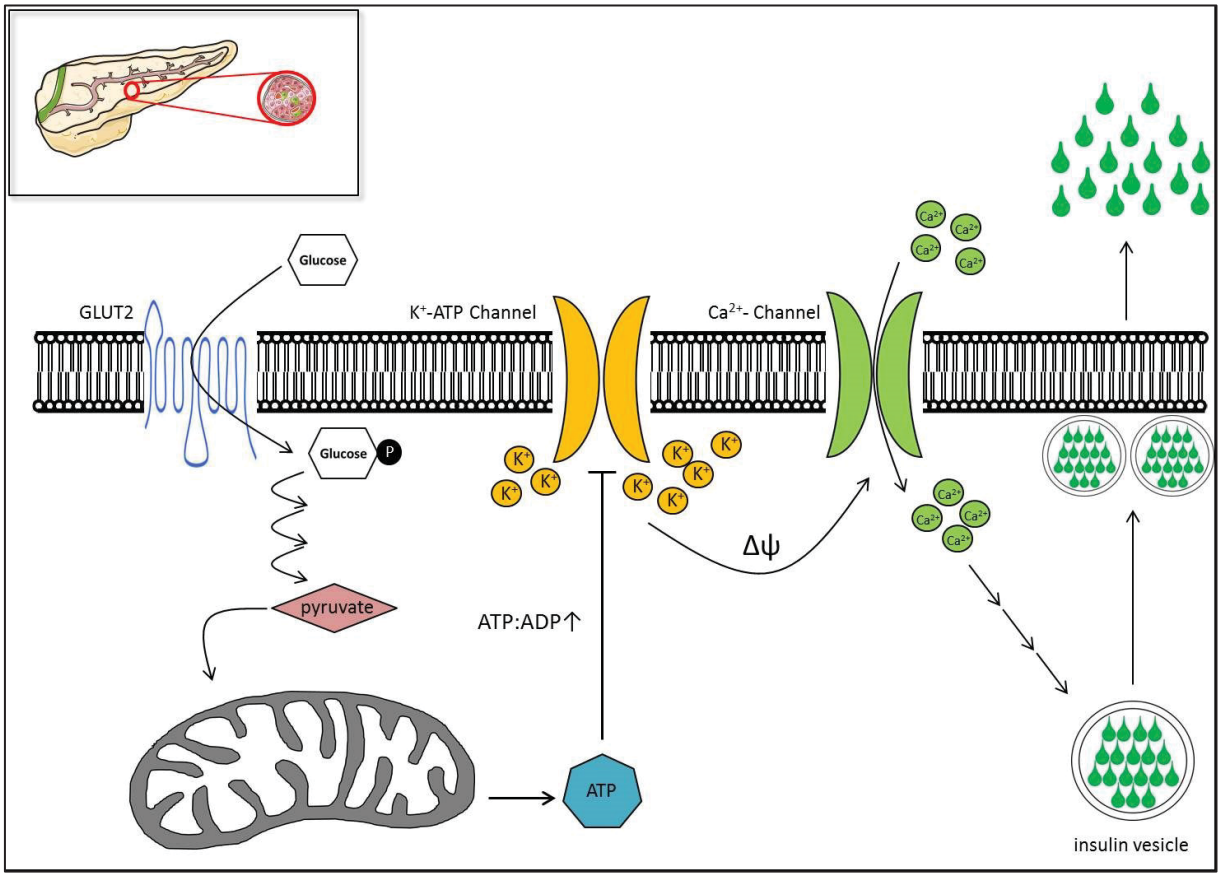

Figure 3: Schematic representation of the triggering pathway that leads to first phase glucose-stimulated insulin secretion in pancreatic β-cells.

1.3.2 Other known modulators of insulin secretion

Insulin secretion from β-cells is not only stimulated by glucose, but also by a broad variety of other modulators. Some of them stimulate insulin secretion only in the presence of glucose. Others can provoke insulin secretion also in the absence of glucose.

Two major modulators that are produced naturally in the body increasing insulin secretion upon an oral glucose uptake are the incretin hormones glucagon-like peptide-1 (GLP-1) and the glucose-dependent insulinotropic polypeptide (GIP) [49-51]. Both are produced by special cells of the gut and bind to G-protein coupled receptors on the cell surface of β-cells [52] to potentiate glucose-stimulated insulin secretion (known as incretin effect).

In addition to the incretins, also an acute stimulation with free fatty acids can potentiate insulin secretion in the presence of glucose [53-56]. Most of this potentiating effect is mediated by the free fatty acid receptor 1 (GPR40) [57]. Also amino acids like arginine and leucine are capable of potentiating insulin secretion at stimulatory glucose concentrations [58].

Another interesting study describes the effect of the artificial chemical substance 5-aminoimidazol-4-carboxamid 1-β-D-ribo-furanoside (AICAR) on the potentiation of glucose-stimulated insulin secretion [59]. The active metabolite of AICAR, 5-amino-1-β-D-ribofuranosylimidazole-4-carboxamide-5′-monophosphate (ZMP) mimics the effect of AMP and activates AMPK by phosphorylation [60]. The presence of AMP and the AMP-mediated AMPK phosphorylation and activation is usually linked to a low cellular energy status [61].

For many years it has been known that the ability for glucose-induced insulin secretion from pancreatic β-cells strongly depends on cell-cell interactions [62-66]. This is of particular importance when working with cell culture or with sorted β-cells from dispersed islets. The latest report describes the importance of the EphA-ephrinA pathway in the regulation of insulin secretion. Pancreatic β-cells express the EphA5 cell surface receptors and also the ephrinA5 ligands. The interaction of both proteins and the phosphorylation status of the EphA5 receptors determine either the EphA forward signaling at low glucose levels or the ephrinA reverse signaling at elevated glucose levels [64]. Manipulation of this pathway by inhibiting the EphA receptors can be used to increase insulin secretion and to promote the ephrinA reverse signaling [67].

Stimulators of insulin secretion that are independent of glucose are mostly substances that interfere with the triggering pathway of insulin secretion by mimicking the appearance of glucose. These are for example sulfonylureas (glibenclamide, tolbutamide) that inhibit the ATP-sensitive K^+ channels [68-71], potassium chloride (KCl) that induces a cell membrane depo-

larization [72] and a calcium ionophore (A23187) that incorporates into the cell membrane to build a pore permeable for Ca^{2+} ions [73].

Beside these possibilities mentioned above to increase or induce insulin secretion, there are many more reports on either endogenous or exogenous substances that modulate insulin secretion [67, 74-83].

1.3.3 Components of the insulin granules necessary for insulin secretion

Secretory granules for exocytosis need special molecules to be able to fuse with the cell membrane to secrete their contents. Similar to the mechanism of neurotransmitter release in nervous cells, insulin exocytosis is regulated by a variety of molecules [84]. Most of them belong to the SNARE complex that includes synaptobrevin-2 (VAMP-2), syntaxin-1A, and SNAP-25. They are the key components that enable membrane fusion and exocytosis [85]. Beside these proteins, many more components are necessary to ensure a regulated exocytosis of secretory granules, especially from β-cells [86]. Proteomic techniques uncovered the appearance of many additional proteins in the insulin secretory granule, including cysteine string protein alpha (CSPα), Rab3A, Rab27A, Rab37, ryanodine receptor RyR, Eph receptors, ATP-sensitive K^+ channels and many others [87, 88]. Not all of these proteins are necessary for a regulated exocytosis of the granule but are still somehow crucial for the mechanism of insulin secretion. For instance, the role of CSPα in insulin exocytosis is not completely understood, but it seems to have an important part by interacting with syntaxin-1A and SNAP-25 to promote the SNARE-complex assembly [89-93]. Interestingly, the exocytosis mechanisms and the involved molecules of insulin release in the pancreas and GLUT4 translocation in the skeletal muscle share some similarities by both using Munc18c and syntaxin-4 [94].

1.4 Glucose disposal in the periphery

Regardless of the major role of the pancreas in the regulatory system of glucose homeostasis also the insulin-sensitive target tissues contribute substantially to glucose homeostasis. In skeletal muscle, liver and adipose tissue, insulin triggers cellular glucose uptake that leads to a decrease in blood glucose concentration [4]. Figure 4 illustrates the main steps in this process which is described in this paragraph. Insulin binds to its special insulin receptor tyrosine kinase on the cell surface [95], which is, in contrast to other receptor tyrosine kinases, a co-

valently maintained dimer [96]. Due to conformational changes the receptor becomes phosphorylated at the cytosolic part due to its kinase activity [97]. This recruits IRS-1 (insulin receptor substrate 1) to bind the insulin receptor at the intracellular NPXY motif with its PTB (phospho-tyrosine-binding) domain [98, 99]. Upon insulin binding, multiple tyrosine residues of IRS-1 become phosphorylated by the receptor [100] and activate the PI3 kinase (phosphatidylinositol-4,5-bisphosphate 3-kinase) pathway [101, 102]. This leads to the translocation of GLUT4 containing vesicles to integrate GLUT4 into the cell membrane [103]. After activation, PI3 kinase phosphorylates PIP2 (phosphatidylinositol (3,4)-bisphosphate) to form PIP3 (phosphatidylinositol (3,4,5)-trisphosphate) [104]. On the one hand, protein kinase B (AKT) is now able to bind PIP3 with its pleckstrin homology domain [105] on the other hand PDK1 (phosphoinositide-dependent kinase-1) binds to PIP3 [106]. AKT becomes phosphorylated due to the interaction of these two molecules [107]. As this just leads to a partial activation of AKT another phosphorylation step is executed by the mTOR (mammalian target of rapamycin) protein kinase to reach full activation of AKT [108]. Phosphorylated AKT subsequently binds to RabGAPs (GTPase activating proteins) TBC1D1 and/or TBC1D4 (AS160) and inactivates them by phosphorylation [109-112]. Inactivation of these RabGAPs leads to the initiation of GLUT4 containing vesicle trafficking to the plasma membrane [111]. GLUT4 becomes integrated into the membrane and transports glucose from the blood into the cell.

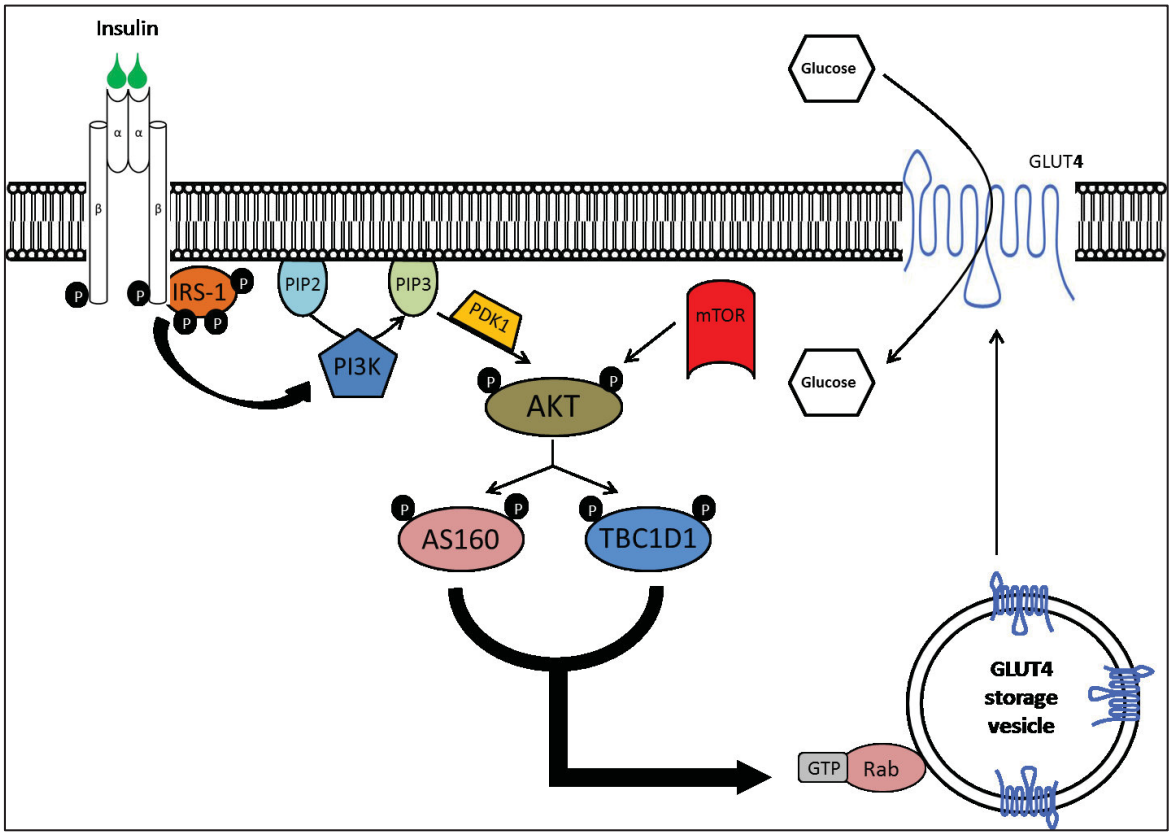

Figure 4: Schematic representation of the pathway that leads to insulin-induced translocation of GLUT4 containing vesicles to the plasma membrane in skeletal muscle cells or adipocytes.

1.5 Diabetes mellitus

Disturbances in the production, secretion or the peripheral use of pancreatic hormones can lead to severe pathophysiological consequences and diseases. The most prominent disease that is caused by malfunctions in the glucose homeostasis is *Diabetes mellitus*. This metabolic disease is classified into two major subtypes, based on its pathophysiology.

1.5.1 Type 1 *diabetes mellitus*

Type 1 *diabetes mellitus* represents an insulin-dependent disease. Due to autoimmune processes the β-cells of the islets of Langerhans are recognized as foreign cells and are destroyed by the immune system [113]. As a consequence the body is not able to produce and secrete insulin anymore. Therefore, individuals with type 1 *diabetes* require a lifelong daily administration of insulin to regulate their blood glucose concentration appropriately. The onset of this type of diabetes usually begins at juvenile or teenager age but can also start at older ages [114]. There is a genetic inheritance of this disease, but it is also accompanied by environmental factors and viral infections that play a role in the onset and progression of type 1 *diabetes* [115]. To date there are about 50 genes that have been associated with the development of type 1 *diabetes* [116]. There are four types of antibodies that can be detected in relation with type 1 *diabetes*: antibodies against islet cell antibody (ICA), GADA (glutamic acid-decarboxylase), tyrosine phosphatase IA-2, and insulin autoantibody (IAA) [114].

1.5.2 Type 2 *diabetes mellitus*

The pathophysiology of type 2 *diabetes mellitus* is very complex und not yet fully understood. It comprises several factors that can influence the onset and progression of the disease, such as environmental factors, lifestyle, exercise, but also genetic factors [117] and, most importantly, the combination between all previously mentioned factors. Type 2 *diabetes mellitus* is considered to have a polygenic origin combined with different risk factors, such as obesity, elevated blood pressure, elevated fasting plasma glucose, high serum triglycerides and low high-density lipoprotein (HDL) levels [118]. A major risk factor for the development of type 2 *diabetes* is obesity. Type 2 *diabetes mellitus* is classically characterized by the primary development of insulin resistance in the insulin-sensitive target tissues (Diabetes mellitus a guide to patient care). The insulin receptors at skeletal muscle cells and adipocytes be-

come less sensitive towards insulin that leads to an increased secretion of insulin from the β-cells as a compensatory mechanism [119]. This results in hyperglycemia but also hyperinsulinemia. In the progression of the disease the β-cells are not capable of secreting enough insulin anymore, leading to progressive β-cell failure [119]. In this state of the disease, the patients are insulin-dependent. To compensate for the insulin resistance at early stages of the disease, some oral medications, such as sulfonylureas or GLP-1 analoga, intend to increase insulin secretion when blood glucose levels are elevated [120]. As mentioned in 1.4 the peripheral insulin-target tissues regulate the insulin-mediated translocation of GLUT4 containing vesicles to enable glucose uptake. These translocation processes are themselves strongly dependent on a regulatory system that involves small Rab-GTPases and Rab-GTPase activating proteins.

1.6 Small Rab-GTPases regulate vesicle trafficking

1.6.1 Small Rab-GTPases

The complex organization of eukaryotic cells requires a regulated sorting of proteins to their specified location inside the cell. After the expression inside the rough endoplasmic reticulum of most membrane proteins or proteins to be secreted they are budded out in vesicles to transport the proteins to all possible positions. This vesicle trafficking needs to be organized to ensure that the proteins reach their predetermined location. This regulation is amongst others realized by Rab (**Ra**s-related in **b**rain) GTPase proteins [121-123]. Rab-GTPases belong to the Ras-superfamily of monomeric small GTPase proteins [123]. To regulate vesicle trafficking, Rab-GTPases switch between two conformational states, the GTP-bound “active” and the GDP-bound “inactive” state [124]. To enable these conformations, the Rab-GTPases are supported by mainly two other classes of signaling molecules, namely the GEFs (guanine nucleotide exchange factors) and the GAPs (GTPase activating proteins) [125-127]. GEFs catalyze the exchange of GDP with GTP [128], while GAP proteins facilitate the hydrolysis of GTP to GDP, thereby increasing the low intrinsic GTP hydrolysis activity of the Rab-GTPases [129] (Fig. 5).

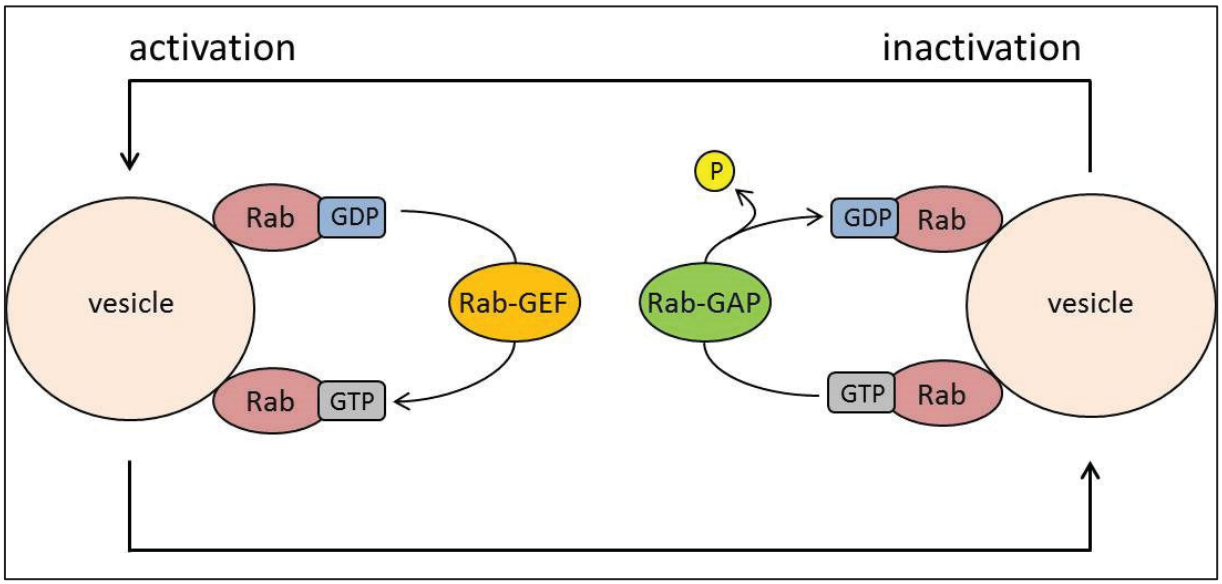

Figure 5: Schematic visualization of the Rab-cycle to activate or inactivate vesicle transport.

1.6.2 Rab-GTPases as regulators of insulin secretion

There are some reports on the relevance of Rab3A and a lot more reports of Rab27A in the control of insulin exocytosis but both proteins are not exclusively expressed in islets. Rab27A was first described as a crucial protein in the regulated secretion in human lymphocytes, platelets and melanocytes [130, 131]. Later Rab27A was also shown to be expressed in pancreatic islets, regulating insulin exocytosis by interacting with granuphilin [132]. A deeper look into the mechanism revealed that glucose-induced Rab27A activity leads to a replenishment of insulin granules [133] by interacting also with Noc2, a Rab-binding protein [134]. Until now, several effectors of Rab27A have been identified as necessary for regulated exocytosis. Interestingly, Rab27A is one of very few Rab proteins for which an effector was identified that binds to Rab27A-GDP [135]. In contrast to Rab27A-GTP-effectors regulating exocytosis, the Rab27A-GDP effector coronin 3 controls endocytotic events [136]. Besides the downstream effectors of Rab27A, also more upstream regulators have been identified. In melanosomes, the RabGAP EPI64 (TBC1D10) was described as Rab27-specific GTPase-activating protein [137]. Although EPI64 could also be shown to be the Rab27-specific RabGAP in pancreatic acinar tissue [138, 139], the responsible RabGAP for Rab27A in pancreatic islets was not identified yet. The fact that there are different Rab-GTPases present on insulin secretory granules illustrates the complexity of regulated sorting and translocation mechanisms and makes it different to unravel the specified roles of one single Rab protein in these processes. In the dynamic process of glucose-induced insulin secretion, Rab27A is

believed to have a more relevant role in the second phase of secretion, that is independent from the K^+-ATP channel [47].

1.7 Rab-GTPase activating proteins

1.7.1 Rab-GTPase activating proteins

The regulated protein sorting under the control of Rab-GTPases needs to have an upstream control system to manage the trafficking events. Usually the active Rab proteins are in the GTP-bound conformation. The switch between GTP- and GDP-conformation is controlled by either GTPase-activating proteins (GAPs) or guanine-nucleotide-exchange factors (GEFs) [123, 125-127, 140]. All known RabGAPs share a common Tre-2/ Bub2/Cdc16 (TBC) protein domain that was first identified in yeast [141] and that is evolutionary conserved [142]. Some RabGAPs have been shown to interact with specific Rab proteins independently of the TBC domain [143, 144], but for most RabGAPs the TBC domain is the catalytically active GTPase-activating domain with a crucial arginine residue [145, 146]. Interestingly, despite the fact that more than 60 different Rab-GTPases are known in humans [121], only approximately 40 different RabGAPs have been described so far [147]. This indicates that the specificity of one RabGAP might be directed towards several Rab-GTPases. In the past years some studies explored the substrate specificity of different RabGAPs towards Rab proteins [147] by either using yeast two-hybrid assays [148, 149] or by analyzing the *in vitro* GAP activity towards several Rab-GTPases [150]. In all of these studies, a recombinantly expressed TBC domain was used to measure *in vitro* GTP hydrolysis activity [111, 151]. In the field of glucose homeostasis, diabetes and obesity the most important RabGAPs so far are TBC1D1 and TBC1D4.

1.7.2 TBC1D1 and TBC1D4

TBC1D1 and TBC1D4 (also known as AS160) belong to the family of RabGAPs and their physiological roles in glucose homeostasis and their implication in human diseases have already been characterized in skeletal muscle and adipocytes in a large number of independent studies [111, 112, 150-170]. Both proteins share about 50 % identity in full length whereas the functional GAP domain is identical to a degree of 79 % between TBC1D1 and TBC1D4 [111, 164]. In contrast to TBC1D1, which is expressed in all animals, TBC1D4 is only present in vertebrates [158].

As represented by Figure 6, both proteins have a similar domain structure, including two phospho-tyrosine-binding (PTB) domains, a calmodulin-binding domain (CBD) and the functional GAP domain responsible for catalyzing GTP hydrolysis. The figure shows the human isoforms with their respective amino acid numbering. Both proteins have distinct tyrosine and serine residues where either AKT or AMPK can directly phosphorylate TBC1D1 or TBC1D4. TBC1D1 is phosphorylated by AKT on Thr^{596} and by AMPK on Ser^{237}. On TBC1D4, four different AKT phosphorylation sites were identified on Ser^{318}, Ser^{588}, Thr^{642} and Ser^{751} [164]. In addition to that, the AMPK phosphorylation site Ser^{711} was identified in TBC1D4 in muscle [171]. The role of the CBD in both proteins is not understood. Although calmodulin binding to the CBD of TBC1D4 was demonstrated before, it was assumed that this binding does not participate in the function of GLUT4 translocation [162].

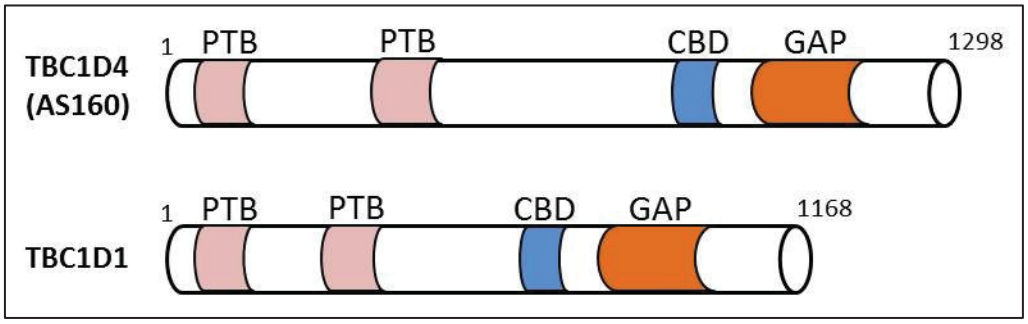

Figure 6: Schematic protein domain organization of human TBC1D1 and TBC1D4 with amino acid count at the C- and N-terminal end.

For both RabGAPs, different splice variants and isoforms have been described [153, 156, 161, 168, 172]. Their respective function in metabolism, however, remains unknown. In previous and unpublished data from our working group, it was shown that the TBC1D1 isoforms differ between the investigated tissues. In the human skeletal muscle TBC1D1 is expressed as multiple isoforms. [168]. While the long isoform is predominant in skeletal muscle, heart and hypothalamus, the short isoform is predominant in pancreas, kidney, white adipose tissue (WAT), brown adipose tissue (BAT) and in the intestines. In mice, the long isoform of TBC1D1 consists of 1255 amino acids coded by 21 exons. The short isoform has 1162 amino acids coded by 19 exons. Thus, the short isoform is lacking two exons. Importantly, the different isoforms have different sites for phosphorylation [168]. The expression of the different isoforms may represent tissue-specific activities.

1.7.3 TBC1D1 and TBC1D4 in pancreas tissue

The role of TBC1D1 and TBC1D4 has been intensely studied in skeletal muscle and white adipose tissue. Recent studies, however, demonstrated expression in the pancreas and enrichment of TBC1D1 and TBC1D4 in islet β-cells [156, 173, 174] but their functional roles have not been extensively investigated so far in this tissue. TBC1D4 was shown to be a glucose-dependent substrate of AKT in sorted mouse β-cells and the reduced expression of this protein, induced by RNA interference technique resulted in an increased basal and decreased glucose-stimulated insulin secretion [173]. Along with this insulin secretion effect, knockdown of *Tbc1d4* in primary mouse β-cells led to a decreased proliferation and an increased apoptosis. Another recent study showed an involvement of TBC1D4 in the regulation of β-cell mass and function in glucocorticoid-treated rodents [175]. TBC1D1 was shown to be phosphorylated in rat β-cells after glucose stimulation and knockdown of *Tbc1d1* in sorted rat β-cells led to a mild increase in both, basal and glucose-stimulated insulin secretion in combination with a reduced proliferation but with no significant changes in apoptosis [174]. Stimulation of insulin secretion with KCl was ineffective in rat β-cells upon *Tbc1d1* knockdown.

A previous study performed in our own working group investigated the implication of a *Tbc1d1*-deficiency in lipid metabolism of pancreatic islets (PhD thesis Franziska Menzel). In accordance to an earlier finding, in which *Tbc1d1*-deficiency in skeletal muscles and cultured C2C12 myotubes led to elevated uptake and oxidation of fatty acids [156], isolated mouse islets and cultured MIN6 cells also showed an increased fatty acid uptake upon *Tbc1d1*-deficiency.

2 AIM OF THE STUDY

The RabGAPs TBC1D1 and TBC1D4 are important regulators of glucose homeostasis in skeletal muscle and adipose tissue. Their functional role in the regulation of GLUT4 containing vesicle translocation upon insulin and contraction stimulation has been demonstrated by us and others in the past. In contrast to the skeletal muscle, the role of TBC1D1 in pancreas tissue is not well defined. Only one published study so far investigated the impact of *Tbc1d1* knockdown in sorted rat β-cells on proliferation, apoptosis and glucose- as well as KCl-stimulated insulin secretion. Although it was shown that *Tbc1d1* knockdown somehow alters glucose- and KCl-induced insulin secretion no deeper insights into a potential mechanism was given [174]. Therefore the aim of this study was to further clarify the role of TBC1D1 in glucose-stimulated insulin secretion to postulate a potential mechanism. For this purpose we used three different mouse models.

1. A recombinant congenic *Tbc1d1*-deficient mouse strain on C57BL/6J background (D1KO) that globally lacks *Tbc1d1* due to a frameshift mutation in exon 18 [156].
2. A transgenic mouse model on C57BL/6J background that overexpresses the 3xFLAG-tagged short isoform of *Tbc1d1* specifically in β-cells under the control of the rat insulin 2 promoter (RIP2-TG). This mouse was created by Franziska Menzel, previously a member of our working group at the German Institute for Human Nutrition (*DIfE*, Potsdam-Rehbruecke, Nuthetal, Germany) together with Fatima Bosch and Anna Pujol (Autonomous University of Barcelona, Barcelona, Spain).
3. A *Tbc1d1*/*Tbc1d4*-double-deficient mouse strain (D1/4KO) that was generated previously by us by crossing the recombinant congenic *Tbc1d1*-deficient mouse strain with a conventional *Tbc1d4*-knockout mouse on C57BL/6J background [155].

We characterized the impact of *Tbc1d1* expression on static and dynamic basic GSIS ad by using different pharmacological approaches, including sulfonylureas, KCl and the Ca^{2+}-ionophore A23187. Furthermore, we specified the role of TBC1D4 in basic GSIS by using isolated islets of D1/4KO mice. Moreover, we performed in vivo glucose tolerance tests, histological analyses to determine islet morphometry and number as well as ultrastructural insulin granule density in D1KO mice and controls. In addition we investigated expression of both, mRNA and protein abundance of crucial regulatory factors of insulin secretion, β-cell integrity and vesicle sorting as a function of *Tbc1d1* deficiency.

3 MATERIAL AND METHODS

3.1 Animal experiments

3.1.1 Experimental mice

For this thesis three different mouse models were used (Tab. 2). All three strains had already been backcrossed at least 10 times to generate a pure (>99.9 %) C57BL/6J background. The generation of both knockout models, the D1KO and the D1/4KO mouse lines, was already described in the literature [155, 156]. The generation of the transgenic mouse overexpressing the short isoform of *Tbc1d1* specifically in β-cells under the RIP2 promoter was described in the PhD thesis of Franziska Menzel, formerly working in our group at the German Institute for Human Nutrition, *DIfE*, Potsdam-Rehbruecke, Nuthetal, Germany.

Table 2: Overview of the used experimental mice

Systematic strain name	Designation	Expression feature
RCS.B6.SJL.*Nob1.10*	D1KO	*Tbc1d1*-knockout
RIP2-3xFLAG-*Tbc1d1*	RIP2-TG	β-cell specific *Tbc1d1*-overexpression
RCS.B6.SJL.*Nob1.10* x KO-TBC1D4	D1/4KO	*Tbc1d1*-/*Tbc1d4*-double knockout

3.1.2 General animal maintenance

Mice were group-housed with up to six animals per cage after weaning under a 12:12 hour light-dark cycle (light on at 6 a.m.) in macrolon III cages. Mice received a standard chow diet (Ssniff Spezialdiäten, Soest, Germany, 9 kcal % from fat, Tab. 3) directly after weaning at the age of 3 weeks and drinking water *ad libitum* throughout the whole project. For certain experiments mice received a chow diet until the age of 12 weeks and subsequently a high-fat diet (Research Diets, New Brunswick, NJ, USA: 60 kcal % from fat, Tab. 3) for 4 weeks. Tail tip biopsies were collected at the age of 3 weeks after weaning for later genotyping. We used male mice at the age of 12 to 16 weeks and, for certain experiments, also old male mice at the age of 50 to 52 weeks. All animal experiments were approved by the Ethics Committee of the State Agency for Nature, Environment and Consumer Protection (LANUV, North Rhine-Westphalia, Germany), reference number 84-02.04.2013.A225.

Table 3: Overview of animal diets and compositions

Diet	Supplier	Catalog number	Composition
Chow diet	Ssniff Spezialdiäten	V1534-3	Protein 33 kcal % Carbohydrate 58 kcal % Fat 9 kcal %
High-fat diet	Research Diets, Inc.	D12492	Protein 20 kcal% Carbohydrate 20 kcal % Fat 60 kcal %

3.1.3 Pancreatic islet isolation

Prior to the isolation, a collagenase solution (Liberase TL Research Grade, Tab. 12) was prepared by dissolving 5 mg of collagenase with 200 µL of DMEM-1 (Tab. 14) to a concentration of 25 mg/mL. 140 µL aliquots were diluted in 19 mL DMEM-1 to reach a final collagenase working concentration of 0.18 mg/mL. This working solution was stored on ice. Experimental mice were sacrificed by cervical dislocation and the abdominal part was disinfected with 70 % ethanol. The abdominal organs were exposed and the major part of the intestines was laid aside. Under the stereomicroscope the *Papilla duodeni major* was identified and blocked with a Bulldog clamp. 3 mL of the collagenase working solution (0.55 mg) were injected into the *Ductus choledochus* with a syringe and a 30G needle (Tab. 15) to perfuse the pancreas (Fig. 7). Afterwards, the inflated pancreas was dissected and stored in a 50 mL Falcon tube on ice until the procedure was finished with all animals. The collagenase was activated by incubation in a 37 °C shaking waterbath for exactly 18 min. The collagenase activity was stopped immediately by adding DMEM-2 (Tab. 14) to a total volume of 50 mL followed by vigorous hand shaking. The disrupted pancreas was pelleted at 900 rcf for 3 min and the supernatant was discarded. The pellet was resuspended with 10 mL DMEM-1 and poured over a tissue sieve with a mesh size of 380 µm via a plastic funnel into a new Falcon tube. The old Falcon tube and the sieve were rinsed with DMEM-1 and the new Falcon was filled up with DMEM-1 to 50 mL. After another centrifugation at 900 rcf for 3 min the supernatant was discarded and the pellet resuspended in 10 mL Histopaque-1077 (Tab. 13). The suspension was carefully covered with 13 mL of DMEM-1 to shape a phase separation. The tubes were centrifuged at 1200 rcf for 25 min without brake and both phases were transferred into a new Falcon tube and filled up with DMEM-1 to 50 mL. After another centrifugation at 900 rcf for 3 min with installed brake and the elimination of the supernatant the remaining tiny pellet was resuspended with 10 mL of islet medium (Tab. 14) and the suspen-

sion was transferred to a 10 cm disposable petri dish and the purity of the islets was estimated under the stereomicroscope (Tab. 16). Finally the islets were handpicked into a new petri dish with 13 mL islet medium to have the islets completely separated from residual exocrine tissue. The isolated islets were allowed to regenerate overnight in a 37 °C / 5 % CO_2 / 90 % humidity incubator.

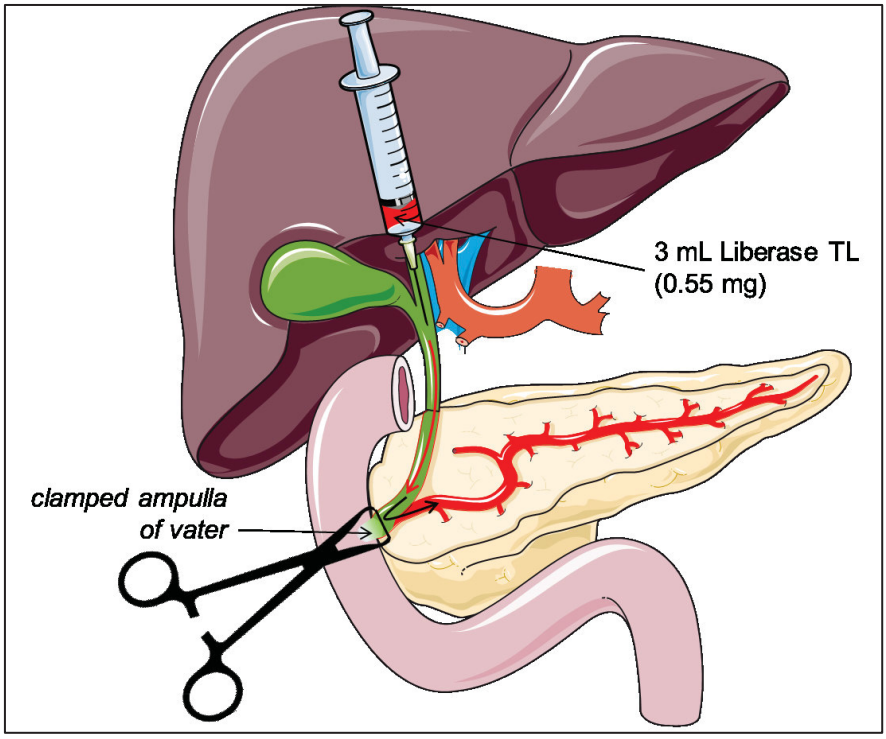

Figure 7: Visual description of the collagenase perfusion of the pancreas. The *Papilla duodeni major* (ampulla of Vater) is clamped and collagenase is injected into the *Ductus choledochus* to reach the pancreatic duct and to perfuse the entire pancreas.

3.1.4 Pancreas dissection

Experimental mice were sacrificed by cervical dislocation and the abdominal part was disinfected with 70 % ethanol. The abdominal organs were exposed and the major part of the intestines was laid aside. With a fine forceps the pancreas was removed from the adjacent intestines and visceral fat and stored according to the planned subsequent analysis. For total pancreatic insulin content the spleen was removed and the pancreas was snap frozen in liquid nitrogen and stored at -80 °C until use. For immunohistochemistry the pancreas (with attached spleen!) was arranged in an embedding cassette and fixed in 4 % paraformaldehyde (PFA, Tab. 12) solution for 24 hours.

3.1.5 Intraperitoneal glucose tolerance test

Prior to the test the mice were fasted for 6 hours by maintaining them overnight in cages connected to a system, that takes away the food at a preset time automatically (2 a.m.). At 8 a.m. body weight was determined, the tail tip of the mice was cut and blood glucose concentration was measured with a glucometer (Tab. 16) for the baseline value. Additional blood (approx. 30 µl) was collected in a microcuvette (Tab. 15) and stored on ice. Mice were then kept in individual cages without food but with water throughout the experiment. Mice were injected with 2 mg glucose per gram body weight intraperitoneally and blood glucose was measured at 15, 30, 60 and 120 min after injection with a glucometer. When using old animals (50-52 weeks) for glucose tolerance test, an additional time point at 240 min after injection was included due to the slower glucose disposal from the blood. At each time point blood was collected in microcuvettes and stored on ice. After the test the microcuvettes with blood were centrifuged 15 min at 21000 rcf at 4 °C, blood plasma was collected and used for insulin quantification with Insulin (Mouse) Ultrasensitive ELISA kit (3.3.6) after appropriate dilutions or stored at -80 °C.

3.2 Molecular biology methods

3.2.1 DNA isolation from mouse tail tips and concentration measurement

To specify the genotypes of the mice which were used in the experiments, approx. 1.5 mm mouse tail tip was collected after weaning in a reaction tube. Genomic DNA isolation from the tail tip was performed with the Invisorb® Genomic DNA Kit II (Tab. 10) according to the manufacturer's handbook. The tail tip was lysed with 10 µL Proteinase K and 200 µL Lysis Buffer G for three to four hours (or overnight) at 60 °C with 1200 rpm stirring. The lysate was centrifuged for 1 min at 16000 rcf in a table centrifuge (Tab. 16) and the supernatant was mixed with 450 µL Binding Buffer. To ensure the effective binding of the DNA to the silica particles of the buffer, the sample was incubated for 5 min at room temperature and mixed again afterwards. The suspension was centrifuged for at least 15 seconds at 16000 rcf and the supernatant was aspirated with a vacuum pump. The pelleted silica particles were washed with 650 µL of the prepared Wash Buffer, resuspended thoroughly in a gyrator (Tab. 16) for approx. 1 min and again pelleted for at least 15 seconds at 16000 rcf. The supernatant was discarded and the washing procedure was repeated twice. After the last washing the supernatant was aspirated entirely and the silica pellet dried at 60 °C with 1200 rpm stir-

ring for 10 min. The sample was cooled at room temperature for 3 min and the DNA was finally eluted with 200 µL Elution Buffer, heated to 60 °C. Before the sample was placed again to 60 °C with 1200 rpm stirring for 3 min it was mixed in the gyrator. Finally the tube was centrifuged for 2 min at 18,000 rcf and the DNA containing supernatant was collected in a new reaction tube. DNA concentration was measured via NanoDrop.

3.2.2 Genotyping of experimental mice

The genotypes of mice were determined by PCR for the designated genes from isolated genomic DNA and subsequent agarose gel analysis of the amplified DNA fragments. The isolated DNA was used at a concentration of 10 ng/µL. Agarose gel electrophoresis with ethidium bromide staining was performed according to standard procedures.

3.2.2.1 Genotyping of D1KO mice

The reaction setup for one sample had a total volume of 20 µL and comprised 5.8 µL MQ-H_2O, 4 µL 5x HF Buffer, 2 µL dNTPs (8 mM), 1 µL of each primer (10 nM, Appendix Tab. 19), 0.2 µL Phusion® High-Fidelity DNA Polymerase (2 u/µL) and 4 µL of DNA. Table 21 (Appendix) shows the temperature properties of the different cycling steps of the thermocycler for the DNA amplification. The forward primer to detect the D1KO mice is located on exon 18 directly at the site of the frameshift mutation, so that it can only bind to DNA derived from D1KO mice. The reverse primer is located in the adjacent intron. The forward primer to detect the WT mice is located in the intron prior to exon 18, whereas the reverse primer is located on exon 18 directly at the site of the frameshift mutation so that it can only bind to DNA derived from WT mice. With this protocol the amplified DNA fragment of wildtype mice was expected with a size of 585 bp, the fragment of D1KO mice was expected with a size of 347 bp.

3.2.2.2 Genotyping of RIP2-3xFLAG-*Tbc1d1* mice

The reaction setup for one sample had a total volume of 10 µL and comprised 3.8 µL MQH_2O, 2 µL 5x DreamTaq Green Buffer, 1 µL dNTPs (8 mM), 0.5 µL of each primer (10 nM, Appendix Tab. 19), 0.2 µL DreamTaq Polymerase (5 u/µL) and 2 µL of DNA. Table 21

(Appendix) shows the temperature properties of the different cycling steps of the thermocycler for the DNA amplification. One primer is located on the FLAG-expression DNA sequence, so that it can only bind to DNA derived from RIP2-TG mice. In the RIP2-WT mice the primer cannot bind, thus no amplification is expected. The PCR was designed to amplify a 374 bp fragment in the presence of FLAG. Since FLAG was not present in the wildtype animals, no band was expected for these animals.

3.2.2.3 Genotyping of D4KO and D1/4KO mice

The reaction setup for one sample had a total volume of 20 µL and comprised 5.8 µL MQH_2O, 4 µL 5x DreamTaq Green Buffer, 2 µL dNTPs (8 mM), 2 µL of the forward primer and 1 µL of each reverse primer, respectively (10 nM, Appendix Tab. 19), 0.2 µL DreamTaq Polymerase (5 u/µL) and 4 µL of DNA. Table 21 (Appendix) shows the temperature properties of the different cycling steps of the thermocycler for the DNA amplification. With this protocol the amplified DNA fragment of wildtype mice was expected with a size of 350 bp, the fragment of D4KO mice was expected with a size of 250 bp.

3.2.3 RNA isolation from isolated mouse islets and concentration measurement

Total RNA from isolated mouse islets was extracted with the RNeasy mini kit (Tab. 10) according to the manufacturer`s instructions. Isolated islets were collected in a reaction tube with islet medium and centrifuged for 5 min at 4 °C and 6000 rcf. Medium supernatant was discarded and the islets were lysed in 350 µL Lysis Buffer RLT (containing 1 % β-mercaptoethanol, Tab. 12) and disrupted in a gyratory shaker for 10 min. After another centrifugation the supernatant was mixed with one volume of 70 % ethanol and applied on the spin columns to centrifuge shortly. While the flow through was discarded, the spin column was washed with Wash Buffer RW1 and centrifuged again. To remove DNA contaminations the sample in the spin column was incubated for 15 min at room temperature with an RNAse-free DNAse (Tab. 10). Afterwards, the spin column was washed again with Wash Buffer RW1 and centrifuged as described above. The flow-through was discarded and the column was washed twice with Buffer RP1 and the RNA was finally eluted with 30 µL of nuclease-free water. RNA concentration was measured via NanoDrop. In case the measured RNA concentration was too low to use for subsequent methods, the RNA concentration was enriched in a vacuum centrifuge (Tab. 16). In this centrifuge the volume of the RNA solution

was reduced to a remaining little drop of water. The RNA was reconstituted with 11 µL of RNAse free water and the concentration was measured again.

3.2.4 Quality control of isolated RNA with a BioAnalyzer

To evaluate the quality of the isolated RNA (3.2.3), especially after concentration in the vacuum centrifuge, the RNA fragments were separated by their size in a chip-based approach (RNA 6000 Nano Kit, Tab. 10) to measure 18s and 28s rRNA. The chips were initially loaded with a special gel and a fluorescent dye before the RNA samples were loaded to the sample wells. One well was loaded with a size reference and an electric circuit was applied to the chip. The results of the measurements were graphically analyzed by the respective Agilent BioAnalyzer software (Tab. 17). In some exemplary samples, RNA quality was unaffected neither by RNA concentration enrichment nor HFD feeding of the mice.

3.2.5 Reverse transcription

To synthesize cDNA for subsequent gene expression measurements, 500 ng (for qPCR) or 1 µg (for qRT-PCR) of RNA was used in a reverse transcription reaction with the GoScript™ Reverse Transcriptase Kit (Tab. 10). In a first step, the isolated RNA was mixed with random hexanucleotide primers (Tab. 10) and a PCR nucleotide mix and incubated for 5 min at 65 °C. In this step the primers should anneal to the RNA templates. In the second step, a reaction buffer, $MgCl_2$ and the reverse transcriptase were added and subjected to another set of temperature properties in a thermocycler (Biorad T100™ Thermal Cycler, Tab. 16) that are summarized in Table 4.

Table 4: Thermocycler settings to synthesize cDNA from RNA template

Stage	Temperature	Duration
Lid heating	40 °C	∞
Annealing	25 °C	5 min
Elongation	42 °C	60 min
Inactivation of reverse transcriptase	72 °C	15 min
	4 °C	∞

The cDNA was finally diluted 1:10 with nuclease-free water for subsequent expression analyses.

3.2.6 RT-PCR to identify *Tbc1d1* isoforms in different tissues

cDNA samples of islets, heart and skeletal muscle from C57BL/6J mice, that were prepared from 1 µg RNA by reverse transcription (3.2.5), were subjected to a PCR approach according to chapter 3.2.2.1. The reaction setup for one sample had a total volume of 20 µL and comprised 10.8 µL MQH_2O, 4 µL 5x HF Buffer, 2 µL dNTPs (8 mM), 1 µL of each primer (10 nM, Appendix Tab. 19), 0.2 µL Phusion® High-Fidelity DNA Polymerase (2 u/µL) and 1 µL of islet and muscle cDNA, but 2 µL of heart cDNA. Table 20 (Appendix) shows the temperature properties of the different cycling steps of the thermocycler for the cDNA amplification. The amplified DNA fragments were analyzed on a 2 % agarose gel.

3.2.7 Quantitative Real-time PCR (qPCR)

The relative amount of cDNA in a sample can be measured in a special PCR approach, where after each amplification cycle the fluorescence intensity of a DNA-intercalating dye (SYBR® Green) is measured. This quantitative Real-time PCR (qPCR) approach is a very sensitive method for the determination of relative gene expression levels. In the end a special value (C_t – cycle threshold) gives the threshold where the fluorescence is significantly higher than the baseline fluorescence. The lower the C_t-value, the higher was the amount of mRNA/cDNA in the starting material. In the end of the amplification period, a dissociating melt curve of each sample is recorded by increasing the temperature from 65 °C stepwise to 95 °C with an increment of 0.3 °C. The reaction setup for one sample had a total volume of 10 µL and was comprised of 3 µL nuclease free H_2O, 5 µL 2x GoTaq® qPCR Master Mix, containing 20 µL CXR reference dye per mL (Tab. 10), 0.5 µL of each primer (10 nM, Appendix Tab. 18) and 1 µL of the synthesized and 1:10 diluted cDNA. The primers were either self-designed with the help of the web-based online tool “Primer3” (http://bioinfo.ut.ee/primer3-0.4.0/) or were taken from the literature (Appendix Tab. 18). Whenever possible, the primer pairs were chosen to be located on two different exons to avoid amplification of genomic DNA. Table 5 shows the temperature properties of the cycling steps for the cDNA amplification.

Table 5: Thermocycler settings to amplify the target cDNA in a qRT-PCR

Stage	Temperature	Duration	Repeats
Lid heating	105 °C	∞	Throughout the entire cycling
Hot start	95 °C	2 min	-
Denaturation	95 °C	15 s	40 x
Annealing / Elongation	60 °C	60 s	
Dissociation / Melt curve	65 – 95 °C		-

3.2.8 Determination of *Tbc1d1* and *Tbc1d4* copy number in islet cDNA from mice

Due to different product lengths, different amounts of intercalating dye can be present in the amplified fragments. Thus, the measured fluorescence intensity does not correlate with the number of DNA fragments. In addition the amplification efficiency can differ between different targets. Therefore, to calculate total amounts of mRNA in a specific sample, the Ct values after qPCR are not a suitable surrogate. Hence, different expression vectors containing either *Tbc1d1* or *Tbc1d4* were used to generate a standard curve for quantification (Tab. 6). The original concentration of both vectors was measured and adjusted to a starting concentration of 10 ng/µL. Serial dilutions of 46 times 1:2 were prepared and subjected to amplification by qPCR (3.2.7) with primers for *Tbc1d1* and *Tbc1d4* (Appendix Tab. 18). The resulting Ct values were used to refer to the concentration of the vector in the respective dilution and to receive a linear equation. With this equation the amounts of *Tbc1d1* and *Tbc1d4* template in the isolated islet RNA samples were calculated and referred to the amount of the housekeeping gene *36b4*.

Table 6: Expression vectors for *Tbc1d1* and *Tbc1d4*

Expression vector	Vector size	Starting amount	Plasmid source
pcDNA3-CMV-3xFLAG-*Tbc1d1*	9319 bp	9400 pg	Thermo Fisher
PCR2.1-*Tbc1d4*	7916 bp	11275 pg	Thermo Fisher

3.3 Biochemical methods

3.3.1 Protein isolation from isolated mouse pancreatic islets

Isolated islets were collected after overnight recovery with 1 mL islet medium in a 1.5 mL reaction tube on ice. After centrifugation at 4 °C for 5 min at 6000 rcf, the supernatant medium was discarded and the pelleted islets were washed with 1 mL islet medium without supplements (pure CMRL medium). Afterwards, the islets were lysed with 30 µL lysis buffer (Tab. 13). To support the lysis the samples were homogenized in a gyratory shaker for 10 min and finally centrifuged at 4 °C for 10 min at 21000 rcf. The protein containing supernatant was collected in a new reaction tube and stored at -20 °C. Protein concentration was measured in a micro plate reader after application of the BCA Protein Assay Kit (Tab. 11) according to the manufacturer's handbook.

3.3.2 Western Blot analysis

The western blot technique was developed in 1979 to detect a certain protein in a complex protein mixture or tissue lysate [176]. In a first step, the protein mixture was separated by size in a discontinuous SDS-PAGE [177]. In the second step, the separated proteins were transferred via tank blotting onto a chemically inert PVDF (polyvinylidene difluoride) membrane [178]. In the last step, the membrane was incubated with specific antibodies (Tab. 7) against the desired protein. Finally the primary antibodies were detected with conjugated secondary antibodies (Tab. 7) via either Western Lightning ECL Pro or Western Lightning ECL Ultra (Tab. 11) in the ChemiDoc Illuminator (Tab. 16) and analyzed with the Image Lab software (Tab. 17).

Table 7: Antibodies for western blot

Designation	Host	Immunogen	Supplier
β-Actin (AC-15)	Mouse	DDDIAALVIDNGSGK	Abcam, Cambridge, UK
TBC1D4	Rabbit	Amino acids 1178-1189 rat TBC1D4	Merck Millipore, Darmstadt, Germany
CSPα	Rabbit	Amino acids 182-198 rat CSP	Synaptic Systems, Göttingen, Germany
FLAG (M2)	Mouse	DYKDDDDK	Sigma Aldrich, Steinheim, Germany

Designation	Host	Immunogen	Supplier
GAPDH	Mouse	Whole rabbit muscle GAPDH	Thermo Fisher Scientific, Darmstadt, Germany
GLUT2 (H-67)	Rabbit	Amino acids 32-98 human GLUT2	Santa Cruz, Dallas, TX, USA
IRS2	Rabbit	Total human IRS2	Cell Signaling Technologies, Danvers, MA, USA
TBC1D1 (V796)	Rabbit	Around Val796 mouse TBC1D1	Cell Signaling Technologies, Danvers, MA, USA
α-Tubulin (DM1A)	Mouse	native chick brain microtubules	Calbiochem – Merck Millipore, Darmstadt, Germany
Anti-rabbit-HRP	Goat	-	Dianova, Hamburg, Germany
Anti-mouse-HRP	Rabbit	-	Dianova, Hamburg, Germany

3.3.3 Measurement of total pancreatic insulin content

Dissected total pancreas (3.1.4) was homogenized in a 2 mL reaction tube with 1 mL ice-cold acid ethanol solution (Tab. 13) and a small stainless steel bead (Tab. 15) under harsh disrupting conditions in the TissueLyser II (Tab. 16). The homogenate was stirred overnight at 4 °C and centrifuged the next day at 5000 rcf, 4 °C for 15 min. The clear supernatant was stored at -20 °C until insulin (3.3.6) and protein concentration measurement (3.3.1).

3.3.4 Preparation of palmitate stock solution

Initially, a 10 % BSA solution was prepared by mixing 1.6 g fatty acid free BSA (Tab. 12) with 16 mL KHB buffer (Tab. 13) overnight at 4 °C. A 20 mM palmitate solution was prepared by mixing 14.14 mg palmitic acid (Tab. 12) with 3 mL freshly prepared 100 mM NaOH solution at 70 °C in a heat block. The BSA solution was heated to 50 °C. To prepare a 5 mM palmitate stock solution, a total of 2.5 mL clear palmitate solution (20 mM) was added quickly to 7.5 mL warm BSA solution (10 %) with a pre-heated pipette tip with a maximum of 1 mL at a time. The solution was stored at -20 °C.

3.3.5 Secretagogue-stimulated insulin secretion in isolated mouse islets

3.3.5.1 Static secretagogue-stimulated insulin secretion

Static GSIS assay was performed in a U-bottom 96 well plate with eight islets (3.1.3) of equal size in 4 replicates per genotype. The respective wells were loaded with 80 µL KRH buffer (Tab. 13) with 2 mM glucose and islets were added in a volume of 20 µL islet medium. To wash the samples from the added islet medium, 80 µL were discarded and 80 µL fresh KRH buffer with 2 mM glucose was added again. After another washing step, the islets were allowed to equilibrate for 1 h at 37 °C, 5 % CO_2. Thereafter, always the same islets were incubated 1 h at 37 °C, 5 % CO_2 with KRH buffer containing the designated secretagogue (11 mM / 25 mM glucose, 1 µM glibenclamide, 30 mM KCl or 5 µM A23187, 0.5 mM AICAR, 0.3 mM palmitate) according to the experimental setups shown in Figure 8. When certain substances were dissolved in DMSO, the same volume of DMSO was also applied to the respective control conditions. Always 80 µL of supernatant was collected and replaced with the same volume of the next secretagogue-containing buffer after the incubation time. Insulin values in the supernatants were quantified with the Insulin ELISA Kit (Tab. 11) after appropriate dilutions.

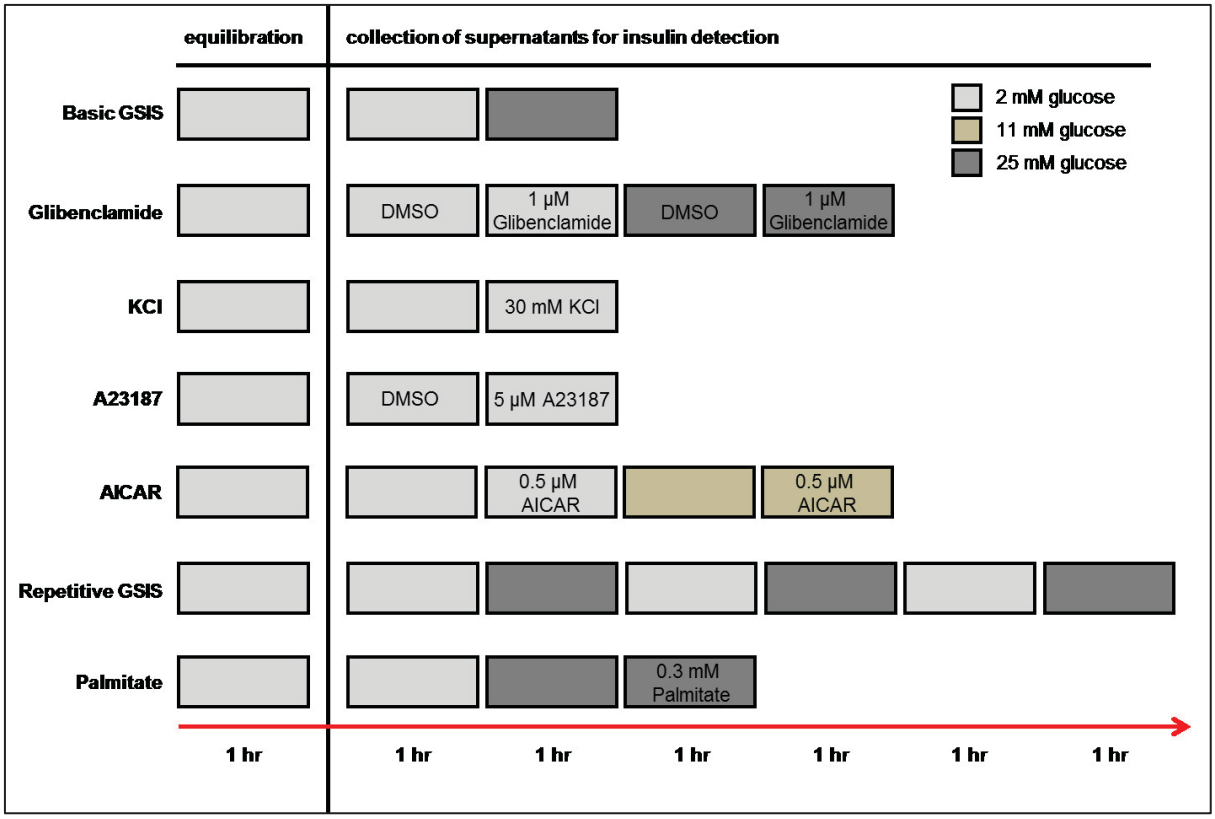

Figure 8: Experimental setups for static secretagogue-induced insulin secretion of isolated islets. For all setups an initial 1 hour equilibration of isolated islets in KRH buffer with 2 mM glucose is followed by the 1 hour

incubation in KRH buffer with 2 mM glucose as the basal control. For later applied secretagogues that were dissolved in DMSO, the same volume of DMSO in the KRH buffer was applied at this stage. **Basic GSIS:** Basic glucose-stimulated insulin secretion with 25 mM glucose. **Glibenclamide:** GSIS under the influence of 1 µM glibenclamide (solubilized in DMSO). **KCl:** KCl-stimulated insulin secretion at 2 mM glucose with 30 mM KCl. **A23187:** Ca^{2+}ionophore A23187-induced insulin secretion at 2 mM glucose with 5 µM A23187 (solubilized in DMSO). **AICAR:** GSIS under the influence of 0.5 µM AICAR. Insulin secretion was stimulated with 11 mM glucose. **Repetitive GSIS:** GSIS with three subsequent repetitive glucose stimulations (25 mM) interrupted by incubation with 2 mM glucose. **Palmitate:** GSIS with an additional acute exposure to 0.3 mM palmitate.

3.3.5.2 Dynamic secretagogue-stimulated insulin secretion (perifusion)

These experiments were performed by Verena Lier-Glaubitz in the lab of Prof. Dr. Ingo Rustenbeck at the Institute of Pharmacology, Toxicology and Clinical Pharmacy (Technical University Braunschweig, Germany). Mice were sacrificed by decapitation, pancreas was removed and manually chopped in KRH buffer. After 8.5 min of collagenase (Tab. 12) digestion in a 37 °C shaking water bath, the tissue was washed with KRH buffer und islets were immediately handpicked from the exocrine tissue. Perifusion of 50 WT and D1KO islets, respectively, was carried out with 5 mM basal glucose and either 30 mM glucose, 500 µM tolbutamide (Tab. 12) and/or 40 mM KCl for stimulated conditions according to the previously described protocols [179] (Hans-Georg Joost et al. (eds.), Animal Models in Diabetes Research, Methods in Molecular Biology).

3.3.6 Insulin quantification with ELISA

The enzyme-linked immunosorbent assay (ELISA) is an antibody-based detection system to quantify very little amounts of proteins in a sample. The assay was carried out according to the manufacturer's instructions with slight adaptations (Tab. 11). 10 µL sample and the supplied insulin standard solutions (for the Insulin ELISA Kit, otherwise 25 µL for the Insulin Ultrasensitive ELISA Kit) were loaded into the antibody-coated wells of a 96 well plate and mixed with 100 µL of a prepared 1x enzyme-conjugate solution. After 2 hours incubation at room temperature with approx. 800 rpm stirring the wells were washed 6 times with 300 µL of a prepared 1x wash buffer. The buffer was discarded and the plate tapped on tissue paper between the washing steps. For the signal development, 200 µL of the TMB (3,3',5,5'-tetramethylbenzidine) substrate was added and incubated for 15 min at room temperature without light exposure. The reaction was stopped by adding 50 µL of a sulfuric acid-containing stop solution by which the blue signal turned yellow. The intensity of the yellow

color was quantified in the iMark Reader at 450 nm and the insulin concentration calculated via cubic spline regression with the help of the insulin standards in the Microplate Manager 6 software (Tab. 17).

3.4 Histological techniques

The histologic and morphometric analysis and the sample preparation were performed in major parts by Carmen Weidlich during her Bachelor thesis (C.W., bachelor thesis, 2014) and Dr. Jürgen Weiß and Kay Jeruschke from the histology unit of the Institute for Clinical Biochemistry and Pathobiochemistry.

3.4.1 Fixation of tissues

As mentioned in 3.1.4, the dissected pancreas with the attached spleen was placed in an embedding cassette and fixed with 4 % PFA for 24 hours at room temperature. PFA acts by crosslinking proteins and therefore stabilizing and maintaining the actual status of the tissue [180].

3.4.2 Paraffin embedding

With the help of an automatic tissue processor (Shandon Excelsior, Tab. 16), the fixed tissues (3.4.1) were prepared for paraffin embedding by firstly dehydration with alcohol and secondly a subsequent substitution of the alcohol with the amphoteric intermedium xylene. In the last steps of the automatic procedure, the tissues were placed into liquid paraffin. The automatic procedure contained different steps that are shown in Table 8. In a manually operated embedding station (Tab. 16) the tissues were filled up with paraffin so that the tissue was fully surrounded by paraffin in a block.

Table 8: Incubation series of formalin-fixed tissues for paraffin embedding

Solution	Temperature	Duration
ethanol 70 %	room temperature	1 h
ethanol 70 %	room temperature	1 h
ethanol 96 %	room temperature	1 h
ethanol 96 %	room temperature	1 h
ethanol 100 %	room temperature	1 h
ethanol 100 %	room temperature	2 h
xylene	room temperature	1 h
xylene	room temperature	1 h
xylene	room temperature	1 h
paraffin	59 °C – 60 °C	1 h
paraffin	59 °C – 60 °C	1 h
paraffin	59 °C – 60 °C	2 h

3.4.3 Preparation of tissue slices by microtome cutting

After embedding the tissue in paraffin (3.4.2), sections of 5 µm thickness were cut with a microtome (Tab. 16) with 10 sections per level series. Between each series 50 µm of tissue (another 10 adjacent sections) were discarded. By doing so, each section of one series has a defined distance of 100 µm to the same section of the next or the previous series. To stretch the sections after the cutting, they were transferred via a water bridge into a 45 °C water bath for a few seconds. When the tissue was stretched, the section was collected onto microscopic slides (Tab. 15) and dried overnight at room temperature.

3.4.4 Hematoxylin and eosin (HE) staining

The HE staining represents a very basic method for the illustration of tissue arrangement in the histologic characterization of tissues. Hematoxylin in the prepared solution oxidizes to hematein which forms a complex with aluminium ions to form hemalum. This is able to stain nuclei of cells and some other cellular components in blue [181]. Afterwards, the tissue can be counterstained with aqueous or alcoholic solutions of eosin y which stains cytoplasmic (eosinophilic) structures of cells in red, pink and orange. Prior to the staining, the tissue had to be deparaffinized and rehydrated to enable the accessibility and binding of the stains. This

was achieved by subsequent incubations of the formalin-fixed paraffin embedded (FFPE) tissue on the microscopic slides (3.4.3) in xylene and different descending concentrations of ethanol. After incubation in 70 % ethanol solution the paraffin disappeared on the slide and the tissue was stained with Mayer's hematoxylin solution (Tab. 13). After the stain, the excessive solution was washed away with water and the tissue was stained with 0.1 % alcoholic eosin solution (Tab. 13). To finalize the stain the slides were incubated again in ethanol and finally in xylene before they were mounted with a specialized medium (Shandon EZ-Mount, Tab. 12) and sealed with a cover slip. The different incubation steps are listed in Table 9.

Table 9: Incubation series of FFPE slices for hematoxylin/eosin staining

Solution	Incubation time
xylene	5 min
xylene	5 min
ethanol 100 %	5 min
ethanol 100 %	5 min
ethanol 96 %	5 min
ethanol 96 %	5 min
ethanol 70 %	5 min
ethanol 70 %	5 min
Mayer's hematoxylin	2 min
double-distilled water	wash
tap water	10 min
eosin 0.1 %	30 seconds
ethanol 100 %	wash
ethanol 100 %	2 min
ethanol 100 %	2 min
ethanol 100 %	2 min
xylene	5 min

3.4.5 Point counting method to determine the pancreas area

The first step in the morphometric analysis was the determination of the pancreas area of each analyzed section. This was accomplished with the point counting method [182]. The slides were projected by an overhead projector onto a paper grid with marker points that had a defined distance of 28 mm to each other. The projected picture was adjusted to a magnification of 28-fold. The marker points that hit the pancreatic tissue in the projected picture (excluding vessels, duct, lymph nodes and spaces) were counted and summed up. One point corresponded to a pancreas area of 1 mm².

3.4.6 Software-assisted morphometric analysis of islets

After determination of the pancreas area per section by point counting (3.4.5), each section was scanned under the microscope (Tab. 16) with 10-fold magnification for the amount and area of islets within the pancreas tissue. Pictures of each islet were taken and analyzed with the cellSense Dimension software (Tab. 17). Each islet was manually surrounded by an integrated polygon tool that determined the islet area and the islet count.

3.4.7 Transmission electron microscopy for insulin granule analysis

To determine the amount of insulin secretory granules in β-cells of D1KO and WT mice isolated islets (3.1.3) were allowed to regenerate overnight. Islets with signs of necrosis (dark spots in the middle of the islet) were sorted out and the remaining islets were incubated with 2 mM or 25 mM glucose in KRH buffer for 1 h at 37 °C, 5 % CO_2 after equilibration in KRH buffer with 2 mM glucose for 1 h at 37 °C, 5 % CO_2. Islets were washed with BSA-free KRH buffer, fixed for 1 h at room temperature by immersion in 2.5 % glutaraldehyde in KRH buffer (Tab. 13), postfixed in 2 % osmium tetroxide in 0.19 M sodium cacodylate buffer, pH 7.4 (Tab. 12, 13), for 30 minutes, and subsequently stained with 2 % uranyl acetate in maleate buffer, pH 4.7 (Tab. 12, 13). The specimens were dehydrated with increasing ethanol concentrations and embedded in epoxy resin [183]. Ultrathin sections were picked up onto Formvarcarbon-coated grids (Tab. 15), stained with lead citrate (Tab. 12) and viewed in a transmission electron microscope (Tab. 16). Processing of the islets and TEM analysis was conducted by Kay Jeruschke and Dr. Jürgen Weiß.

3.5 Chemicals, solutions

3.5.1 Reaction kits

3.5.1.1 Reaction kits for molecular biology methods

Table 10: Reaction kits for molecular biology methods

Kit name	Supplier
Invisorb® Genomic DNA Kit II	STRATEC Molecular GmbH, Berlin, Germany
RNeasy Mini Kit	QIAGEN, Hilden, Germany
RNAse free DNAse Set	QIAGEN, Hilden, Germany
GoScript™ Reverse Transcriptase Kit	Promega, Madison, WI, USA
Hexanucleotide primer	Roche, Mannheim, Germany
GoTaq® qPCR Master Mix	Promega, Madison, WI, USA
100 bp DNA Ladder / 1 kb DNA Ladder	Thermo Scientific, Peqlab, Wilmington, MA, USA
6x Gel Loading Dye	Thermo Scientific, Peqlab, Wilmington, MA, USA
Phusion High-Fidelity DNA Polymerase 500U	Thermo Scientific, Peqlab, Wilmington, MA, USA
5x Phusion HF Buffer	Thermo Scientific, Peqlab, Wilmington, MA, USA
10x DreamTaq Green Buffer	Thermo Scientific, Peqlab, Wilmington, MA, USA
DreamTaq DNA Polymerase 5U/µL	Thermo Scientific, Peqlab, Wilmington, MA, USA
RNA 6000 Nano Kit	Agilent Technologies, Waldbronn, Germany
Customized oligonucleotide primers	Eurogentech, Seraing, Belgium

3.5.1.2 Reaction kits for biochemical methods

Table 11: Reaction kits for biochemical methods

Kit name	Supplier
Pierce™ BCA Protein Assay Kit	Thermo Scientific, Pierce, Rockford, IL, USA
Precision Plus Protein Standard Dual Color	Biorad Laboratories, München, Germany
Western Lightning ECL Pro	Perkin Elmer, Waltham, MA, USA
Western Lightning ECL Ultra	Perkin Elmer, Waltham, MA, USA
Insulin (Mouse) ELISA	DRG Instruments, Marburg, Germany
Insulin (Mouse) Ultrasensitive ELISA	DRG Instruments, Marburg, Germany

3.5.2 Chemicals

All fine chemicals that were used for the described study were purchased from standard suppliers. Specific chemicals are listed in Table 12.

Table 12: Chemicals

Chemical / Solution	Supplier
5-aminoimidazole-4-carboxamide 1-β-D-ribo-furanoside (AICAR)	Enzo Life Sciences, Lörrach, Germany
Ammonium persulfate (APS)	MP Biomedicals, Illkirch, France
Bovine serum albumin (BSA) Fraction V	AppliChem, Darmstadt, Germany
BSA Fraction V, fatty acid free, low endotoxin	Sigma Aldrich, Steinheim, Germany
Bromophenol blue	Merck, Darmstadt, Germany
Cacodylic acid Na-salt x 3 H_2O	Serva, Heidelberg, Germany
Calcium ionophore A23187	Sigma Aldrich, Steinheim, Germany
Chloralhydrate	AppliChem, Darmstadt, Germany
Collagenase	Serva, Heidelberg, Germany
Complete Protease Inhibitor Cocktail	Roche, Mannheim, Germany
Compound 6	Provided by Prof. Dr. Eckhard Lammert
D.E.R 736	Serva, Heidelberg, Germany
Dimethylaminoethanol (DMAE)	Serva, Heidelberg, Germany
Dimethylsulfoxide (DMSO)	AppliChem, Darmstadt, Germany
Dithiothreitol (DTT)	VWR, Darmstadt, Germany
dNTP Set PCR Grade	Roche, Mannheim, Germany
Eosin yellowish	Merck, Darmstadt, Germany
3,4-Epoxycyclohexylmethyl-3,4-epoxycyclohexylcarboxylate (ERL-4221 D)	Serva, Heidelberg, Germany
Ethidium bromide	MP Biomedicals, Illkirch, France
Ethylenediaminetetraacetic acid (EDTA)	Roth, Karlsruhe, Germany
Ethylene glycol tetraacetic acid (EGTA)	Serva, Heidelberg, Germany
Fetal Bovine Serum (FBS)	Thermo Fisher Scientific, Darmstadt, Germany
Glibenclamide	Sigma Aldrich, Steinheim, Germany
Glutaraldehyde (25 % solution)	Serva, Heidelberg, Germany
Hematoxylin	Merck, Darmstadt, Germany
Histopaque-1077	Sigma Aldrich, Steinheim, Germany
Lead citrate	Merck, Darmstadt, Germany
Liberase TL Research Grade	Roche, Mannheim, Germany
Maleic acid	Merck, Darmstadt, Germany

Chemical / Solution	Supplier
β-Mercaptoethanol (50 mM solution)	Thermo Fisher Scientific, Darmstadt, Germany
Nonenylsuccinic anhydride	Serva, Heidelberg, Germany
Osmium tetroxide	Serva, Heidelberg, Germany
Paraffin (Paraplast Plus©)	Sigma Aldrich, Steinheim, Germany
Paraformaldehyde (PFA) extra pure	Merck, Darmstadt, Germany
Penicillin/Streptomycin solution	Thermo Fisher Scientific, Darmstadt, Germany
PhosSTOP Phosphatase Inhibitor	Roche, Mannheim, Germany
Potassium aluminium sulfate ($KAl(SO_4)_2$)	VWR, Darmstadt, Germany
Shandon EZ-Mount	Thermo Electron Corporation, Waltham, MA, USA
Sodium bicarbonate (7.5 % solution)	Thermo Fisher Scientific, Darmstadt, Germany
Sodium iodate	VWR, Darmstadt, Germany
Tetraethylethylenediamin (TEMED)	Roth, Karlsruhe, Germany
Tolbutamide	Serva, Heidelberg, Germany
Tris(hydroxymethyl)aminomethan (TRIS)	Roth, Karlsruhe, Germany
Uranyl acetate 98 %	Polysciences Inc., Warrington, PA, USA
Xylene	AppliChem, Darmstadt, Germany

3.5.3 Solutions

3.5.3.1 Buffers and solutions

Table 13: Buffers and solutions

Solution	Content
KRH (Krebs-Ringer-HEPES) Buffer	15 mM HEPES, 5 mM KCl, 120 mM NaCl, 24 mM $NaHCO_3$, 1 mM $MgCl_2$, 2 mM $CaCl_2$, 1 mg/mL BSA
Stacking gel buffer for SDS-PAGE	500 mM Tris-HCl, 0.4 % SDS, pH 6.8
Separation gel buffer for SDS-PAGE	1,5 M Tris-HCl, 0.4 % SDS, pH 8.8
Electrophoresis Buffer for SDS-PAGE	25 mM Tris-HCl, 192 mM Glycine, 0.1 % (w/v) SDS
Transfer Buffer for tank blotting	25 mM Tris-HCl, 192 mM Glycine, 20 % Methanol
Wash Buffer for Western Blots (TBS-T)	10 mM Tris-HCl, 150 mM NaCl, 0.5 % Tween-20, pH 8.0
4x Lämmli Sample Buffer	20 % vol Glycerol, 8 % SDS, 10 mM EDTA, 250 mM Tris-HCl, 5 % bromophenol blue solution (2 % bromophenol blue + 4 % SDS in water)
1x TAE Buffer	40 mM Tris acetate, 1 mM EDTA
Lysis buffer stock	20 mM Tris-HCl, 150 mM NaCl, 1 mM EDTA, 1 mM EGTA, 1 % Triton X-100
Complete Proteases working solution	1 Tablet dissolved in 2 mL H_2O

Solution	Content
PhosSTOP working solution	1 Tablet dissolved in 1 mL H_2O
Lysis buffer	Lysis Buffer stock with 10 % PhosSTOP and 4 % Complete Proteases
Acid ethanol solution	0.18 M HCl, 75 % Ethanol
Mayer's hematoxylin	50 g Chloralhydrate, 1 g Citric acid, 1 g hematoxylin, 50 g $Kal(SO_4)_2$, 0.2 g Sodium iodate, add 1000 mL H_2O
Eosin y	80 mL Ethanol (70 %), 40 µL Acetic acid, 0.1 % Eosin yellowish
Krebs-Henseleit buffer (KHB) Stock I	118.5 mM NaCl, 4.7 mM KCl, 1.2 mM KH_2PO_4, 25 mM $NaHCO_3$
KHB Stock II	2.5 mM $CaCl_2 \cdot 2\ H_2O$, 1.2 mM $MgSO_4 \cdot 7\ H_2O$, 5 mM HEPES
KHB	10 % (v/v) KHB Stock I, 10 % (v/v) KHB Stock II, 80 % (v/v) H_2O
Sodium cacodylate buffer 0.19 M	0.19 M sodium cacodylate in water
Maleate buffer 0.05 M	0.05 M maleic acid in water

3.5.3.2 Media for islet isolation and maintenance

Table 14: Media for islet isolation and maintenance

Solution	Content	Supplier	Supplements
DMEM-1	DMEM low glucose, L- glutamine, sodium pyruvate and phenol red, without HEPES	Gibco® Thermo Fisher Scientific, Darmstadt, Germany	No Supplements
DMEM-2	DMEM-1	Gibco® Thermo Fisher Scientific, Darmstadt, Germany	15 % FBS
Islet medium	CMRL medium without L-glutamine and HEPES	Gibco® Thermo Fisher Scientific, Darmstadt, Germany	15 % FBS, 0.1 % 50 mM β-Mercaptoethanol, 1 % penicillin/streptomycin, 0.5 % glucose solution (20 %), 2 % $NaHCO_3$ solution (7.5 %)

3.6 Material

3.6.1 Disposables

All standard disposable material that was used for the described study was purchased from standard suppliers. Specific material is listed in Table 15.

Table 15: Disposables

Material	Supplier
BD Microlance™ 3, 30G ½“ 0.3 x 13 mm	BD Drogheda, Ireland
Sterican® needle 26Gx1” 0.45 x 25 mm	Braun, Melsungen, Germany
PVDF Hybond membrane 0.45 µm	GE Healthcare, Buckinghamshire, England
di-K^+-EDTA-coated microcuvettes	Sarstedt, Nümbrecht, Germany
96 well PCR plate for Real time PCR	Applied Biosystems, Darmstadt, Germany
Glucose test stripes Contour Next	Bayer HealthCare, Leverkusen, Germany
Microscope slides HistoBond®	Marienfeld, Lauda-Königshofen, Germany
Plastic Petri dish 10 cm	Greiner Bio One, Kremsmünster, Österreich
Formvar 12438	Serva, Heidelberg, Germany
Copper grids H75 mesh	Veco Gmbh, Marl, Germany
Stainless steel beads	QIAGEN, Hilden, Germany

3.6.2 Devices

Table 16: Devices

Device / Instrument	Supplier
Stereomicroscope SMZ1500	Nikon Instruments, Amsterdam, Netherlands
Shaking waterbath	Köttermann, Uetze/Hänigsen, Germany
Heraeus Megafuge 1.0 (Rotor Cat. No. 2705 with # 2252 F inlays)	Heraeus, Hanau, Germany
Plastic funnel, size 8	Roth, Karlsruhe, Germany
Cooling table centrifuge 5425 R (Rotor FA-45-24-11, KL088, 36927)	Eppendorf, Wesseling-Berzdorf, Germany
Table centrifuge 5425 R (Rotor FA-45-24-11, KL001, 32470)	Eppendorf, Wesseling-Berzdorf, Germany
Thermocycler Mastercycler (personal/gradient)	Eppendorf, Wesseling-Berzdorf, Germany
GelDoc XR+	Biorad Laboratories, München, Germany
ChemiDoc XRS+	Biorad Laboratories, München, Germany

Device / Instrument	Supplier
Gelchambers compact (M/XS/S)	Biometra, Göttingen, Germany
Standard PowerPack P25	Biometra, Göttingen, Germany
Minipac PS304 II	Biometra, Göttingen, Germany
Glucometer Contour XT	Bayer HealthCare, Leverkusen, Germany
Agilent 2100 Bioanalyzer	Agilent Technologies, Waldbronn, Germany
Cell dissociation sieve	Sigma Aldrich, Steinheim, Germany
iMark Microplate Reader	Biorad Laboratories, München, Germany
NanoDrop 2000	Thermo Scientific, Peqlab, Wilmington, MA, USA
Short plates for SDS gels	Biorad Laboratories, München, Germany
Spacer Plates (1.0 mm, 1.5 mm) for SDS gels	Biorad Laboratories, München, Germany
StepOnePlus™ Real-time PCR system	Applied Biosystems, Darmstadt, Germany
Concentrator 5301 (Vacuum centrifuge)	Eppendorf, Wesseling-Berzdorf, Germany
Mini PROTEAN Tetra System	Biorad Laboratories, München, Germany
Power Pac Basic	Biorad Laboratories, München, Germany
Tankblot Eco Mini	Biometra, Göttingen, Germany
Power Pac HC	Biorad Laboratories, München, Germany
Horizontal shaker CAT ST5	CAT, Staufen, Germany
TissueLyser II	QIAGEN, Hilden, Germany
Uniprep Gyrator	UniEquip, Planegg, Germany
Shandon Excelsior Tissue Processor	Thermo Scientific, Peqlab, Wilmington, MA, USA
Histo-Embedder	Leica Microsystems, Wetzlar, Germany
Rotary Microtome HM 360	Thermo Scientific, Peqlab, Wilmington, MA, USA
Microscope DM RBE	Leica Microsystems, Wetzlar, Germany
TEM 910	Zeiss, Oberkochem, Germany

3.7 Software

Table 17: Software applications of different devices for data measurement and analysis

Software	Method	Device	Company
NanoDrop 2000	DNA/RNA concentration	NanoDrop 2000	Thermo Fisher
Image Lab	Agarose gel / Western blot	Gel/Chemi Doc	Bio-Rad Laboratories
StepOne v2.1	qPCR	StepOne Plus	Applied Biosystems
Microplate Manager 6	BCA / ELISA	iMark Reader	Bio-Rad Laboratories
GraphPad Prism 5	Statistical analyses	PC	GraphPad Software Inc
Agilent 2100 BioSizing	RNA quality	BioAnalyzer	Agilent Technologies
cellSense Dimension	Microscopy	Microscope	Leica Microsystems

3.8 Statistical analysis

Statistic operations were applied to identify significant differences between the measured or determined data. Therefore, different statistical tests were applied to determine the significance of differences. All experiments were performed with at least n = 3 samples and shown as mean values ± SEM or mean values ± SD. Exact numbers of experiments (n) are depicted in the figure legends and the text. Statistical significance was calculated with two-tailed student's t-test for paired or unpaired values, one-way ANOVA with Tukey's multiple comparison test, two-way ANOVA with Bonferroni post-hoc-test or with Mann-Whitney-U test. For all tests a p-value ≤ 0.05 was considered to be significant. Statistical analysis was performed with GraphPad Prism 5 software (Tab. 17).

4 RESULTS

4.1 Glucose-stimulated insulin secretion from isolated D1KO islets

Isolated islets from D1KO mice and WT littermates were subjected to the basic GSIS protocol (3.3.5, Fig. 8) and the secreted insulin was measured with ELISA. The results were expressed as pg secreted insulin per islet per 60 minutes (Fig. 9). Insulin secretion at 2 mM glucose was unchanged between both genotypes after 60 min incubation (10.8 ± 2.2 pg/islet/60 min in WT islets vs. 8.1 ± 1.9 pg/islet/60 min in D1KO islets). Stimulated insulin secretion at 25 mM glucose was substantially increased in islets of D1KO mice compared to WT after 60 min incubation (120.5 ± 12.7 pg/islet/60 min in WT islets vs. 178.1 ± 24.0 pg/islet/60 min in D1KO islets; $p < 0.05$).

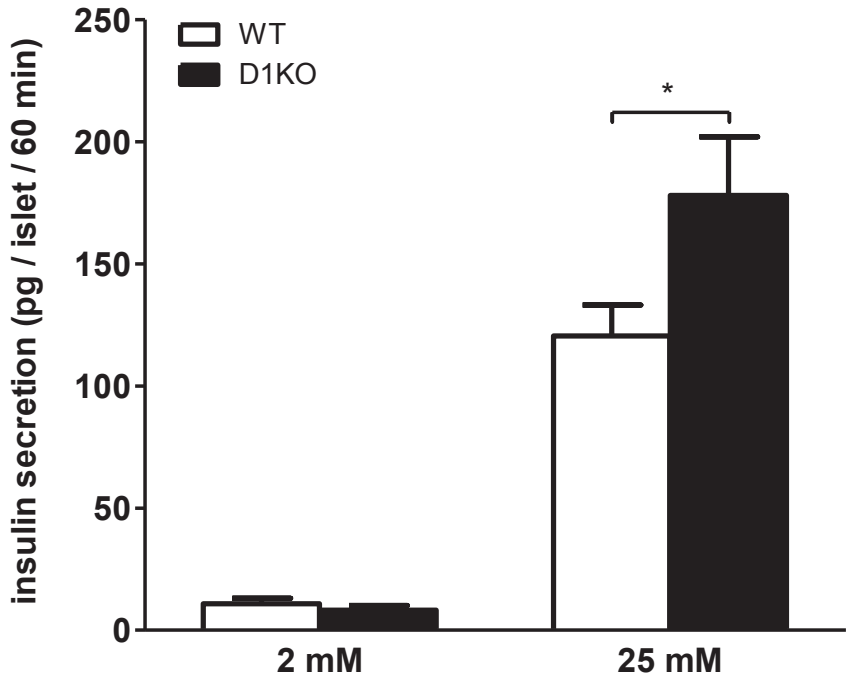

Figure 9: Glucose-stimulated insulin secretion in isolated islets of D1KO mice. Isolated islets of D1KO mice were incubated with 2 mM and 25 mM glucose for 1 h at 37 °C (Basic GSIS setup) and secreted insulin in the supernatants was measured with ELISA. Data are mean values ± SEM (n = 7), two-way ANOVA with Bonferroni post-hoc-test * $p < 0.05$.

The demonstrated differences could be due to several cellular or mechanistic changes. To find the underlying *in vitro* mechanisms and possible *in vivo* consequences, first the total and differential expression of *Tbc1d1* and *Tbc1d4* in isolated islets were investigated.

4.2 RabGAP expression in isolated islets

A qualitative assessment of the expressed *Tbc1d1* isoform in islets and other tissues of wildtype mice was performed. In addition the mRNA copy number of *Tbc1d1* and *Tbc1d4* transcripts in isolated islets of wildtype mice as well as the differential expression of *Tbc1d1* and *Tbc1d4* in isolated islets of D1KO and RIP2-TG mice were determined.

4.2.1 Determination of *Tbc1d1* isoforms in different tissues of C57BL/6J mice

Tbc1d1 is expressed as two major isoforms in different tissues. In the literature it was reported that the skeletal muscle expresses predominantly the long isoform [168] whereas the short *Tbc1d1* isoform is found in pancreas tissue from NZO mice (Katja Leicht, PhD thesis). Therefore, the short isoform was used for the generation of the transgenic mice that were used for this thesis. To verify the previous results heart and muscle tissue (*Musculus quadriceps*) of C57BL/6J mice were used and isolated islets instead of total pancreas (3.2.6). The primers that were described in the methods section (Appendix Tab. 19) bind to DNA regions of exons 11 and 14 that flank exons 12 and 13 that are present in the long isoform but missing in the short isoform. Thus, for the long isoform a 645 bp fragment and for the short isoform a 366 bp fragment was expected to be amplified. The amplified fragment from the cDNA of the skeletal muscle *Musculus quadriceps* represented an intense band between 600 and 700 bp at the expected height of the long isoform. A very faint band was also seen between 300 and 400 bp at the expected height of the short isoform. The amplified fragment from the cDNA of the heart represented a band for both isoforms. The band of the short isoform was a bit more intense, than the band for the long isoform. Notably, an additional band below 600 bp was visible next to the expected band at 645 bp for the long isoform which could neither be seen in the muscle nor in islets. The amplified fragment from the cDNA of the islets represented a band exclusively for the short isoform of *Tbc1d1*. Importantly the negative control without cDNA template did not show up any nucleic acid amplification (Fig. 10).

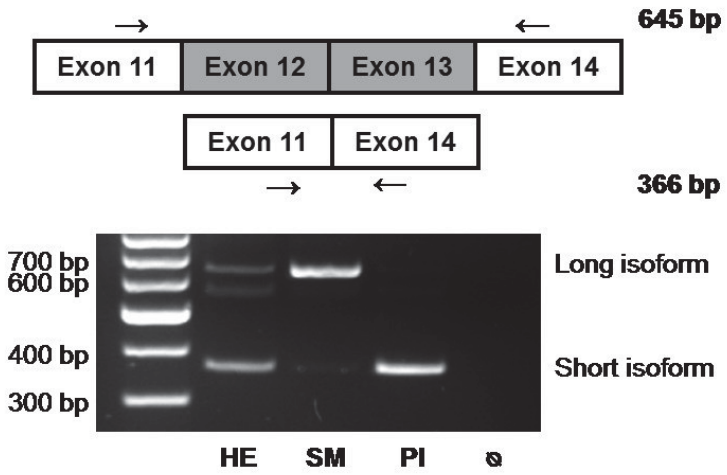

Figure 10: Identification of *Tbc1d1* isoforms in different tissues of C57BL/6J mice. Identification of the expressed *Tbc1d1*-isoforms in heart (HE), *quadriceps* muscle (SM) and pancreatic islets (PI) from C57BL/6J mice. Samples were analyzed by RT-PCR and visualized on a 2 % agarose gel. Schematic primer location is designated with the arrows. The long isoform should produce a 645 bp fragment, the short isoform a 366 bp fragment, due to the lack of exons 12 and 13. ⊘ – negative control without cDNA template

4.2.2 Total gene expression of *Tbc1d1* and *Tbc1d4* in isolated mouse islets

The comparative ΔΔCt method to determine the relative amount of mRNA does not give information about the total amount of mRNA present in a sample [184]. The amplification efficiency of a template depends on the primer pair, on the template itself or on the cycling settings. Therefore the raw Ct values were not suitable to conclude about expression differences in a sample between different genes. This was solved by measuring Ct values of two different expression vectors (pcDNA3-CMV-3xFLAG-*Tbc1d1* and PCR2.1-*Tbc1d4*) containing either *Tbc1d1* or *Tbc1d4* gene in multiple serial 1:2 dilutions (3.2.8). By referring the resulting Ct value to the concentration of the vector in the respective dilution the efficiency of the amplification was determined. As shown in Figure 11A the linear part of the relationship between Ct value and the logarithm of the concentration was equal with the amplification of both, *Tbc1d1* and *Tbc1d4*. With the help of the respective linear equation the amount of template of *Tbc1d1* and *Tbc1d4* in the islet samples was calculated. By normalizing to the reference gene *36b4* the normalized copy-number of mRNA was determined. Figure 11B shows the result of this calculation. *Tbc1d1* copy-number was 7.6-fold higher than *Tbc1d4* copy-number after molar calculation and normalizing to *36b4* (0.440 ± 0.022 for *Tbc1d1* vs. 0.058 ± 0.006 for *Tbc1d4*, $p < 0.0001$). The Ct values of *Tbc1d1* and *Tbc1d4* in the measurement from islets already differed in 3-4 Ct's. At the same time Ct values for *36b4* were not different.

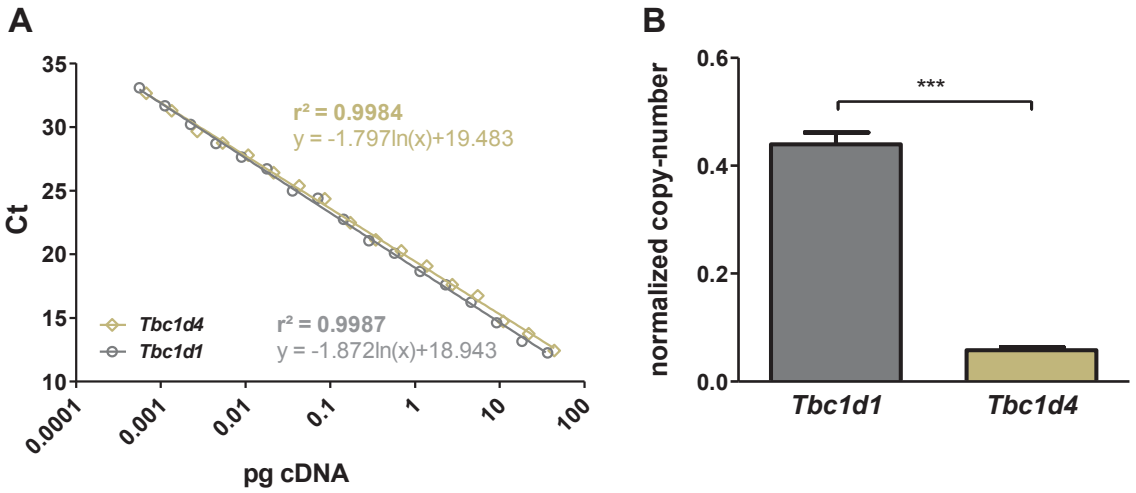

Figure 11: ***Tbc1d1*** **and** ***Tbc1d4*** **mRNA quantification in isolated islets of mice. (A)** 10 ng/µL of expression vectors pcDNA3-CMV-3xFLAG-*Tbc1d1* (9319 bp) and PCR2.1-*Tbc1d4* (7916 bp) with serial 1:2 dilutions were amplified with primers for *Tbc1d1* and *Tbc1d4* in a Real time PCR approach. Resulting Ct values were related to the amount of template in the respective dilution and the linear part of the relationship was plotted in a semi-log (x-axis log) diagram. The characteristics of the linear equation are shown. **(B)** With the help of the equation the molar amount of *Tbc1d1* and *Tbc1d4* template in RNA samples of isolated islets were calculated, normalized to the molar amount of *36b4* and displayed as normalized copy-number. Data are mean values ± SEM (n = 8), Student's t-test, two-tailed, unpaired *** $p < 0.0001$

4.2.3 Detection of TBC1D1 and FLAG in total pancreas lysates of transgenic mice

To test the conditions to detect TBC1D1 protein by western blot in total pancreas lysates from wildtype and RIP2-3xFLAG-*Tbc1d1* mice different amounts (40, 80 and 200 µg) of total protein were loaded to the polyacrylamide gel. Only with 200 µg protein TBC1D1 (Fig. 12A) and FLAG (Fig. 12B) were detected on the PVDF membrane after blotting at approx. 160 kDa. The detection of FLAG was used as a surrogate for TBC1D1 in the transgenic RIP2-TG islets. By using the anti-FLAG antibody the samples of wildtype and transgenic mice could be distinguished from each other.

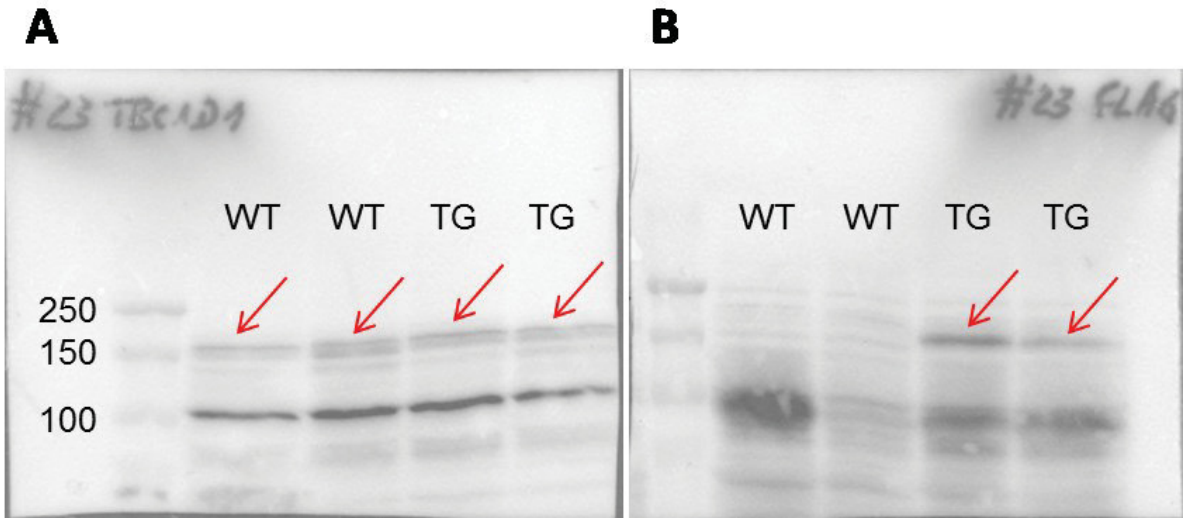

Figure 12: Detection of TBC1D1 and FLAG in lysates of total pancreas from transgenic mice. 200 µg of total protein were separated on an 8 % polyacrylamide gel. After tank blotting onto PVDF membrane TBC1D1 and FLAG were detected with **(A)** anti-TBC1D1 (1:1000) and **(B)** anti-FLAG (1:1000) primary antibodies. Signals were developed with ECL solution in a ChemiDoc device after incubating with HRP-conjugated secondary anti-rabbit (for TBC1D1) or anti-mouse (for FLAG) antibodies (1:20000).

4.2.4 Relative protein and gene expression of *Tbc1d1* and *Tbc1d4* in islets

After islet isolation and overnight regeneration the islets were lysed according to 3.3.1 and 10 µg of total islet protein were separated on an 8 % polyacrylamide gel. After tank blotting onto PVDF membranes the proteins were detected with anti-TBC1D1 and anti-TBC1D4 antibodies (Tab. 7) with a dilution of 1:1000 in 5 % BSA/TBS-T. TBC1D1 was identified at approx. 160 kDa in all samples, except for islets of D1KO mice. TBC1D1 protein expression in RIP2-3xFLAG-*Tbc1d1* islets was 2.6-fold higher compared to the respective control islets. TBC1D4 was also identified at approx. 160 kDa in all samples without differences between the respective genotypic different samples (Fig. 13A).

mRNA expression of both genes was measured in islets of D1KO mice. Expression of *Tbc1d4* mRNA was not different between WT and D1KO islets but *Tbc1d1* mRNA was expressed 10-fold less in D1KO islets compared to WT islets (Fig. 13B). Despite the presence of *Tbc1d1* mRNA in *Tbc1d1*-deficient islets no TBC1D1 protein was detected.

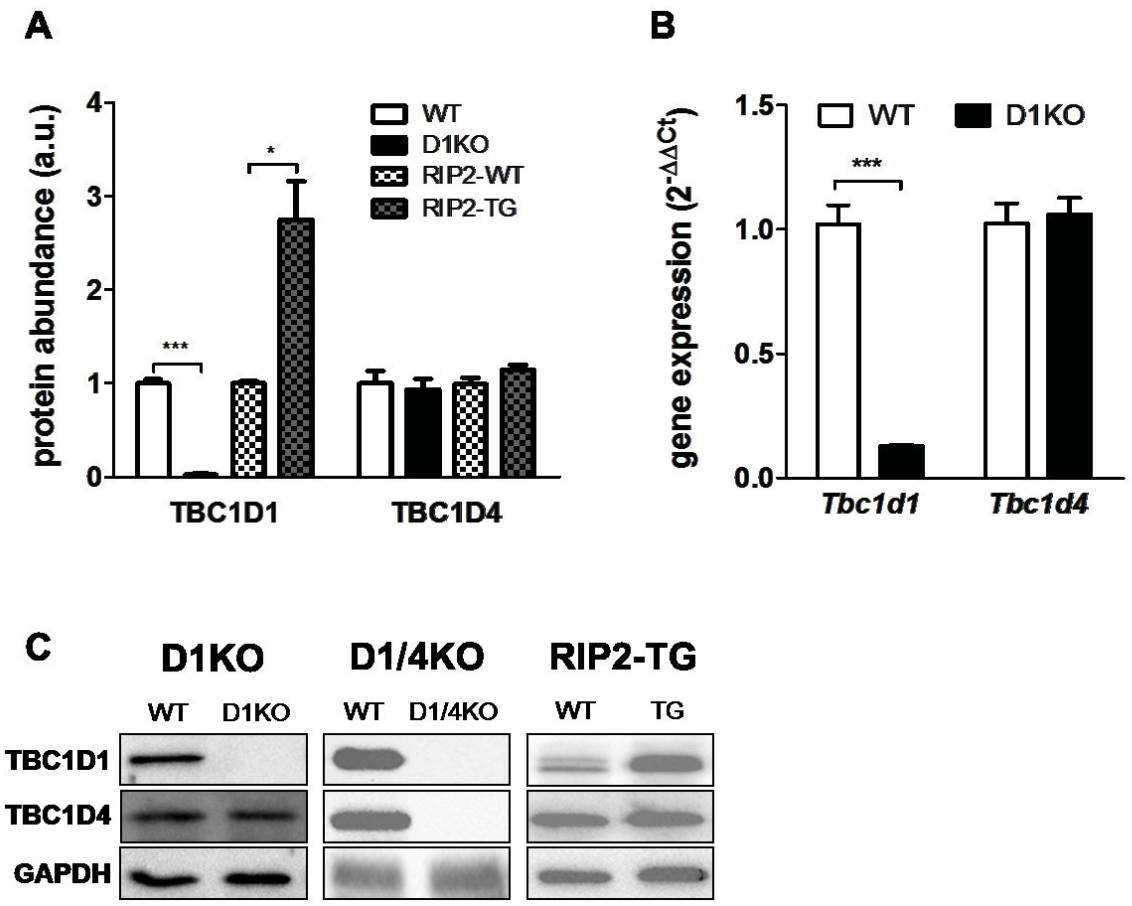

Figure 13: TBC1D1 and TBC1D4 expression in isolated islets of *Tbc1d1*-deficient and transgenic mice. (A) Protein expression of TBC1D1 and TBC1D4 in islets of D1KO and RIP2-TG mice compared to their respective controls. Samples from RIP2-WT and RIP2-TG mice were normalized to GAPDH expression, samples from WT and D1KO mice were normalized to α-tubulin. Data are mean values ± SEM (n = 4-8), Mann-Whitney-U test, two-tailed, * $p < 0.05$, *** $p < 0.001$. **(B)** Relative mRNA expression of *Tbc1d1* and *Tbc1d4* in islets of D1KO mice. Data were normalized to *36b4* expression and are shown as mean values ± SEM (n = 8), Mann-Whitney-U test, two-tailed, *** $p < 0.001$. **(C)** Representative Western Blots for TBC1D1 and TBC1D4 detection in isolated islets are shown in reference to the housekeeping protein GAPDH.

4.3 Static and dynamic GSIS from isolated islets

4.3.1 Static GSIS from islets of transgenic RIP2-3xFLAG-*Tbc1d1* mice

To investigate whether the overexpression of *Tbc1d1* would lead to the opposite effect as seen in the islets of D1KO mice isolated islets of transgenic mice and their respective WT controls were subjected to the basic GSIS protocol (3.3.5, Fig. 8) and the secreted insulin was measured with ELISA. Insulin secretion at 2 mM glucose was unchanged between both genotypes after 60 min incubation (17.5 ± 5.7 pg/islet/60 min in WT islets vs. 16.4 ± 3.3

pg/islet/60 min in RIP2-TG islets). Stimulated insulin secretion at 25 mM glucose was also unchanged between the genotypes after 60 min incubation (136.4 ± 26.0 pg/islet/60 min in WT islets vs. 135.1 ± 42.2 pg/islet/60 min in RIP2-TG islets) as shown in Figure 14.

Insulin secretion at basal 2 mM glucose was higher in islets of both genotypes of the transgenic mouse strain compared to the *Tbc1d1*-knockout strain. However, these differences were statistically not significant when calculating with two-way ANOVA.

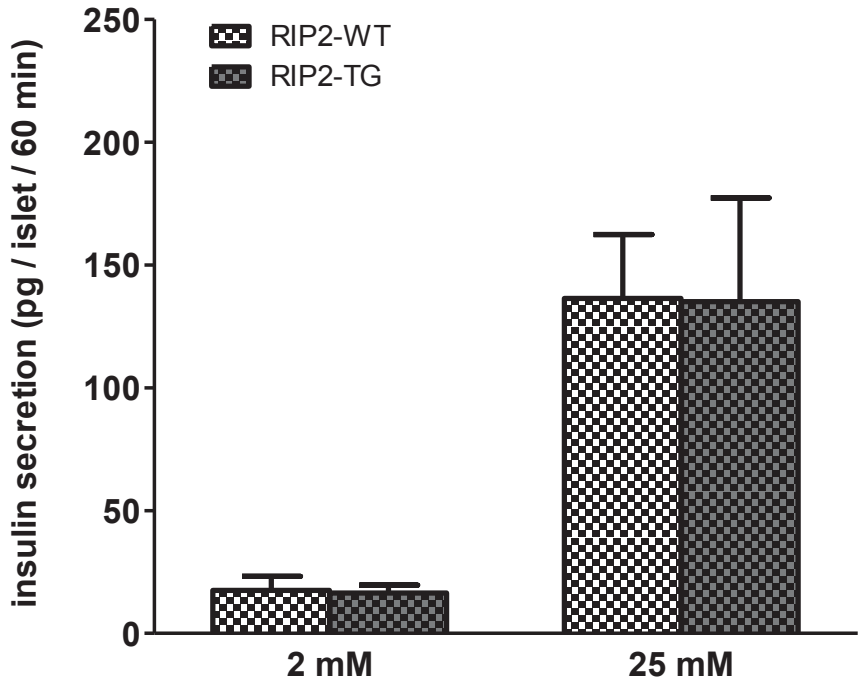

Figure 14: Glucose-stimulated insulin secretion in isolated islets of RIP2-TG mice. Isolated islets of RIP2-TG mice were incubated with 2 mM and 25 mM glucose for 1 h at 37 °C (Basic GSIS setup) and secreted insulin in the supernatants was measured with ELISA. Data are mean values ± SEM (n = 7), two-way ANOVA with Bonferroni post-hoc-test.

4.3.2 Static GSIS from islets of *Tbc1d1*/*Tbc1d4*-double-deficient D1/4KO mice

In a previous study the impact of *Tbc1d4*-knockdown in sorted mouse β-cells on GSIS was reported [173]. Reduced *Tbc1d4* expression led to an increase in basal but a decrease in glucose-stimulated insulin secretion. In this study the role of *Tbc1d4* in GSIS was investigated by using isolated islets of a mouse strain with a double-knockout of *Tbc1d1* and *Tbc1d4*. Isolated islets were subjected to the basic GSIS protocol (3.3.5, Fig. 8) and the secreted insulin was measured with ELISA. Insulin secretion at 2 mM glucose was again unchanged between both genotypes after 60 min incubation (10.9 ± 1.2 pg/islet/60 min in WT islets vs.

13.4 ± 1.8 pg/islet/60 min in D1/4KO islets). Stimulated insulin secretion at 25 mM glucose was significantly increased in islets of D1/4KO mice compared to WT (96.8 ± 17.3 pg/islet/60 min in WT islets vs. 172.8 ± 25.4 pg/islet/60 min in D1/4KO islets) similar to the results with the single knockout of *Tbc1d1* (Fig. 15).

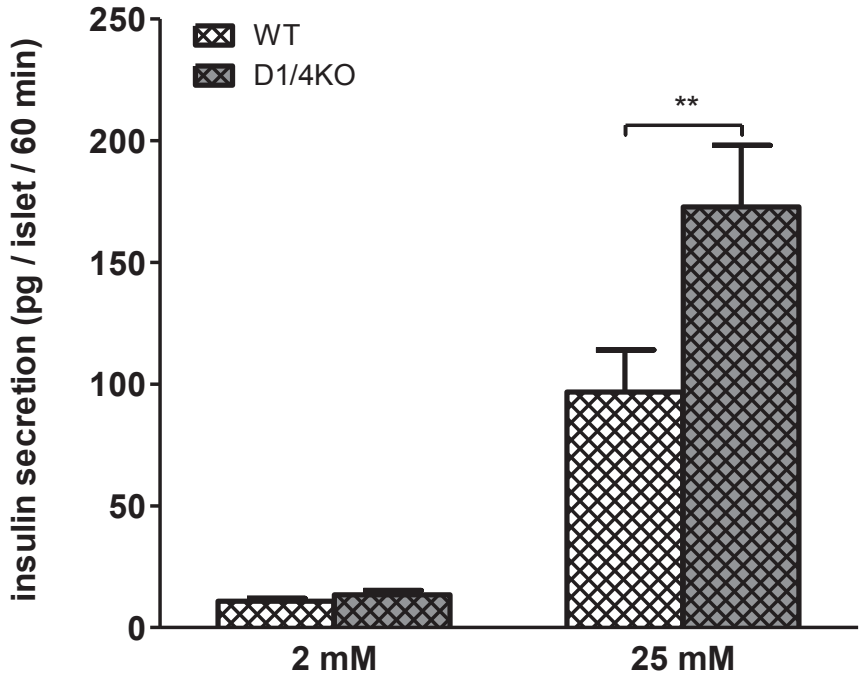

Figure 15: Glucose-stimulated insulin secretion in isolated islets of D1/4KO mice. Isolated islets of D1/4KO mice were incubated with 2 mM and 25 mM glucose for 1 h at 37 °C (Basic GSIS setup) and secreted insulin in the supernatants was measured with ELISA. Data are mean values ± SEM (n = 7), two-way ANOVA with Bonferroni post-hoc-test, ** $p < 0.01$.

4.3.3 Dynamic GSIS from islets of D1KO mice

In the static approach of glucose-stimulated insulin secretion only the sum of secreted insulin is measured at a certain time after stimulation. These data do not allow for a statement regarding insulin secretion phases. In the dynamic perifusion of isolated islets, insulin secretion can be assessed in various fractions of a secretagogue-containing buffer that constantly passes immobilized islets with a constant flow rate. This allows analyzing the different insulin secretion phases and therefore is much more suitable to narrow down the underlying possible mechanism. Since the static glucose-stimulated insulin secretion was changed in islets of *Tbc1d1*-deficient mice, those mice were also used for the dynamic perifusion (3.3.5). Insulin

secretion under basal conditions was determined with 5 mM glucose for approx. 30 min with a subsequent change to 30 mM stimulated glucose for 40 min and a final return to 5 mM basal glucose for another 20 min. The data were expressed as % insulin secretion of the value at 60 min.

As shown in Figure 16A basal insulin secretion was similar in both genotypes and declined in the progression of the basal glucose period to a minimum at 60 minutes. Directly after stimulation with 30 mM glucose, islets of WT mice increased insulin secretion only slightly (maximum 268.57 ± 96.39 %) in the first phase up to minute 70 and a little bit more in the second phase up to minute 100 (maximum 475.04 ± 163.95 %). After the return to basal glucose also insulin secretion fell to approx. 170 %. Islets of D1KO mice showed a much more pronounced insulin response to glucose throughout the entire stimulation period. Directly after stimulation with 30 mM glucose, islets of D1KO mice increased insulin secretion approx. 9-fold (maximum 872.26 ± 321.27 %) in the first phase. After a decline to minute 75 (414.73 ± 101.49 %), insulin secretion in the second phase increased again to a maximum at minute 105 (1223.69 ± 414.76 %). Return to basal glucose led to a decrease in insulin secretion comparable to islets of WT mice to approx. 165 %. The measurement of the area under the curve (AUC) between 60 and 100 minutes as the time of glucose stimulation showed a clear increased area for the D1KO islets but without being statistically significant (Fig. 16B)

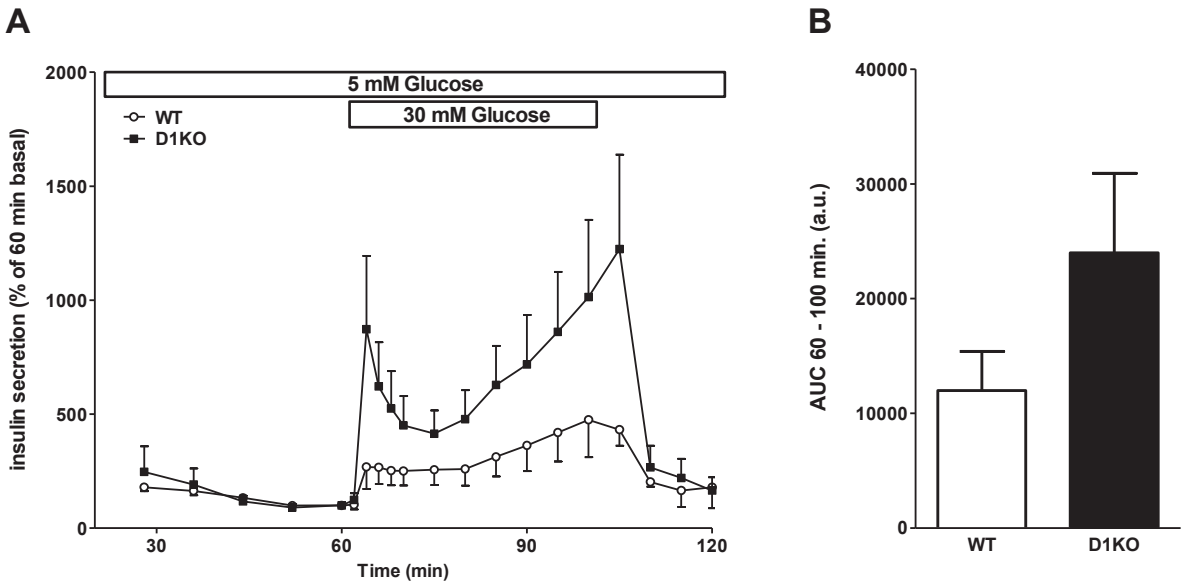

Figure 16: Dynamic glucose-stimulated insulin secretion in isolated islets of D1KO mice. (A) 50 islets per genotype were perifused in a custom-made perifusion chamber with 5 mM glucose and 30 mM glucose for the designated time points. Insulin from the eluate fractions was measured with ELISA and the values are expressed as percentage of the secretion rate at the end of the basal glucose period. Data are mean values ± SEM (n = 5). **(B)** Area under the curve (AUC) between 60 and 100 minutes for glucose stimulation. Data are mean values ± SEM (n = 5).

4.4 Glucose-stimulated insulin secretion in D1KO mice *in vivo*

Islet physiology and hormone secretion affect whole-body glucose homeostasis. In isolated islets of *Tbc1d1*-deficient mice glucose-stimulated insulin secretion was increased in both phases compared to wildtype mice (Fig. 9, 16). In a physiological context increased insulin secretion would lead to an accelerated transport of glucose from the blood into the insulin-sensitive target tissues. In isolated islets, *Tbc1d1*-deficiency led to changes in glucose-stimulated insulin secretion *ex vivo*. To investigate, whether glucose disposal from the blood and plasma insulin levels after an intraperitoneal glucose application to mice is different between wildtype and *Tbc1d1*-deficient mice *in vivo* an intraperitoneal glucose tolerance test was performed. The application of glucose intraperitoneally leads to a rapid bioavailability and resorption into the blood without activating incretin hormones to further increase insulin secretion (in contrast to an oral glucose tolerance test). In collected blood samples insulin concentration was measured to refer the glucose tolerance to the insulin values.

4.4.1 Glucose tolerance and plasma insulin in 14-16 weeks old mice

Prior to the test 14-16 weeks old mice were fasted overnight for 6 hours and the test was performed according to 3.1.5. Glucose tolerance was not different between both genotypes (Fig. 17A). 60 min after intraperitoneal glucose application D1KO mice had slightly lower blood glucose levels. Fasting blood glucose levels were also not different between both genotypes (Fig. 17D). Although glucose tolerance was not different within the tested mice the plasma insulin levels showed some differences between wildtype and D1KO mice. As shown in Figures 17B and 17E, fasting plasma insulin levels were significantly lower in D1KO mice (0.445 ± 0.038 ng/µL in WT mice vs 0.311 ± 0.030 ng/µL in D1KO mice; $p = 0.0112$). Throughout all other time points of the test no significant differences were observed in plasma insulin concentrations (Fig. 17B). The rise in plasma insulin after the first 30 minutes of the test seemed to be higher in D1KO mice compared to WT mice. In the remaining test time the course of plasma insulin was similar in both genotypes. By expressing the data relative to the fasting plasma insulin levels for both genotypes individually an increased secretion of insulin into the plasma in D1KO mice became visible (Fig 17C). In this expression the insulin values at 30, 60 and 120 min were significantly higher in D1KO mice compared to WT mice. Calculating the area under the curve (AUC) by integration of the relatively expressed data (Fig. 17F) demonstrated also a significantly increased AUC in D1KO mice (19977.1 ± 1402.7) compared to WT mice (15847.4 ± 1261.0) ($p = 0.044$).

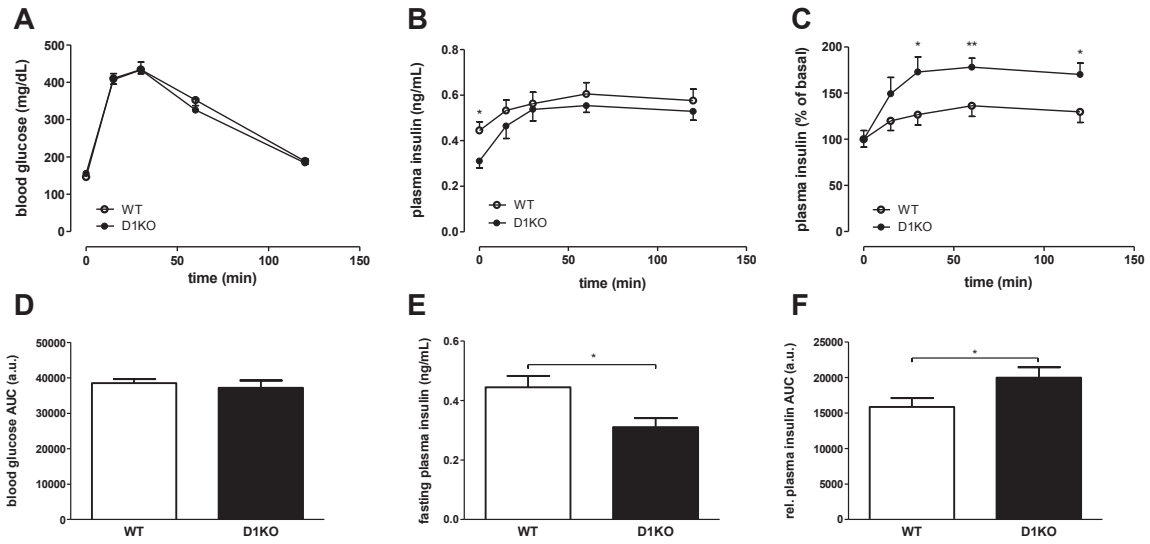

Figure 17: Intraperitoneal glucose tolerance test in 14-16 weeks D1KO mice compared to WT mice. (A, D) Glucose tolerance as a measure of glucose clearance from peripheral tail blood within 120 min after glucose injection was the same in D1KO and WT mice (n = 14). **(B, E)** Absolute plasma insulin levels were significantly lower in the fasted state in D1KO mice but were unchanged in the progression of the test (n = 12-14). **(C, F)** Plasma insulin levels and the AUC were significantly higher in D1KO mice when expressed as the percentage of the basal values of D1KO and WT mice, respectively. Data are mean values ± SEM with indicated number of individuals. Student's t-test, two-tailed, unpaired. * $p < 0.05$, ** $p < 0.01$

4.4.2 Glucose tolerance and plasma insulin in 50-52 weeks old mice

Because the young mice analyzed in 4.4.1 did not show a marked difference in the absolute plasma insulin levels throughout the test between both genotypes some of the previously tested mice were analyzed again in the same experimental setup at older ages. To ensure that blood glucose levels return to baseline levels at the end of the test the late time point at 240 min after i.p. injection was included for blood glucose and plasma insulin measurements. Glucose tolerance of old WT mice was significantly impaired in comparison to old D1KO mice (Fig. 18A). This was also illustrated by the AUC in Figure 18C (82951.3 ± 7122.2 in WT mice vs. 60771.3 ± 5396.8 in D1KO mice; $p = 0.041$). This difference in glucose tolerance between the genotypes was mostly due to differences in the blood glucose values at 60 and 120 min after glucose injection. Importantly fasting blood glucose levels and glucose levels at 15 and 30 min after glucose injection were unchanged between WT and D1KO mice. WT mice had an impaired glucose disposal from the blood 60 and 120 min after glucose injection compared to D1KO mice. The corresponding plasma insulin levels of the old mice were approx. twice as high as in the young mice (Fig. 18B). Fasting plasma insulin levels were unchanged between old WT and D1KO mice (Fig. 18D) although still a trend towards de-

creased levels of plasma insulin was determined in D1KO mice (p = 0.18). In the time course of the experiment plasma insulin levels of WT mice continuously increased from 0.957 ± 0.146 ng/µL at baseline until 2.375 ± 0.346 ng/µL 240 min after glucose injection. In contrast in D1KO mice plasma insulin continuously increased from 0.649 ± 0.090 ng/µL at baseline to 1.009 ± 0.084 ng/µL 30 min after glucose injection and reached more or less a plateau until 1.286 ± 0.229 ng/µL 240 min after glucose injection. Importantly plasma insulin levels after 240 min were significantly lower in D1KO mice compared to WT mice (Fig. 18E: p = 0.041).

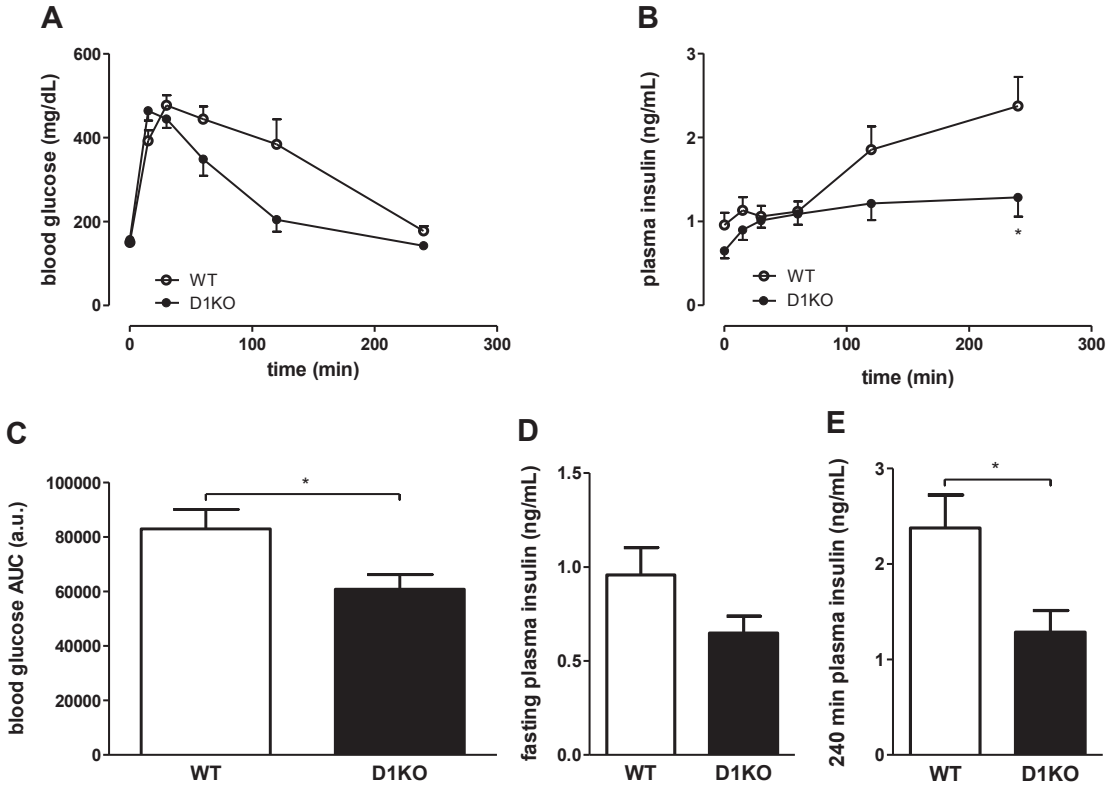

Figure 18: Intraperitoneal glucose tolerance test in 50-52 weeks D1KO mice compared to WT mice. (A, C) Glucose tolerance as a measure of glucose clearance from peripheral tail blood within 240 min after glucose injection was significantly improved in D1KO mice compared to WT mice (n = 6). **(B)** Plasma insulin levels showed an increased rise within 240 min in WT mice compared to D1KO mice (n = 6). **(D)** Fasting plasma insulin levels were unchanged between the genotypes but **(E)** were significantly lower in D1KO mice at the end of the test. Data are mean values ± SEM with indicated number of individuals. Mann-Whitney-U test, two-tailed. * p < 0.05

4.5 Total insulin content

4.5.1 Insulin content after glucose stimulation

Dependent on the *Tbc1d1* expression glucose-stimulated insulin secretion from isolated islets was altered. To exclude that the increased insulin secretion in D1KO islets was due to increased insulin content in the islets, insulin concentration in islet lysates after glucose stimulation was measured. Insulin content in the islet lysates of all genotypes were not different compared to their respective controls. Moreover, insulin content was unchanged in the comparison between all genotypes (Fig. 19).

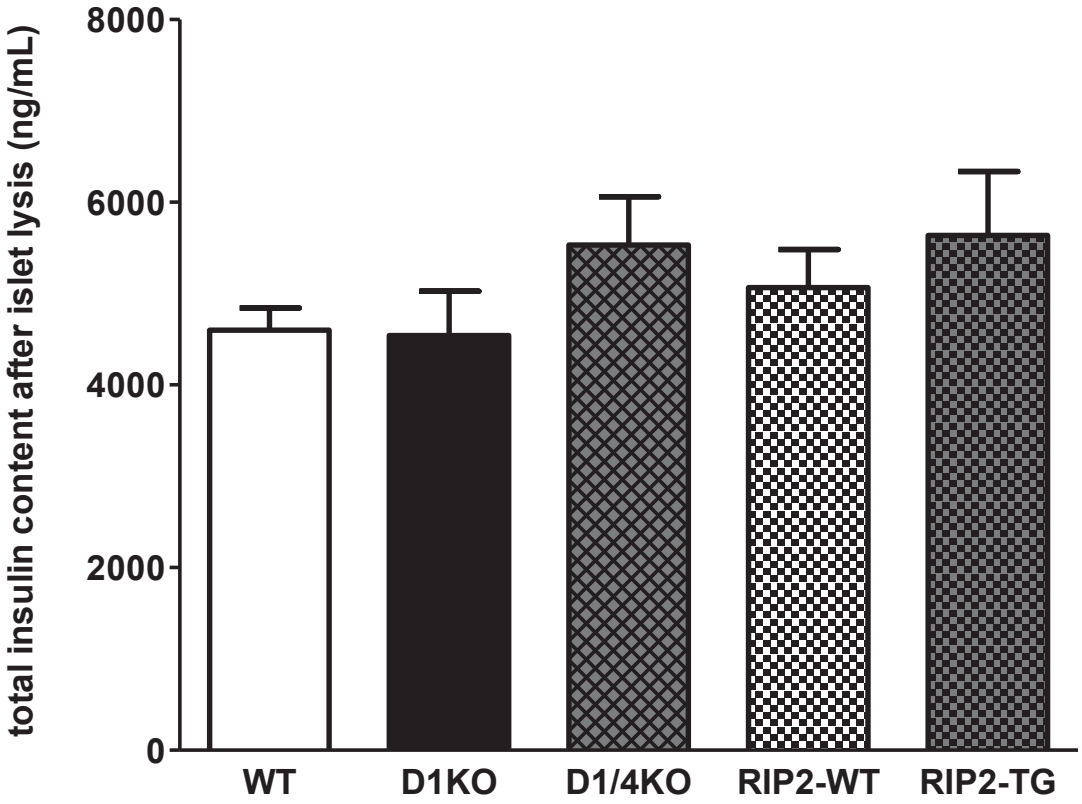

Figure 19: Insulin content of isolated islets after glucose stimulation. Isolated islets of D1KO, RIP2-TG and D1/4KO mice were lysed after 25 mM glucose stimulation and insulin in the lysates was measured with ELISA. Data are mean values ± SEM (n = 7), One-way ANOVA with Tukey's multiple comparison test.

4.5.2 Total pancreatic insulin content of D1KO mice

In young mice the course of absolute plasma insulin levels after glucose administration was unchanged between D1KO and WT mice. Similar to the demonstrated *ex vivo* data on isolated islets, here, total pancreatic insulin content was measured in pancreases from *Tbc1d1*-deficient mice according to 3.3.3. The amount of insulin was normalized to the amount of protein in the same sample.

Total pancreatic insulin content was not different between D1KO and WT mice (9.3 ± 1.1 µg/mg protein in WT mice vs. 9.6 ± 1.0 µg/mg protein in D1KO mice; n=6) as shown in Figure 20C. Importantly also the amount of insulin (Fig. 20A) and total protein (Fig. 20B) per pancreas were unchanged (62.7 ± 5.8 µg insulin in WT vs. 73.0 ± 4.7 µg insulin in D1KO and 6.9 ± 0.4 mg protein in WT vs. 7.8 ± 0.4 mg protein in D1KO).

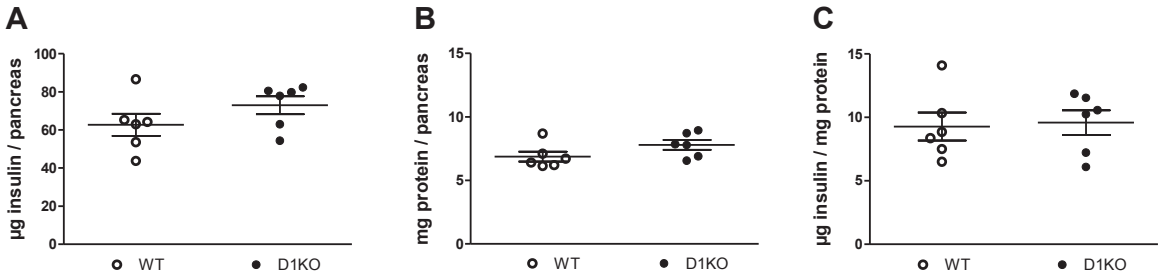

Figure 20: Total pancreatic insulin content from D1KO mice. The snap frozen pancreas was homogenized in acid ethanol. Insulin was measured with ELISA and protein amount was measured with BCA assay. **(A)** Amount of insulin per pancreas in D1KO and WT mice. **(B)** Amount of protein per pancreas in D1KO and WT mice. **(C)** Amount of insulin per mg protein. Data are mean values ± SEM (n = 6), Student's t-test, two-tailed, unpaired.

4.6 Islet morphometry and β-cell insulin granules from *Tbc1d1*-deficient mice

The following data of the histologic and morphometric analysis were gained in collaboration with Carmen Weidlich, Dr. Jürgen Weiß and Kay Jeruschke.

4.6.1 Basic morphology

After HE staining of the pancreas sections the islet structures could be well distinguished from the exocrine cells of the pancreas as indicated by arrows in Figure 21. Without applying

quantitative measures the basic morphology of the islets seemed to be the same in both, WT and D1KO mice. Most of the islets were localized around the main pancreatic duct and in the tail of the pancreas.

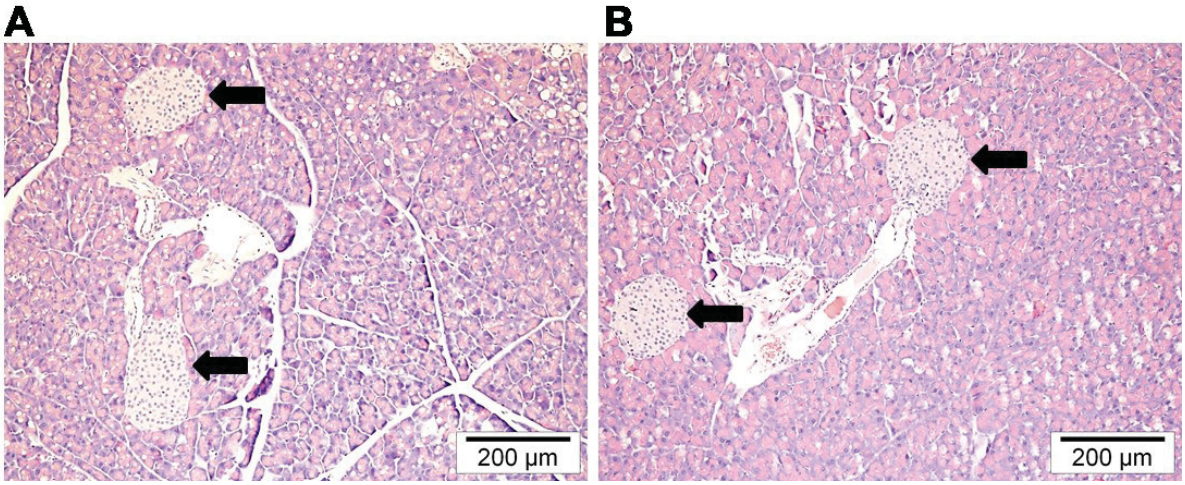

Figure 21: Pancreas sections of D1KO and WT mice stained with HE. Organization of exocrine and endocrine cells in pancreas sections of **(A)** WT mice and **(B)** D1KO mice. Islets can be distinguished from the exocrine cells by the staining and by the borderline peri-insular basement membrane. Arrows indicate islets of Langerhans. Scale bar = 200 µm

4.6.2 Morphometry

After analyzing three animals per genotype there were no differences found in any of the measured parameters between WT and D1KO mice. The pancreas area, measured by point counting (3.4.5) was 53.26 ± 3.07 mm² in WT vs. 53.88 ± 2.74 mm² in D1KO mice (Fig. 22A). In all of the analyzed sections every islet was counted and the islet area was measured. The amount of islets in the wildtype mice were 738.3 ± 121.3 vs. 718.0 ± 52.3 in D1KO mice (Fig. 22B). When normalizing the amount of islets to the pancreas area also no differences were found as shown in Figure 22C (0.74 ± 0.02 islets/mm² pancreas in WT vs. 0.75 ± 0.04 islets/mm² pancreas in D1KO mice). The portion of the pancreas area that was covered with islets, analyzed for each slide individually and summed up was expressed as percentage. Figure 22D showed no differences between the genotypes (0.51 ± 0.01 % in WT vs. 0.54 ± 0.08 % in D1KO mice). In addition the amount of islets of different areas as percentage of the total islet area was compared between WT and D1KO mice (Fig. 22E). In summary there were no big changes between the genotypes. Statistical analysis with two-tailed, unpaired student's t-test showed only significant differences between the genotypes in the area cluster 1000-1500 µm² ($p = 0.030$) and 8500-9000 µm² ($p = 0.046$). While there were less islets of

1000-1500 µm² in D1KO mice compared to WT the opposite was seen with the 8500-9000 µm² islets.

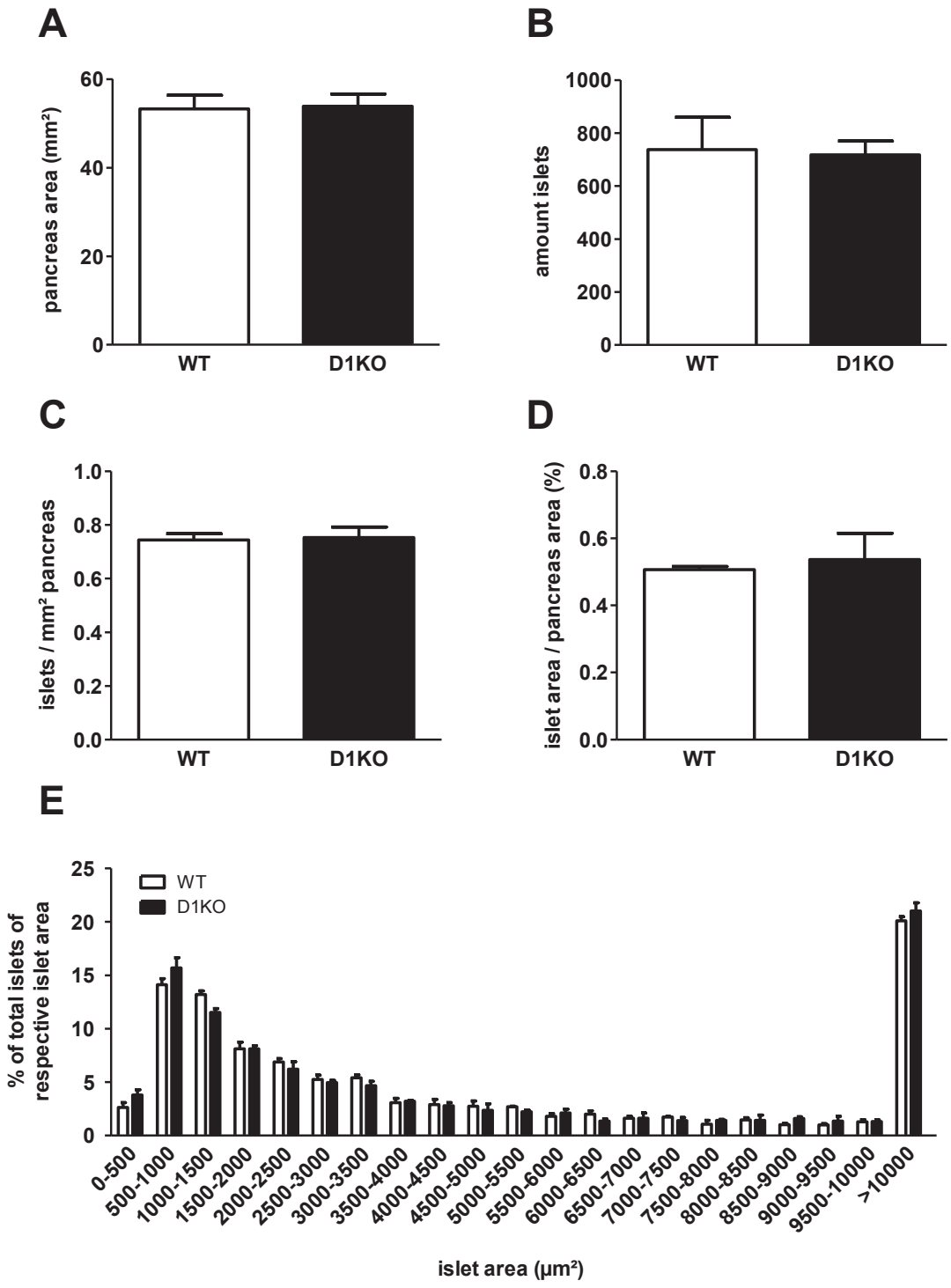

Figure 22: Morphometric analysis of islets from D1KO mice. Pancreas from D1KO mice was dissected and H/E-stained slices of formalin-fixed and paraffin embedded pancreas were analyzed for **(A)** pancreas area by point counting, **(B)** amount of islets, **(C)** amount of islets per mm² pancreas and **(D)** % of islet area per pancreas area. **(E)** Islet sizes of different size clusters show the same distribution within the pancreas in both, WT and D1KO mice. Data are mean values ± SEM (n = 3 with 14-21 sections per n).

4.6.3 Ultrastructure of D1KO islets

The perifusion experiment demonstrated that both, first and second phase of insulin secretion were increased in isolated islets of D1KO mice. To investigate whether this might be due to a change in insulin granule dynamics transmission electron microscopy was used to visualize and analyze insulin granules of single β-cells in isolated islets of D1KO and WT mice. Therefore, islets were isolated and regenerated overnight. After incubation for one hour with either 2 mM or 25 mM glucose the islets were fixed with glutaraldehyde and ultrathin sections were picked onto Formvarcarbon-coated grids to view in the transmission electron microscope (3.4.7). Single β-cells of the islets were identified and the area of the cells was measured. The secretory granules that contained readily processed and condensed insulin were identified with a threshold analysis of gray scales and therefore distinguished from the pale granules that contain precursor forms of insulin. Those granules were identified and counted manually. The amount of both types of insulin granules was normalized to the respective β-cell area. As shown in Figure 23A the density of dark insulin granule was significantly increased in β-cells of D1KO islets after 25 mM glucose compared to WT islets with glucose stimulation (1.388 ± 0.042 in WT vs. 1.608 ± 0.177 dark granules/β-cell area in D1KO, $p < 0.05$). Dark insulin granule density did not differ in D1KO cells between 2 mM and 25 mM glucose stimulation. In contrast, dark insulin granule density significantly decreased in WT cells after 25 mM glucose stimulation compared to 2 mM glucose (1.756 ± 0.105 at 2 mM glucose vs. 1.388 ± 0.042 dark granules/β-cell area at 25 mM glucose, $p < 0.001$). As shown in Figure 23B, pale insulin granule density was significantly increased in D1KO cells compared to WT cells after 25 mM glucose stimulation (0.066 ± 0.009 in WT vs. 0.088 ± 0.022 pale granules/β-cell area in D1KO, $p < 0.05$).

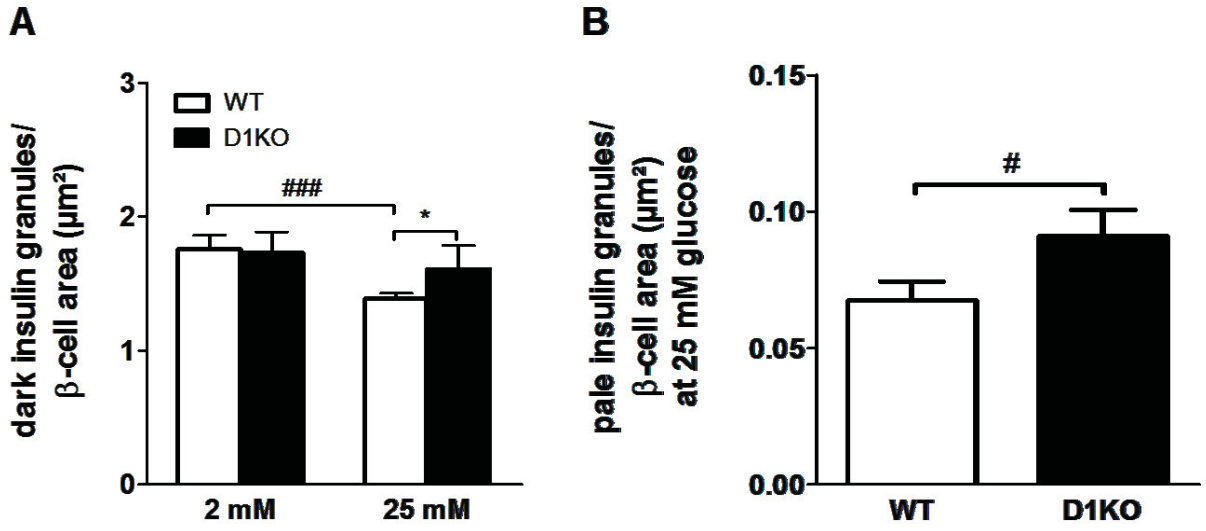

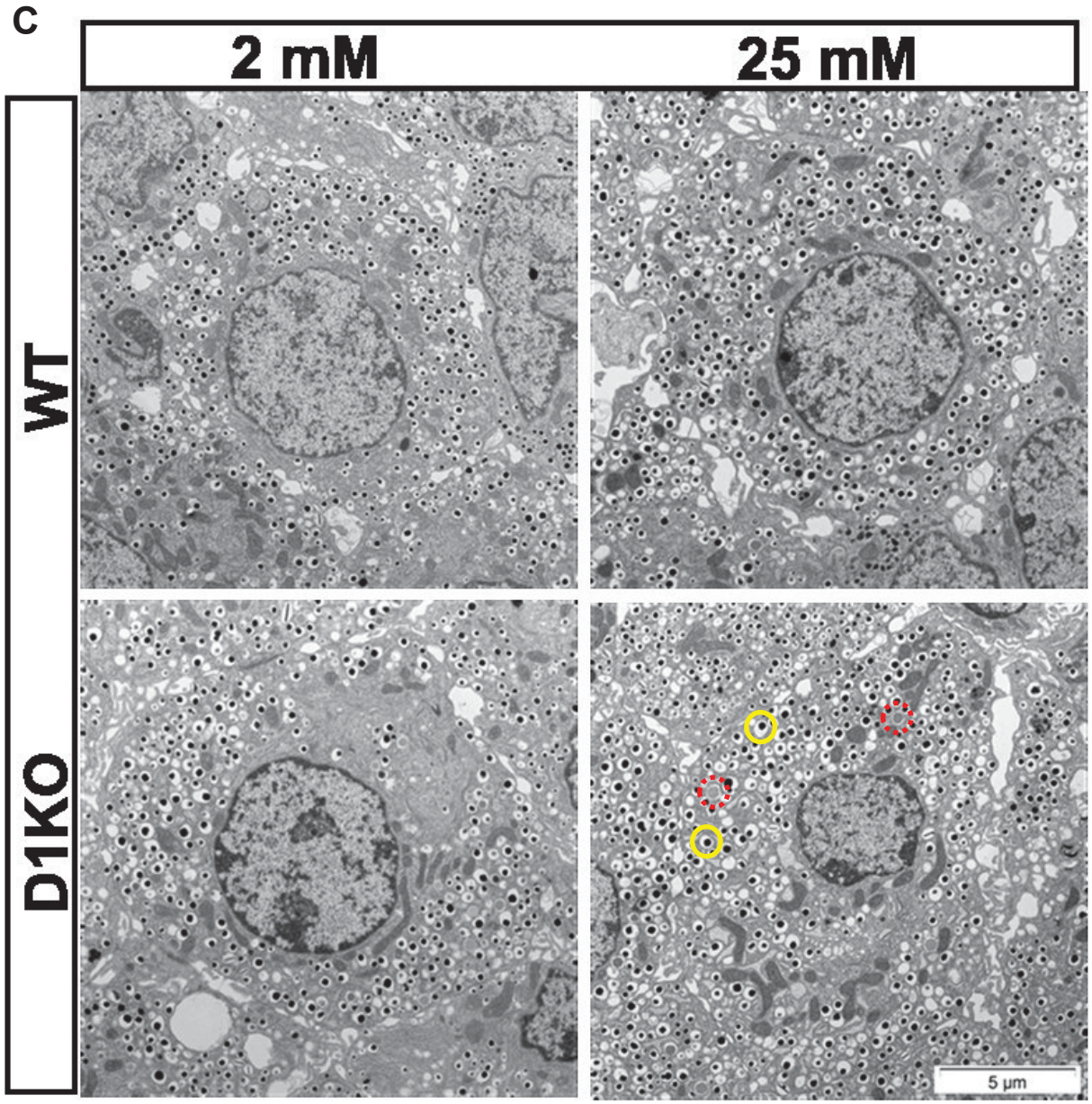

Figure 23: Density of insulin granules in β-cells of WT and D1KO islets with or without glucose stimulation. Pancreatic islets of three different mice per genotype were isolated and regenerated overnight. After rejection of necrotic islets all islets per genotype were pooled. After 1 h stimulation with 2 mM or 25 mM glucose islets were fixed in 2.5 % glutaraldehyde and prepared for transmission electron microscopy. **(A)** Granules with readily processed insulin were identified by gray scale threshold analysis and the amount of dark granules was referred to the β-cell area (µm²). Data are mean values ± SD from 10 β-cells of 3-5 different islets per condition, respectively. Two-way ANOVA with Bonferroni post-hoc-test. * $p < 0.05$. Student's t-test, two-tailed, unpaired, ### $p < 0.001$. **(B)** Pale granules were identified and counted manually and the amount was referred to the β-cell area (µm²). Data are mean values ± SD from 10 β-cells of 4-5 different islets, respectively. Student's t-test, two-tailed, unpaired, # $p < 0.05$. **(C)** TEM images of WT and D1KO β-cells after 2 mM or 25 mM glucose stimulation with insulin containing granules. The red dotted circles indicate pale granules, the yellow closed circles indicate dark granules. Islets of WT and D1KO mice, respectively, were treated with 2 mM versus 25 mM glucose for 60 min. Bar (5 µm) fits to all images.

4.7 Gene expression analysis

Basic islet histology and morphometry was not altered in pancreatic sections of both WT and D1KO mice. However, insulin granule density was increased in β-cells of isolated islets of D1KO mice after 25 mM glucose stimulation compared to WT littermates. To further characterize islet-cell identity and dedifferentiation, as well as insulin exocytosis mechanisms a panel of various genes were analyzed by qPCR in islets of both genotypes.

4.7.1 Expression of genes that confer islet-cell identity and dedifferentiation

A panel of genes that mediate basic cell function or dedifferentiation of islets was analyzed by qPCR (Fig. 24). Interestingly isolated islets of D1KO mice expressed 50 % less *Mafa* mRNA compared to islets of WT mice (1.06 ± 0.14 in WT vs. 0.53 ± 0.09 in D1KO; p = 0.0019). *Mafa* is a key transcription factor for the insulin gene that is exclusively expressed in β-cells of adult islets [185]. In contrast, *Mafb* that is exclusively expressed in adult α-cells was not differentially expressed between islets of both genotypes (1.02 ± 0.09 in WT vs. 1.18 ± 0.17 in D1KO). In accordance with the decreased *Mafa* mRNA in D1KO islets also the expression of the insulin 2 (*Ins2*) gene was slightly repressed in D1KO islets, although not significantly (1.02 ± 0.09 in WT vs. 0.85 ± 0.05 in D1KO; p = 0.195). The pancreatic and duodenal homeobox protein Pdx1 is a transcription factor that is necessary for the development of the entire pancreas but also for β-cells within the islets [186]. Together with FoxA2 and Nkx2.2 Pdx1 regulates MafA expression in islet β-cells [187]. Although *Mafa* mRNA abundance was significantly lower in D1KO islets *Pdx1* mRNA was unchanged (1.01 ± 0.05 in WT vs. 0.91 ± 0.06 in D1KO). Neurogenin3 (*Ngn3*) is a marker that is expressed in β-cell progenitor-like cells and is associated with dedifferentiation of pancreatic β-cells in diabetic β-cell failure [188]. *Ngn3* mRNA expression was also unchanged between islets of WT and D1KO mice (1.02 ± 0.08 in WT vs. 1.06 ± 0.09 in D1KO).

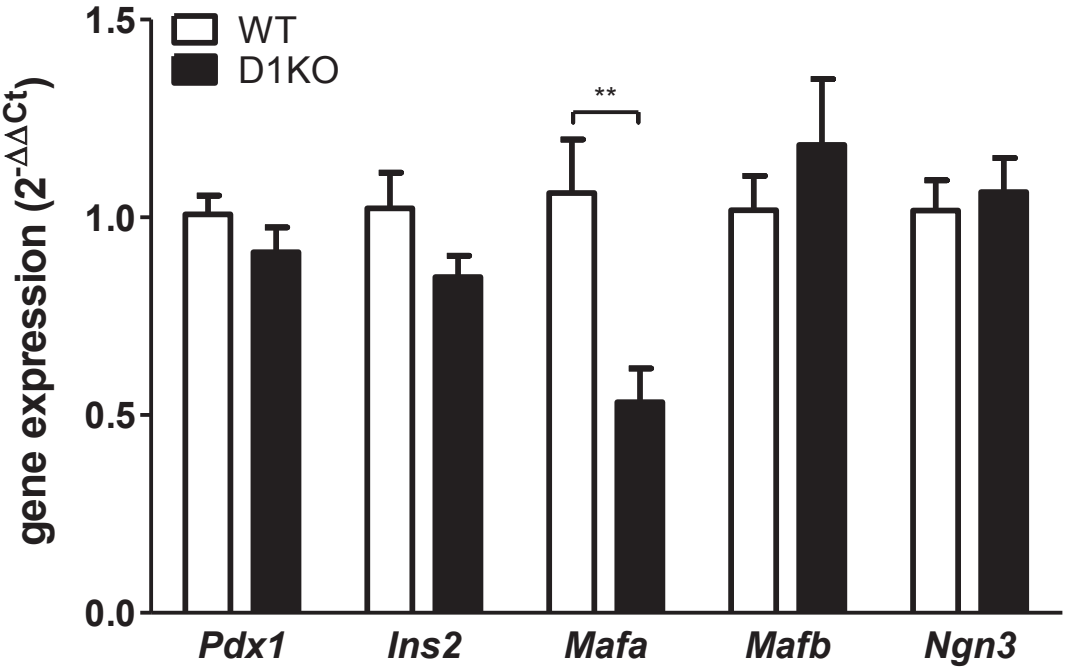

Figure 24: Expression of genes that confer islet cell identity and dedifferentiation. Relative mRNA expression of *Pdx1*, *Ins2*, *Mafa*, *Mafb* and *Ngn3* from isolated islets of D1KO mice compared to WT mice in reference to *36b4* mRNA expression. Data are mean values ± SEM (n = 7-8), Mann-Whitney-U test, two-tailed, ** p < 0.01. *Pdx1* - pancreatic and duodenal homeobox protein 1, *Ins2* – Insulin 2, *Maf* - v-maf musculoaponeurotic fibrosarcoma oncogene family, protein, *Ngn3* – Neurogenin

4.7.2 Gene expression of *Rab27a* and *Tbc1d10a*

It has been shown previously that Rab27A is an important regulator of insulin vesicle translocation [132-134]. In pancreatic acinar cells and in melanosomes the protein EPI64 was shown to be the RabGAP for Rab27 that hydrolyzes Rab27-GTP [137-139]. The expression of both genes was measured by qPCR (3.2.7). No significant differences were found in mRNA expression of both genes (Fig. 25A). *Tbc1d10a* expression in D1KO islets was slightly increased compared to WT islets (1.005 ± 0.037 in WT vs. 1.093 ± 0.044 in D1KO; p = 0.152). In line with the mRNA expression also protein expression of Rab27A in isolated islets was unchanged between WT and D1KO mice (Fig. 25B).

4.7.3 Expression of SNARE genes

Beside the genes responsible for the regulation of vesicle translocation another set of important exocytosis genes control different steps in tethering, docking and fusion of the vesicles. These so called SNARE (Soluble N-ethylmaleimide-sensitive factor attachment protein receptor) genes mainly comprise genes encoding syntaxin-1a (*Stx1a*), synaptobrevin-2 (*Vamp2* – vesicle-associated membrane protein) and synaptosomal-associated protein 25 (*Snap25*) [85]. Syntaxin-1a interacts with VAMP2 and SNAP25 to enable tethering and fusion of the vesicles with the plasma membrane [189]. After measuring relative mRNA expression none of the mentioned genes were differentially expressed between islets of D1KO and WT mice (Fig. 25A). Although *Vamp2* expression in D1KO islets seemed less that in WT islets, the calculated p-value by Mann-Whitney-U test was 0.235 (n = 8).

4.7.4 Expression of other insulin secretion genes

Insulin vesicles contain numerous proteins that play a role in the regulated exocytosis of insulin from pancreatic β-cells. Amongst all the genes *Dnajc5*, *Prkcb*, *Sytl4, Snca, Irs1 and Irs2* were chosen for analysis. *Dnajc5* encodes a protein called cysteine-string protein α (CSPα). This is a DnaJ homologue that shows guanine nucleotide exchange activity for G_α proteins [190] and has been shown to regulate insulin exocytosis via interaction with syntaxin-1a [89, 191]. *Prkcb* encodes the protein kinase C-β (PKCβ) that has been implicated in Ca^{2+}-mediated regulation of insulin release [192, 193]. *Sytl4* (synaptotagmin-like 4) encodes for granuphilin and has been shown to interact with Rab27A to regulate insulin secretion [132]. *Snca* encodes the protein α-synuclein. Binding of α-synuclein to the K^+-ATP channel has been demonstrated to inhibit insulin secretion [194]. *Irs1* and *Irs2* as components of the insulin signaling pathway have been linked to insulin secretion and synthesis as well [195, 196]. Expression analysis showed no changes in mRNA expression of most of the genes between D1KO and WT islets (Fig. 25A). *Dnajc5* mRNA was significantly increased by approx. 20 % in islets of D1KO mice (1.007 ± 0.044 in WT vs. 1.206 ± 0.045 in D1KO; p = 0.007). In contrast, the corresponding protein CSPα was not differentially expressed between the genotypes (Fig. 25B). Expression of *Sytl4* was less in D1KO islets compared to WT islets and showed a clear statistical trend (p = 0.097, n = 8). *Irs2* expression was significantly upregulated in D1KO islets by approx. 30 % (1.015 ± 0.076 in WT vs. 1.325 ± 0.101 in D1KO; p = 0.022), while protein abundance remained unchanged (Fig. 25C).

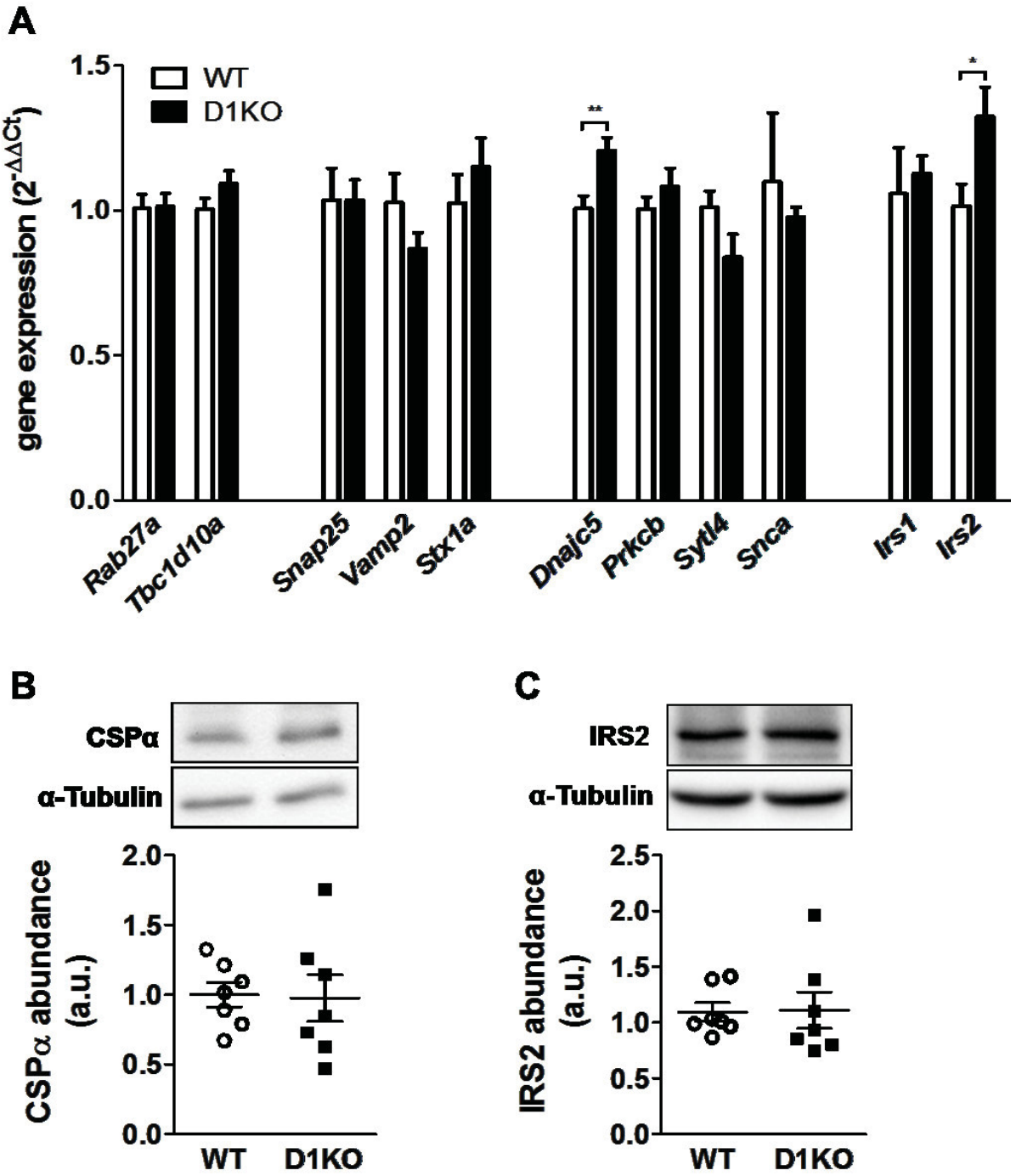

Figure 25: Expression of genes encoding different proteins that play a role in insulin exocytosis. (A) Relative mRNA expression of the designated genes from isolated islets of D1KO mice compared to WT mice in reference to *36b4* mRNA expression. Data are mean values ± SEM (n = 6-8), Student's t-test, two-tailed, unpaired. ** $p < 0.01$. *Snap25* - Synaptosomal-associated protein 25, *Vamp2* – Vesicle-associated membrane protein 2, *Stx1a* – Syntaxin 1A, *Dnajc5* – DnaJ Heat Shock Protein Family (Hsp40) Member C5, *Prkcb* – Protein Kinase Cβ, *Snca* – Synuclein α, *Irs1* – Insulin receptor substrate 1, *Irs2* – Insulin receptor substrate 2 **(B)** Relative CSPα protein abundance from isolated islets of D1KO mice compared to WT mice in reference to α-Tubulin. Primary CSPα and α-Tubulin antibodies were diluted 1:1000, respectively. Data are mean values ± SEM (n = 7). **(C)** Relative IRS2 protein abundance from isolated islets of D1KO mice compared to WT mice in reference to α-Tubulin. Primary IRS2 antibody was diluted 1:500, α-Tubulin antibody was diluted 1:2000. Data are mean values ± SEM (n = 7).

4.8 Manipulation of the triggering pathway of insulin secretion in D1KO islets

Isolated islets of *Tbc1d1*-deficient mice secrete more insulin upon glucose stimulation compared to islets of the respective wildtype mice. This increase could neither be attributed to morphometric changes (4.6) nor changes in total pancreatic and islet insulin content (4.5). Moreover, the effect that was observed in isolated islets *ex vivo* was not clearly seen in the entire organism *in vivo* (4.4). The results of the perifusion showed that both insulin secretion phases were increased (Fig. 16). Therefore, a mechanistic and pharmacologic approach aiming to investigate or manipulate insulin secretion at different steps of the triggering pathway of insulin secretion (Fig. 3) was initiated.

4.8.1 Protein abundance of GLUT2

Insulin secretion is initially triggered by the uptake of glucose into the β-cells via GLUT2 in mice. Therefore GLUT2 protein abundance was measured in isolated islets of both genotypes in comparison to the reference protein β-actin. With seven individual samples per genotype no expression differences were found after quantification (Fig. 26: 0.96 ± 0.10 in WT vs. 1.08 ± 0.07 in D1KO). As illustrated, expression of GLUT2 showed higher variability than expression of β-actin.

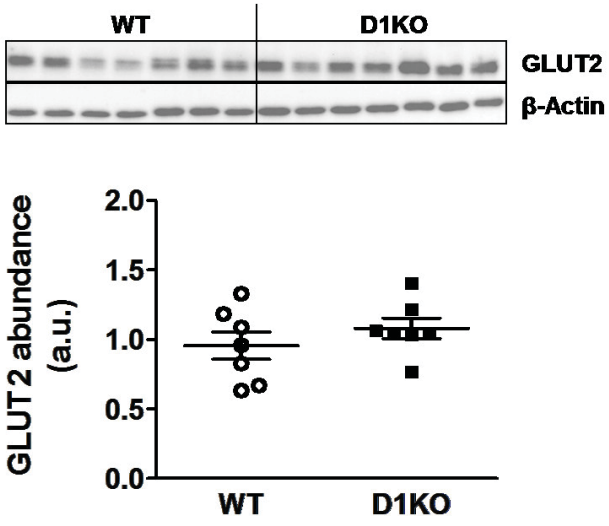

Figure 26: GLUT2 protein abundance from isolated islets of D1KO mice. Protein abundance of GLUT2 in islets of D1KO mice compared to controls. Primary GLUT2 antibody was diluted 1:1000. Primary β-actin antibody was diluted 1:1000.Expression was normalized to β-actin and quantified. Data are mean values ± SEM (n = 7), Mann-Whitney-U test, two-tailed.

4.8.2 Potentiation of insulin secretion by glibenclamide

Glibenclamide is a pharmacologic substance belonging to the group of sulfonylureas. As such it binds the sulfonylurea receptor at the intracellular SUR1 subunit of ATP-sensitive K^+-channels in pancreatic β-cells to block potassium flux and to induce insulin secretion [71]. Due to this mechanism glibenclamide does not require glucose for its efficacy. Previously, an increase in insulin secretion could be seen at both, basal (2 mM) and stimulated (20 mM) glucose concentrations with 1 µM glibenclamide [79]. After performing the GSIS assay according to the Glibenclamide protocol (3.3.5, Fig. 8) potentiation of insulin secretion at 2 mM glucose with 1 µM glibenclamide was significantly higher in islets of D1KO mice compared to wildtype littermates (154.4 ± 10.4 pg/islet/60 min in WT vs. 229.1 ± 13.8 pg/islet/60 min in D1KO; $p = 0.0012$). Supplementation of 25 mM glucose with 1 µM glibenclamide led to a pronounced increase in insulin secretion only in WT (425.8 ± 47.6 pg/islet/60 min without glibenclamide vs. 573.2 ± 54.6 pg/islet/60 min with glibenclamide; $p = 0.065$) but not in D1KO islets (789.6 ± 41.9 pg/islet/60 min without glibenclamide vs. 865.0 ± 57.2 pg/islet/60 min with glibenclamide; $p = 0.311$) The potentiating effect of *Tbc1d1*-deficiency on insulin secretion at 25 mM glucose was observed with (573.2 ± 54.6 pg/islet/60 min in WT vs. 865.0 ± 57.2 pg/islet/60 min in D1KO; $p < 0.001$) or without (425.8 ± 47.6 pg/islet/60 min in WT vs. 789.6 ± 41.9 pg/islet/60 min in D1KO; $p < 0.001$) addition of glibenclamide (Fig. 27).

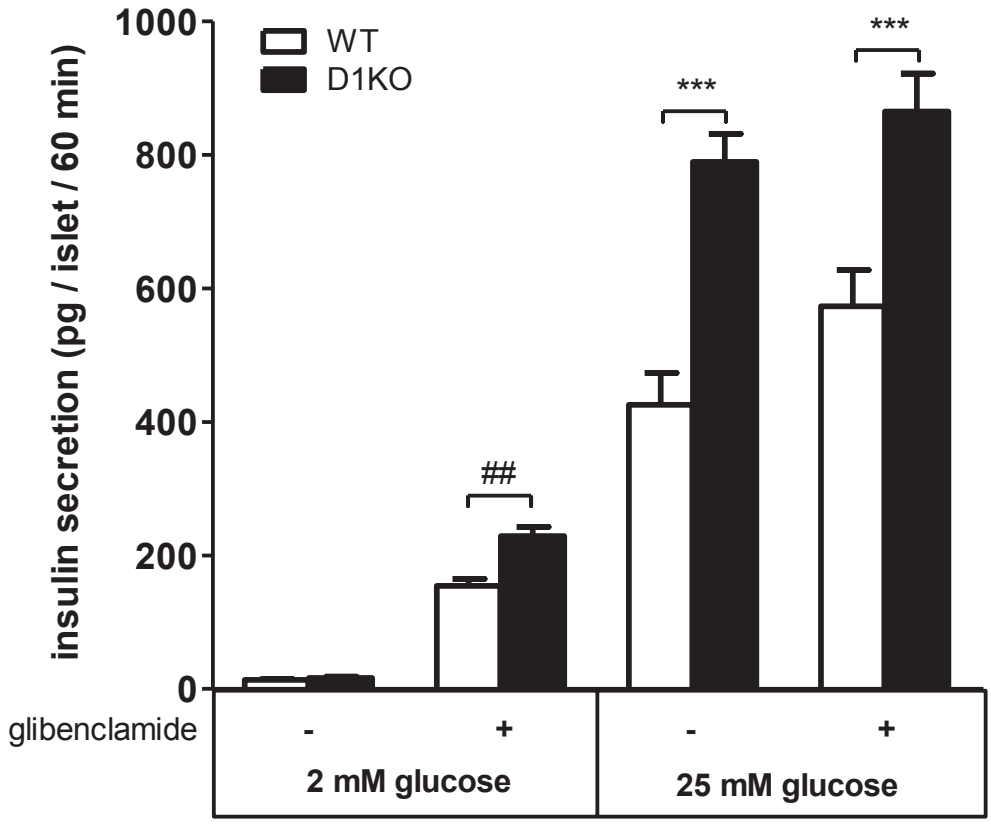

Figure 27: GSIS from isolated islets of D1KO mice with or without 1 µM glibenclamide. Isolated islets of D1KO mice were incubated with 2 mM and 25 mM glucose, with or without 1 µM glibenclamide (solubilized in DMSO) for 1 h at 37 °C and secreted insulin in the supernatants was measured with ELISA. Data are mean values ± SEM (n = 7), two-way ANOVA with Bonferroni post-hoc-test. *** $p < 0.001$; Student's t-test, two-tailed, unpaired. ## $p < 0.01$.

4.8.3 KCl-induced insulin secretion

Exposure of isolated islets to high concentrations of K^+ ions leads to a rapid increase in β-cell depolarization and mimics the closure of K^+-ATP channels [72]. This results in insulin secretion also in the absence of stimulatory glucose concentrations. For the following result the KCl protocol (3.3.5, Fig. 8) was applied. As shown in Figure 28 insulin secretion at 2 mM glucose was substantially potentiated after 60 min with 30 mM KCl in islets of both genotypes (500.6 ±60.9 pg/islet/60 min in WT vs. 558.1 ± 45.4 pg/islet/60 min in D1KO). Potentiation was approx. five times higher than stimulation with 25 mM glucose (compared to Figure 9). Differences in the KCl-induced potentiation fold were not observed between the genotypes.

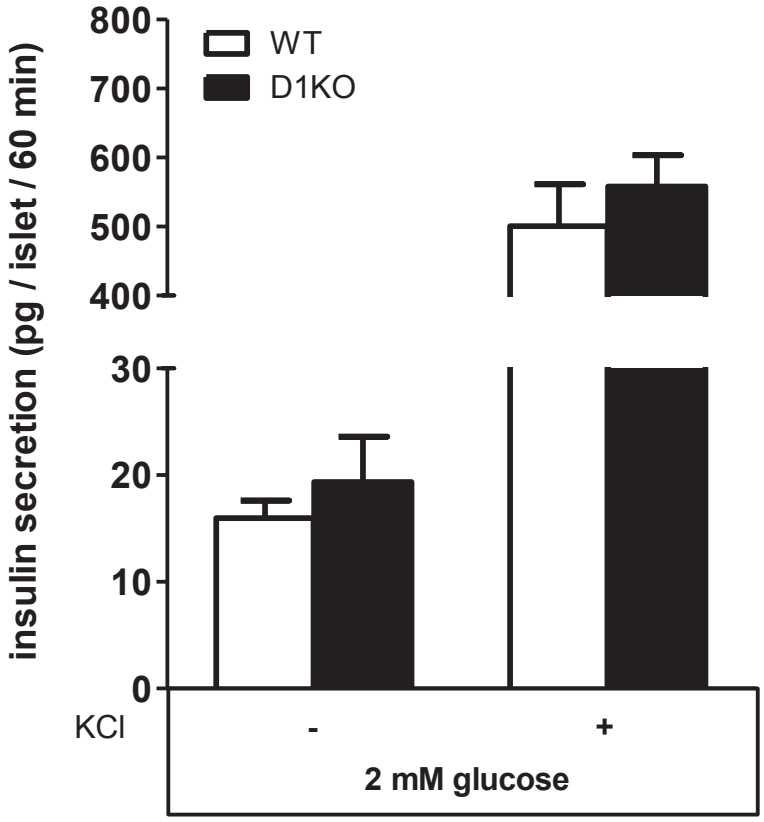

Figure 28: Insulin secretion from isolated islets of D1KO mice induced by 30 mM KCl. Isolated islets of D1KO mice were incubated with 2 mM glucose, with or without 30 mM KCl for 1 h at 37 °C and secreted insulin in the supernatants was measured with ELISA. Data are mean values ± SEM (n = 5), Mann-Whitney-U-test, two-tailed.

4.8.4 Ca^{2+}-ionophore A23187-induced insulin secretion

In the triggering insulin secretion pathway the voltage-dependent L-type Ca^{2+} channel is downstream of the K^+-ATP channel (Fig. 3). Membrane depolarization due to the closure of K^+-ATP channels mediates the opening of the Ca^{2+} channel. The resulting influx of Ca^{2+} ions into the cell triggers insulin exocytosis. To initiate Ca^{2+}-mediated insulin release without increasing the membrane potential, the ionophore A23187 was introduced into the cell membrane [73]. This ionophore is highly selective for Ca^{2+} to increase intracellular Ca^{2+} concentrations [197, 198]. 5 µM A23187 were shown to significantly increase insulin secretion in cultured INS-1 cells under basal glucose conditions by approx. 2-fold after 15 min [199]. Insulin secretion at 2 mM glucose was also moderately potentiated with 5 µM A23187 approx. 2-fold after 60 min when applying the A23187 protocol (3.3.5, Fig. 8) in islets of both geno-

types (Fig. 29). Differences in the A23187-induced potentiation fold were not observed between the genotypes.

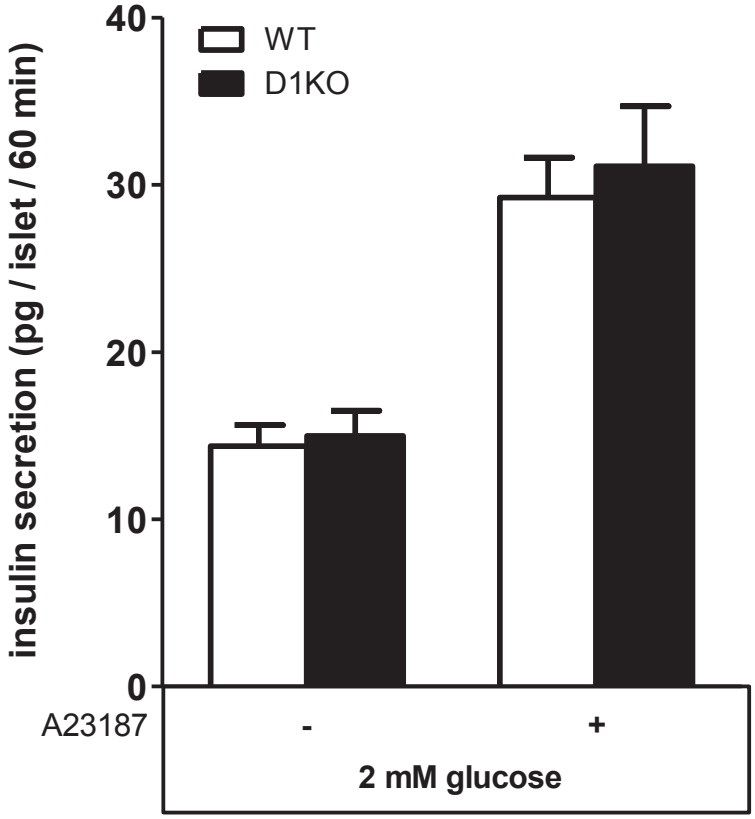

Figure 29: Insulin secretion from isolated islets of D1KO mice induced by 5 µM Ca^{2+}-ionophore A23187. Isolated islets of D1KO mice were incubated with 2 mM glucose, with or without 5 µM A23187 for 1 h at 37 °C and secreted insulin in the supernatants was measured with ELISA. Data are mean values ± SEM (n = 6), Mann-Whitney-U-test, two-tailed.

4.8.5 Perifusion of isolated islets with tolbutamide and KCl

The pharmacologic approach in the static insulin secretion assay demonstrated an increase in glibenclamide-stimulated insulin secretion at basal glucose levels upon *Tbc1d1*-deficiency. By manipulating further downstream targets in the triggering pathway insulin secretion showed no differences between WT and D1KO islets. To validate these results, another sulfonylurea, tolbutamide, and KCl were applied in a perifusion experiment at 5 mM basal glucose, according to the same settings already explained in 4.3.3.

Insulin secretion under basal conditions was determined with 5 mM glucose for approx. 30 min with a subsequent addition of 500 µM tolbutamide. 30 min after tolbutamide addition 40

mM KCl were added for another 10 min and finally removed again. The data were expressed as % insulin secretion of the value at 60 min.

As shown in Figure 30A basal insulin secretion was already different between WT and D1KO islets. Islets of WT mice showed only minor changes in insulin secretion up to 60 minutes (maximum 133.48 ± 36.45 %) whereas islets of D1KO showed a straighter decline of insulin secretion from the beginning of the test up to 60 min (maximum 196.28 ± 23.11 %). Directly after addition of 500 µM tolbutamide, insulin secretion of WT islets increased only moderately (maximum 193.44 ± 35.21 %) and fell down to baseline rapidly. Islets of D1KO mice showed a greater insulin response to tolbutamide. Directly after stimulation insulin secretion of D1KO islets increased to a maximum of 356.61 ± 94.92 % in minute 66. Insulin secretion rate fell down initially to approx. 210 % and later down to 132 % at minute 90. The addition of KCl led again to a sudden rise in insulin secretion to a maximum of approx. 445 % in both genotypes. The secretion rate of WT islets again fell down faster compared to D1KO islets. After returning to basal glucose with tolbutamide at minute 100, insulin secretion increased shortly in both genotypes. The measurement of the area under the curve (AUC) between 60 and 90 minutes as the first time of tolbutamide stimulation showed a significantly increased area for the D1KO islets (Fig. 30B). In contrast, the AUC between 90 and 100 minutes as the time for KCl stimulation is not different between the genotypes.

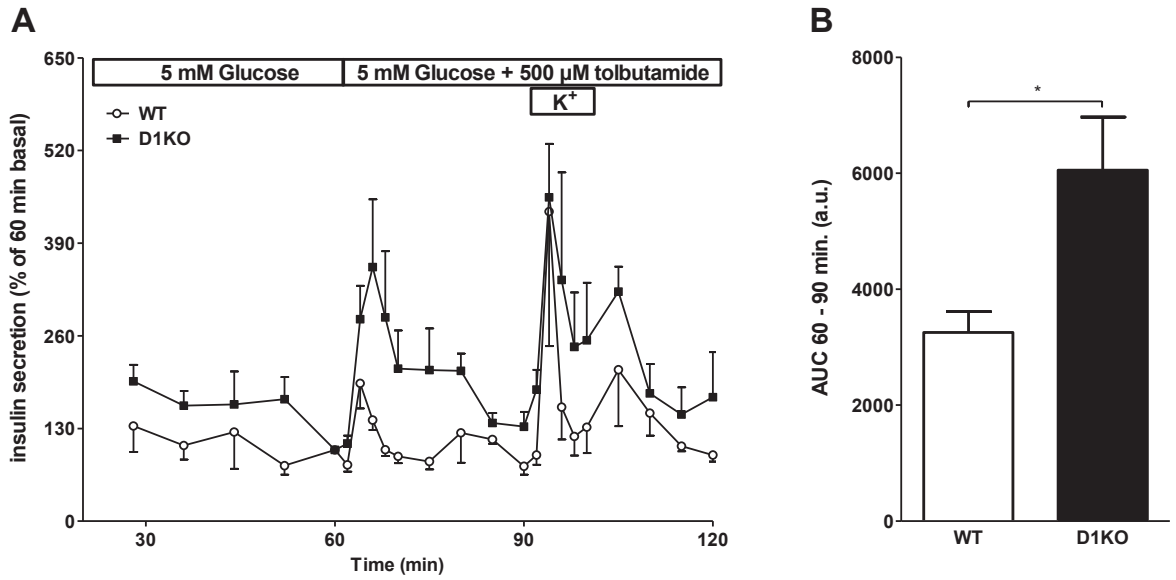

Figure 30: Dynamic secretagogue-stimulated insulin secretion in isolated islets of D1KO mice. (A) 50 islets per genotype were perifused in a custom-made perifusion chamber with 5 mM glucose and together with 500 µM tolbutamide and 40 mM KCl for the designated time points. Insulin from the eluate fractions was measured with ELISA and the values are expressed as percentage of the secretion rate at the end of the basal glucose period. Data are mean values ± SEM (n = 5). **(B)** Area under the curve (AUC) between 60 and 90 minutes for Tolbutamide stimulation. Data are mean values ± SEM (n = 5). Student's t-test, two-tailed, unpaired, * $p < 0.05$.

4.8.6 Relative gene expression of K^+-ATP-channel subunits

Since insulin secretion was potentiated in D1KO islets by two different sulfonylureas but not with KCl or A23187 the expression of the single subunits composing the ATP-sensitive K^+ channel was analyzed by qPCR (3.2.7). The genes encoding both subunits of the channel, *Kcnj11* (K_{ir}6.2) and *Abcc8* (SUR1) were unchanged in mRNA expression between WT and D1KO islets (Fig. 31).

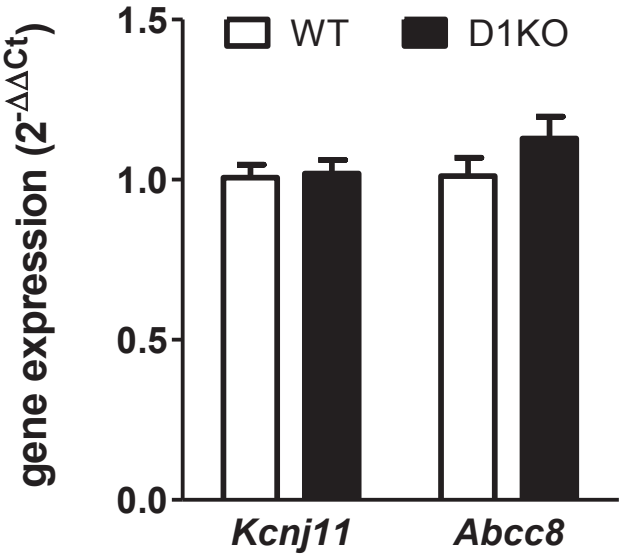

Figure 31: Expression of genes encoding the subunits of ATP-sensitive K^+ channel. Relative mRNA expression of *Kcnj11* (K_{ir}6.2) and *Abcc8* (SUR1) from isolated islets of D1KO mice compared to WT mice in reference to *36b4* mRNA expression. Data are mean values ± SEM (n = 8), Student's t-test, two-tailed, unpaired.

4.8.7 Potentiation of insulin secretion by AICAR

AICAR is a synthetic compound that phosphorylates AMPK. AICAR is converted to the metabolite 5-amino-1-β-D-ribofuranosylimidazole-4-carboxamide-5′-monophosphate (ZMP) that mimics the effect of AMP [60]. Exposure of isolated mouse islets to 0.5 mM AICAR with increasing concentrations of glucose showed a dose-dependent potentiation of insulin secretion upon stimulated glucose concentrations [59]. TBC1D1 is a direct target of AMPK in the skeletal muscle to mediate contraction-induced GLUT4 translocation [155]. Moreover, K^+-ATP channel trafficking was shown to be regulated by AMPK [200, 201], thus the effect of AICAR on insulin secretion in D1KO islets was investigated (AICAR protocol, 3.3.5, Fig. 8). To cover the range of glucose stimulation used in the previously mentioned study [59], 11 mM glucose were chosen for stimulation. Figure 32 shows the results. Insulin secretion at 2

mM glucose was not altered in islets of both genotypes with (9.7 ± 1.3 pg/islet/60 min in WT vs. 13.5 ± 1.6 pg/islet/60 min in D1KO) or without (8.5 ± 1.3 pg/islet/60 min in WT vs. 10.9 ± 0.6 pg/islet/60 min in D1KO) 0.5 mM AICAR application. In D1KO islets insulin secretion was slightly higher compared to wildtype islets, independent of AICAR (120.9 ± 15.7 pg/islet/60 min in WT vs. 168.1 ± 25.9 pg/islet/60 min in D1KO without AICAR and 167.7 ± 22.9 pg/islet/60 min in WT vs. 219.9 ±27.4 pg/islet/60 min in D1KO with AICAR). At 11 mM glucose 0.5 mM AICAR was able to significantly potentiate insulin secretion in both, D1KO (168.1 ± 25.9 pg/islet/60 min without vs. 219.9 ±27.4 pg/islet/60 min with AICAR; p = 0.0019) and WT islets (120.9 ± 15.7 pg/islet/60 min without vs. 167.7 ± 22.9 pg/islet/60 min with AICAR; p = 0.0016) to the same extent. However, *Tbc1d1*-deficiency did not result in a significant increase in insulin secretion at 11 mM glucose with or without AICAR supplementation.

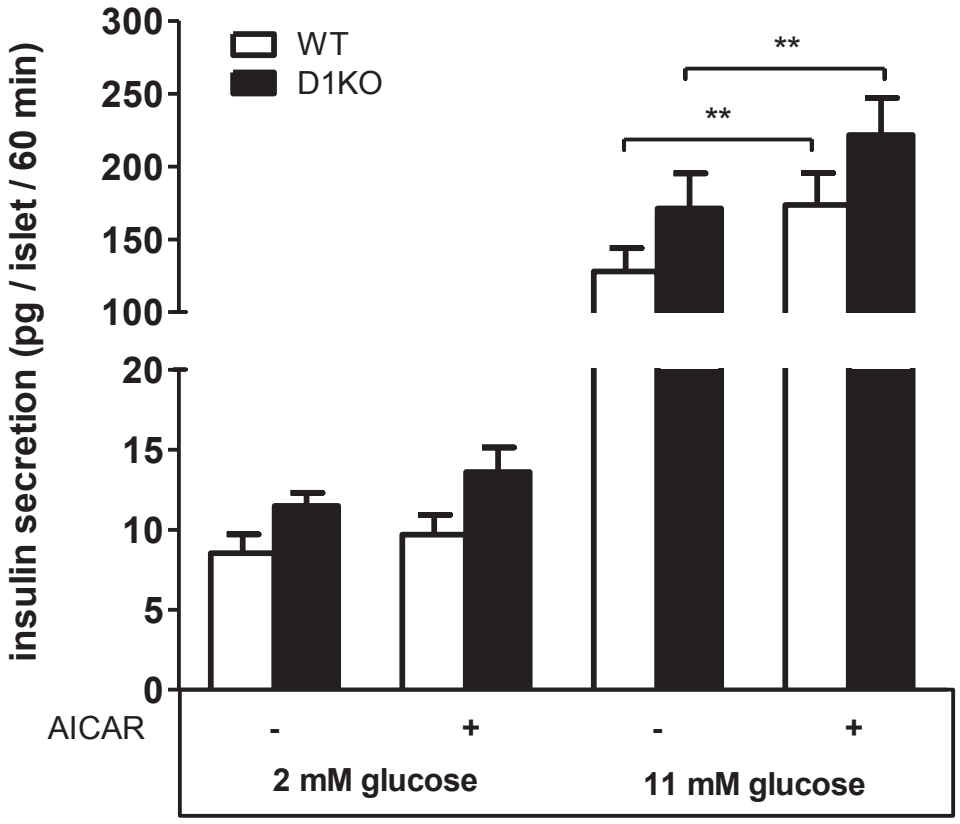

Figure 32: GSIS from isolated islets of D1KO mice with or without 0.5 mM AICAR. Isolated islets of D1KO mice were incubated with 2 mM and 11 mM glucose, with or without 0.5 mM AICAR for 1 h at 37 °C and secreted insulin in the supernatants was measured with ELISA. Data are mean values ± SEM (n = 8), Student's t-test, two-tailed, paired. ** p < 0.01.

4.8.8 GSIS with repetitive glucose stimulation

In a physiologic context glucose stimulation by food intake occurs in a repetitive manner. To more accurately represent the physiologic situation for triggering insulin secretion, a repetitive glucose stimulation of isolated islets for three times was assessed according to the repetitive GSIS protocol (3.3.5, Fig. 8). As demonstrated in Figure 33, *Tbc1d1*-deficiency failed to increase GSIS in the first two stimulations (1.37-fold potentiation in D1KO in the first stimulation and 1.29-fold potentiation in D1KO in the second stimulation) but the third repetitive stimulation with 25 mM glucose showed an increased insulin secretion in D1KO islets compared to WT islets (415.1 ± 44.1 pg/islet/60 min in WT vs. 589.4 ± 69.2 pg/islet/60 min in D1KO, 1.42-fold; $p < 0.05$). Notably, potentiation of insulin secretion after the last stimulation was two times higher in both genotypes compared to the respective genotype after the first stimulation.

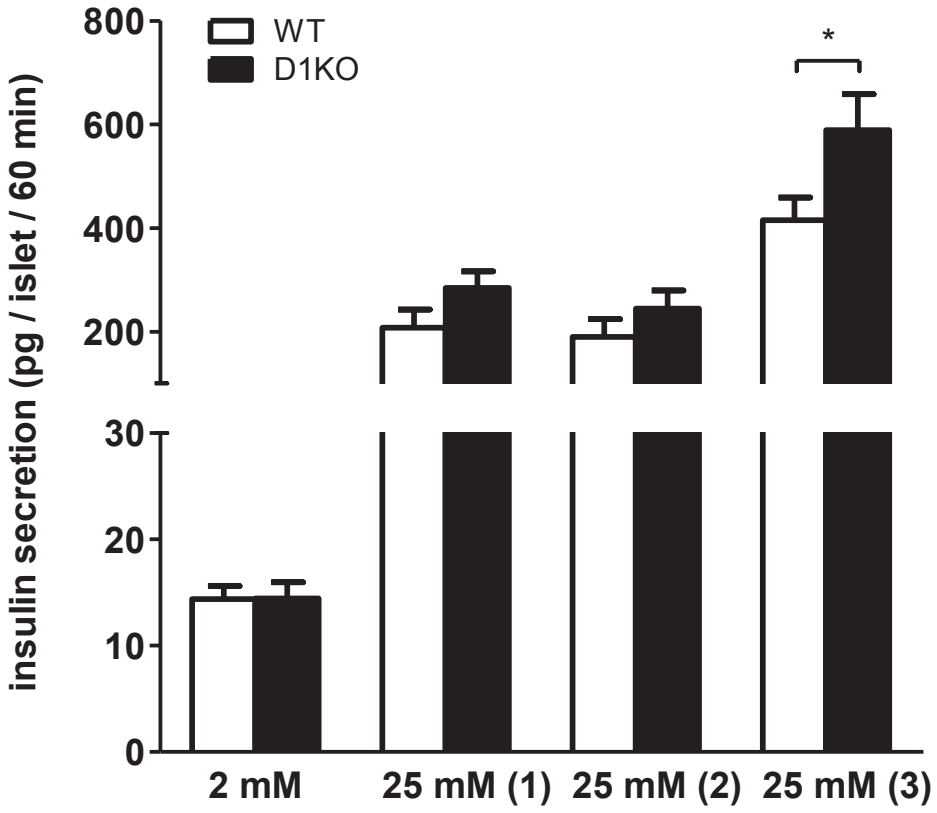

Figure 33: GSIS from isolated islets of D1KO mice after three repetitive glucose stimulations. Isolated islets of D1KO mice were incubated three times with 2 mM and 25 mM glucose, respectively for 1 h at 37 °C and secreted insulin in the supernatants was measured with ELISA. Data are mean values ± SEM (n = 5), two-way ANOVA with Bonferroni post-hoc-test. * $p < 0.05$.

4.9 Static GSIS after acute and chronic exposure to fatty acids

4.9.1 GSIS of islets from D1KO mice after acute exposure to palmitate

It is known from the literature that *Tbc1d1*-deficiency in skeletal muscle and cultured C2C12 myotubes leads to increased fatty acid uptake and oxidation accompanied with decreased glucose uptake and oxidation [156]. To test whether *Tbc1d1*-deficient islets respond differently in insulin secretion upon treatment with fatty acids isolated islets were acutely incubated with 0.3 mM palmitate according to the Palmitate protocol (3.3.5, Fig. 8). From previous work it has already been shown that acute exposure of islets to fatty acids should potentiate glucose-induced insulin secretion without affecting insulin secretion at basal glucose concentrations [56]. Therefore palmitate in this setup was only supplemented to 25 mM glucose. The results (Fig. 34A) showed that no significant differences were found in any of the incubation parameters. Insulin secretion at 2 mM glucose was in the same range as with the previously reported experiments (9.8 ± 1.3 pg/islet/60 min in WT islets vs. 10.9 ± 1.1 pg/islet/60 min in D1KO islets). In contrast to the result in Figure 9 insulin secretion at 25 mM glucose was not different in islets of both genotypes without palmitate (209.9 ± 21.6 pg/islet/60 min in WT islets vs. 206.1 ± 22.1 pg/islet/60 min in D1KO islets). The secreted insulin reached higher amounts compared to the result shown in Figure 9. Supplementation of 25 mM glucose with 0.3 mM palmitate (bound to BSA) effectively boosted insulin secretion approx. 3.5-fold compared to the same conditions without palmitate (714.9 ± 129.9 pg/islet/60 min in WT islets vs. 786.8 ± 226.4 pg/islet/60 min in D1KO islets). However, no differences between the genotypes were observed.

4.9.2 GSIS of islets from D1KO mice after chronic exposure to high-fat diet

Since acute exposure of islets with fatty acids had no influence on genotype-dependent differences in GSIS, mice were chronically fed a HFD for four weeks. Then, islets were isolated and subjected to the basic GSIS protocol (3.3.5, Fig. 8). Previous work showed that chronic exposure of islets to fatty acids decreased insulin secretion performance [53, 55]. In a short pilot study with mice that were fed a HFD for 14 weeks, isolated islets did not meet the quality criteria for a GSIS assay so that the time for HFD-feeding was reduced to four weeks. The results (Fig. 34B) showed a marked decrease in GSIS compared to islets of mice that were fed a standard diet (Fig. 9) but also showed no differences between the genotypes (39.2 ± 4.3 pg/islet/60 min in WT islets vs. 43.1 ± 9.9 pg/islet/60 min in D1KO islets). Insulin secre-

tion at 2 mM glucose was again in the same range as with the previously reported experiments (14.9 ± 3.4 pg/islet/60 min in WT islets vs. 10.7 ± 1.2 pg/islet/60 min in D1KO islets).

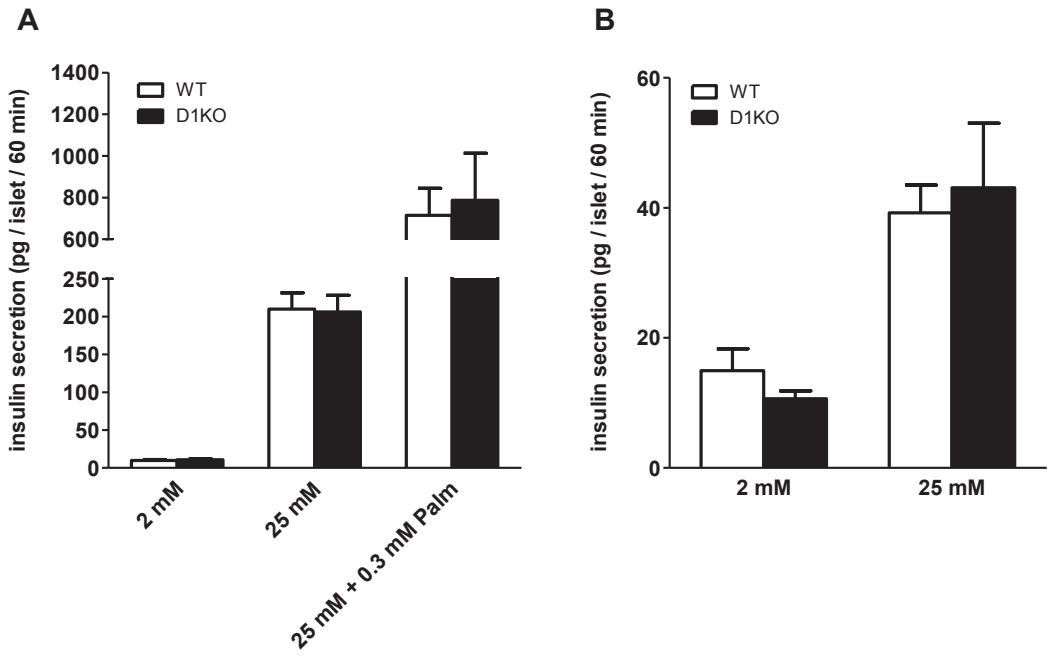

Figure 34: GSIS in isolated islets of D1KO mice with acute or chronic fatty acid exposure. (A) Isolated islets of D1KO mice on standard diet were incubated with 2 mM, 25 mM glucose and 25 mM glucose + 0.3 mM palmitate for 1 h at 37 °C and secreted insulin in the supernatants was measured with ELISA. Data are mean values ± SEM (n = 6). **(B)** Isolated islets of D1KO mice on high-fat diet (4 weeks) were incubated with 2 mM and 25 mM glucose for 1 h at 37 °C and secreted insulin in the supernatants was measured with ELISA. Data are mean values ± SEM (n = 5).

4.9.3 Expression of genes involved in lipid signaling and metabolism in islets

Previous studies have shown that isolated islets of D1KO mice exhibit an increased uptake of radioactively labelled palmitic acid compared to islets of wildtype littermates (Franziska Menzel, PhD thesis). *Tbc1d1* was therefore believed to act as a molecular switch for nutrient preference to use for energy production [156]. To determine, whether the increased fatty acid uptake is due to changes in the expression of fatty acid transporters or other important proteins in lipid metabolism the relative mRNA expression of various genes in WT and D1KO islets was measured. The expression of the G-protein coupled free fatty acid receptors *Ffar1*, *Ffar2*, *Ffar3*, *Gpr119* and *Gpr120*, known for their role in lipid-induced cellular signaling, were not different between WT and D1KO islets (Fig. 35). *Ffar1* shows a trend towards a decreased expression in islets of D1KO mice compared to WT littermates (1.025 ± 0.087 in WT islets vs. 0.868 ± 0.041 in D1KO islets; p = 0.126). No expression differences were also

found for *Cd36*, *Fabp3*, *Fabp5* and *Fatp1* (Fig. 35). Those are genes that are important for cellular but also mitochondrial uptake of fatty acids. Finally the genes *Acadl*, *Pgc1a* and *Cpt1a*, that encode key enzymes and proteins in mitochondrial uptake and oxidation of fatty acids showed no differences between the genotype (Fig. 35).

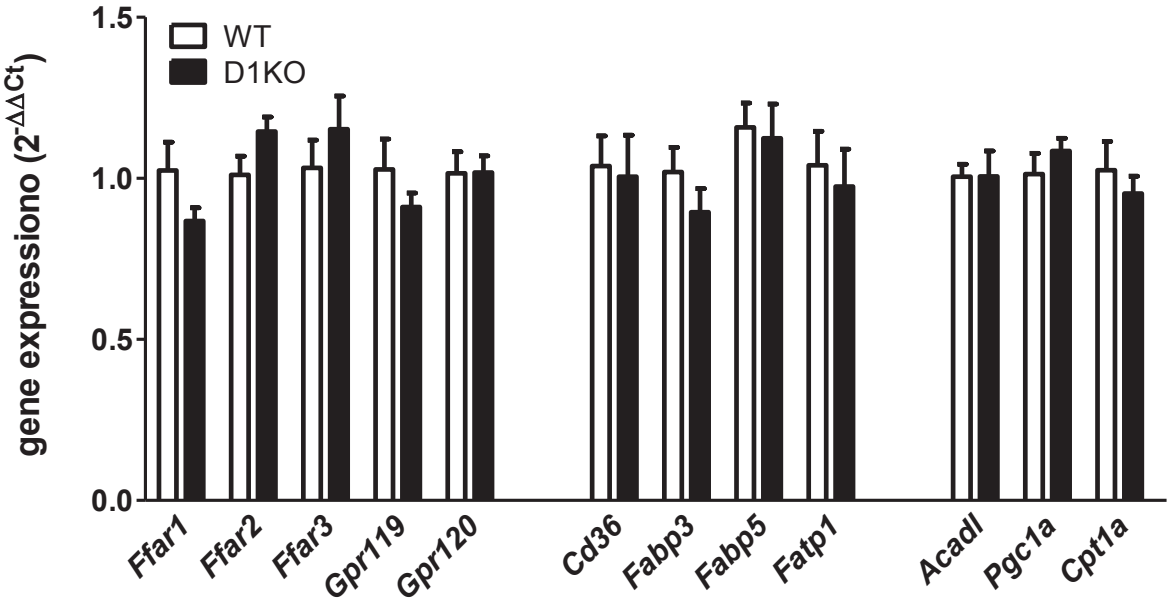

Figure 35: Expression of genes encoding receptors, transporters and key enzymes in islet lipid metabolism. Relative mRNA expression of *Ffar1, Ffar2, Ffar3, Gpr119, Gpr120, Cd36, Fabp3, Fabp5, Fatp1, Acadl, Pgc1a* and *Cpt1a* from isolated islets of D1KO mice compared to WT mice in reference to *36b4* mRNA expression. Data are mean values ± SEM (n = 7-8). *Ffar* – Free fatty acid receptor; *Gpr* – G-protein coupled receptor; *Fabp* – Fatty acid binding protein; *Fatp* – Fatty acid transport protein; *Acadl* – Acyl-CoA dehydrogenase long-chain; *Pgc1a* – PPARγ Coactivator 1α; *Cpt1a* – Carnitine palmitoyltransferase 1α

5 DISCUSSION

Previous studies have shown that the two related proteins TBC1D1 and TBC1D4 are involved in the insulin-stimulated GLUT4 translocation in skeletal muscle [111, 155]. More recently, both RabGAPs have also been implicated to play roles in GSIS in pancreatic β-cells [173, 174].

Here the involvement of *Tbc1d1* in GSIS was investigated using freshly isolated pancreatic islets from *Tbc1d1*-deficient mice (D1KO), transgenic mice overexpressing *Tbc1d1* in pancreatic β-cells under the control of the rat insulin 2 promoter (RIP2-TG), and mice deficient in both *Tbc1d1* and *Tbc1d4* (D1/4KO).

This thesis demonstrated for the first time, that the whole-body knockout of the RabGAP *Tbc1d1* in mice resulted in a pronounced increase in glucose-stimulated insulin secretion in isolated islets without affecting basal insulin secretion. The same effect was found in isolated islets of mice with an additional knockout of the *Tbc1d1* homologue *Tbc1d4*. Conversely, isolated islets with *Tbc1d1* overexpression in β-cells showed no difference in GSIS compared to their wildtype littermates.

5.1 Insulin secretion from isolated islets of experimental mice

The main finding of this thesis was a substantial increase in glucose-stimulated insulin secretion in intact isolated islets from genetically modified mice globally lacking the RabGAP *Tbc1d1* (D1KO) (Fig. 9). “Moreover, islets from *Tbc1d1*/*Tbc1d4* double-deficient mice (D1/4KO) were not different in GSIS than islets from *Tbc1d1* single knockout mice (Fig. 15). At least under non-challenging conditions, TBC1D1 protein appears not to be rate-limiting for GSIS in islets, as overexpression of *Tbc1d1* in RIP2-TG mice did neither change basal nor glucose-stimulated insulin secretion, when compared to the wildtype littermate controls (Fig. 14).” The observed changes in insulin secretion were not attributed to changes in insulin content of the assayed islets, since they appeared unchanged between all genotypes (Fig. 19)

“A recent study with sorted rat β-cells showed that the siRNA-mediated knockdown of *Tbc1d1* moderately increased insulin secretion at both, basal and glucose-stimulated conditions [174]. In isolated D1KO mouse islets, where TBC1D1 protein was undetected, basal insulin secretion was not changed, which demonstrates that loss of *Tbc1d1* affects only glucose-induced insulin secretion. Bouzakri and colleagues reported that siRNA-mediated knockdown of *Tbc1d4* in sorted mouse β-cells led to increased basal and decreased glu-

cose-stimulated insulin secretion, respectively [173].” If TBC1D4 affects insulin secretion in the opposite way from TBC1D1 with a similar impact this would be expected to yield in an intermediate phenotype regarding insulin secretion in the D1/4KO islets. However, islets with genetic deletion of both RabGAPs *Tbc1d1* and *Tbc1d4* showed the same insulin secretion phenotype than islets with a single *Tbc1d1* knockout. “Consistent with this finding, the analysis of mRNA copy numbers showed that in freshly isolated mouse islets *Tbc1d1* was the predominantly expressed RabGAP (Fig. 11). The knockdown of both, *Tbc1d1* and *Tbc1d4* in the previous studies was reported to reduce the abundance of the respective RabGAP by approx. 40-70 % [173, 174], whereas genetic ablation of *Tbc1d1* and *Tbc1d4* results in a complete loss of the proteins [155]. Thus, the presence of residual RabGAPs and compensatory mechanisms may explain the divergent results of the studies.”

These results suggest for the first time a regulatory role for TBC1D1 in isolated mouse islets in a process that is not known to be associated with the trafficking of GLUT4 [111, 155].

To date it seems evident that TBC1D1 regulates GLUT4 vesicle trafficking in skeletal muscle cells [155, 164, 202]. One study reports the expression of GLUT4 also in the endocrine pancreas of rats, mice and humans, which might have an influence on islet physiology [203]. However, mRNA expression of GLUT4 (*Slc2a4*) in INS1 cells was much lower than GLUT2 (*Slc2a2*) expression. Since INS1 cells derive from rat islets, this does not necessarily represent the same situation in freshly isolated mouse islets. Moreover it is not known, whether GLUT4 in islets undergoes the same trafficking as in muscle cells [165, 170, 204, 205] and if this is regulated the same way. A supportive study identified single players of an insulin signaling system in β-cells, including AKT, insulin receptor and insulin receptor substrates [206]. Since TBC1D1-regulated GLUT4 translocation plays an important role after activation of the insulin signaling this could also be a role for TBC1D1 in pancreatic β-cells. At least for TBC1D4 it was shown that it became phosphorylated by protein kinase B (AKT) after glucose stimulation in β-cells [173]. TBC1D1 in rat β-cells was also phosphorylated after glucose stimulation but it was not specified, whether this phosphorylation was AKT or AMPK dependent [174]. At least Rab8A and Rab10, which are important for GLUT4 translocation in skeletal muscle, were also shown to be enriched in mouse islets compared to total pancreas in the bachelor thesis of Dario Gosman from our working group. It is still an open question if and how insulin signaling in the β-cells is important for insulin secretion. An interesting regulator in this pathway could be APPL1. It modulates substrate specificity and activity of AKT and thereby initiates the expression of exocytotic genes to enhance insulin secretion in β-cells [207, 208]. At least for the APPL1-homologue APPL2 an interaction with TBC1D1 was shown [209]. However, since the major exocytotic genes were unchanged in D1KO mice (Fig. 25) an involvement of APPL1 in D1KO-mediated increase in insulin secretion seems unlikely.

Nevertheless, the presented data demonstrate for the first time a regulatory role of TBC1D1 in GSIS in mouse pancreatic islets.

The observed differences in insulin secretion upon *Tbc1d1*-deficiency could be due to several cellular or mechanistic changes. To investigate the underlying *in vitro* mechanisms and possible *in vivo* consequences the following additional questions were asked:

- Does an increased expression of *Tbc1d4* compensate for the loss of *Tbc1d1* in islets?
- Do islets of D1KO mice have more total pancreatic insulin than WT littermate controls?
- Is islet morphology and morphometry changed upon *Tbc1d1*-deficiency?
- Which insulin secretion phases are altered in islets of D1KO mice?
- Is TBC1D1 involved in insulin granule mobility and dynamics?
- Does TBC1D1 act on the triggering pathway of insulin secretion?
- Are possible changes of these parameters accompanied with altered gene expression?
- Do D1KO mice show increased insulin secretion and improved glucose tolerance *in vivo*?
- Does high-fat diet feeding affect insulin secretion of D1KO and WT mice?

5.2 RabGAP expression in mouse islets

The expression and function of Rab GTPase-activating proteins in pancreatic islets and β-cells is not well characterized. So far, TBC1D1 and TBC1D4 were reported to be expressed in mouse, rat and human pancreatic β-cells, as well as TBC1D10A (EPI64), which was shown just recently [173, 174, 210]. TBC1D10A was reported to be the RabGAP for Rab27A which has been previously associated with the trafficking of insulin secretory granules [47, 132, 136]. The substrate Rabs for TBC1D1 and TBC1D4 in β-cells are still unknown. For various Rabs TBC1D1 and TBC1D4 GAP domains were tested for their GTPase activity *in vitro*. TBC1D1 GAP domain showed GTPase activity towards Rab27A compared to the Rab alone or the RK-mutant of the TBC1D1 GAP domain, although the effect size was much smaller compared to the activity towards other Rabs [111]. In contrast TBC1D4 GAP domain showed no GTPase activity towards Rab27A [151]. The present study demonstrated that TBC1D1 is expressed in islets as a different isoform, compared to skeletal muscle (Fig. 10). Although the structure of the functional GAP domain is the same in both TBC1D1 isoforms [168] it is possible that the lack of two exons in the short isoform in islets alters the secondary structure of the protein accompanied with altered substrate specificity for Rabs. It was shown, that the short isoform of TBC1D1 is missing two serine-phosphorylation sites (S^{660} and S^{700}) which were linked to inhibition of GLUT4 translocation in adipocytes [111, 112, 168].

The present study confirms that TBC1D1 and TBC1D4 are expressed in islets but for the first time it demonstrates significantly higher *Tbc1d1* transcripts compared to *Tbc1d4* in freshly isolated mouse islets (Fig. 11) indicating a more relevant role of TBC1D1 in mouse islet physiology. If Rab27A is involved in the insulin secretion effect of D1KO and D1/4KO islets, this would be in line with the previously mentioned observation that TBC1D4 GAP domain has no GTPase activity towards Rab27A. Although it was shown that skeletal muscle also expresses a functionally relevant alternative splice variant of TBC1D4 [153] the predominant splice variant in islets was not investigated. However, the amplification of *Tbc1d4* transcripts with custom made oligonucleotide primers for quantification in mouse islets included both splice variants.

Interestingly mRNA for *Tbc1d1* was strongly reduced in the islets of the recombinant congenic D1KO mice (Fig. 13B). This is attributed to nonsense-mediated mRNA decay. The SJL variant of *Tbc1d1* in the D1KO mice exhibits a 7 bp-deletion compared to wildtype *Tbc1d1*, leading to the formation of a premature translation termination codon [156]. This might constitute a cellular signal to execute the posttranscriptional nonsense-mediated mRNA decay [211-215]. In fact, the truncated form of the mutant TBC1D1 protein appears to be highly unstable *in vivo* and has only been detected through *in vitro* translation assays [156]. Importantly this study showed that neither deficiency nor overexpression of TBC1D1 in islets of D1KO or RIP2-TG mice led to compensatory alterations in TBC1D4 protein expression in islets. Although *Tbc1d4* transcripts were shown to be significantly less expressed in normal mouse islets the detection of TBC1D4 protein in islet lysates were as effective as for TBC1D1. Antibody affinity and binding conditions in a western blot can be totally different between different antibodies, thus the signal intensities after western blot detection do not necessarily correlate with the protein abundance when comparing to another protein. Such correlation is even not possible by normalizing to a housekeeping protein. For this purpose a stain-free gel with known amounts of protein as an intensity reference after coomassie staining might be used to determine absolute amounts of a certain protein present in a given protein lysate.

TBC1D1 detection by western blot in total pancreas lysates of transgenic RIP2-TG mice and their respective control littermates was only possible with the application of 200 µg of total protein (Fig. 12). For isolated islets already 10 µg of total protein was sufficient to detect TBC1D1 with comparable experimental conditions (Fig. 13). This indicates that TBC1D1 expression in pancreas tissue is highly enriched in endocrine islet cells. Previously it was shown that RNA expression of both RabGAPs *Tbc1d1* and *Tbc1d4* was similar in isolated human islets, but *Tbc1d4* was the major RabGAP in FACS-sorted human β-cells [174]. As shown in this study the differential RNA expression of *Tbc1d1* and *Tbc1d4* in isolated mouse islets was totally different compared to the study with human islets. Although Rütti and col-

leagues showed an involvement of TBC1D1 in rat islet function and GSIS, they did not show which RabGAP is the major form in rat islets or β-cells [174].

The present study also made use of a mouse lacking both RabGAPs TBC1D1 and TBC1D4 (D1/4KO). In isolated islets of those mice, neither TBC1D1 nor TBC1D4 protein were detected. A previous study also demonstrated the loss of both proteins in WAT, *TA*, *EDL* and Soleus muscle in the same mouse model [155].

Finally, the data showed for the first time that *Tbc1d1* is predominant over *Tbc1d4* in mouse islets and that upon *Tbc1d1*-deficiency no compensatory overexpression of *Tbc1d4* was observed.

5.3 Total pancreatic insulin content and islet morphometry

To exclude the possibility that the insulin secretion effect observed upon *Tbc1d1*-deficiency was not due to increased pancreatic insulin content, accompanied with morphologic or morphometric changes, pancreatic insulin content was analyzed by ELISA and the histologic properties of pancreatic islets were characterized by light microscopy in pancreatic sections.

Total pancreatic insulin content normalized to total protein content was unaffected by *Tbc1d1*-deficiency (Fig. 20). Insulin content (~ 10 µg/mg protein) accounted for approx. 1% of total pancreatic protein in D1KO and WT control mice. Although unchanged pancreatic insulin content suggested no relevant changes in the number of islets, the morphology and morphometry of pancreas sections from D1KO and WT mice were analyzed. “In line with the data from total pancreatic insulin content the morphometric analysis showed no major differences in islet morphology, number or islet size distribution between D1KO and WT mice as analyzed by light microscopy after HE staining of pancreatic sections (Fig. 22).”

5.4 Dynamic glucose-stimulated insulin secretion

Isolated islets of *Tbc1d1*-deficient mice secrete more insulin upon glucose stimulation compared to islets of the respective wildtype mice. This increase could neither be attributed to morphometric changes (4.6) nor changes in total pancreatic and islet insulin content (4.5). To investigate, whether first or second phase of insulin secretion is affected by *Tbc1d1*-deficiency, isolated islets were applied to perifusion in the lab of Prof. Dr. Ingo Rustenbeck (Institute of Pharmacology, Toxicology and Clinical Pharmacy, Technical University Braun-

schweig, Germany). The results demonstrated for the first time that *Tbc1d1*-deficiency increased both, first and second phase of insulin secretion in the dynamic perifusion of isolated islets (Fig. 16). Apparently the islets of WT mice showed a very poor response to glucose stimulation compared to the D1KO islets. It has been shown earlier that insulin secretion *ex vivo* and *in vivo* differs markedly between different inbred mouse strains when stimulating with different secretagogues [216-219]. Isolated islets of C57BL/6 mice thereby showed the weakest response to glucose, IBMX [220] and tolbutamide in a perifusion experiment when compared to islets of 129X1/Sv, FVB/N and DBA/2 mice. In contrast, insulin secretion to the plasma in an *in vivo* hyperglycemic clamp experiment was pronounced from C57BL/6 mice [217]. Notably, the mice were fasted 5 h prior to the *in vivo* assessment, while they were not fasted for *ex vivo* perifusion. Interestingly C57BL/6J mice carry a mutation in the nicotinamide nucleotide transhydrogenase (*Nnt*) gene resulting in a lack of a proton pump involved in mitochondrial NADPH production [221]. It was reported that this loss-of-function mutation had no effect on insulin secretion and glucose tolerance, when compared to C57BL/6 *Nnt*-wildtype (C57BL/6N) control mice [221]. However, a recent study showed a reduced insulin secretion in C57BL/6J mice after intravenous glucose infusion compared to C57BL/6N mice [218]. Although the same mice were used, the experimental conditions (age of mice and amount of glucose administered) differed in these two studies which might account for the different findings related to insulin secretion. Metabolism of glucose regulates insulin secretion via two main pathways. “Both, the triggering and the amplifying pathway derive from the end products of β-cell mitochondria [78, 222]. The triggering pathway initiates insulin secretion but does not specify its total amount [222]. This depends on the amplifying pathway, which includes the export of mitochondrial metabolites, but remains to be elucidated [223]. Importantly, first phase insulin secretion is affected by the amplifying pathway. Thus, the collective stimulated secretion is critically dependent on continuous mitochondrial activity [224, 225].” While first phase insulin secretion is in large part a result of depleting granules that are pre-docked to the plasma membrane [41, 46], second phase insulin secretion is supposed to be attributed to newly synthesized insulin granules that have to be translocated to the plasma membrane [45]. “However, recent studies unraveled that freshly synthesized newcomer granules were also visible and used during early stages of stimulated insulin secretion [226-229].” Since both phases were increased in islets of D1KO mice, this could either point to an involvement of TBC1D1 in insulin vesicle movement and dynamics or to an accelerated activity of mitochondria or an increase in mitochondrial number and area.

5.5 Ultrastructural insulin granule density in β-cells

The loss of *Tbc1d1* as a RabGAP will most likely affect vesicle trafficking events, rather than activity or number of mitochondria. Therefore the insulin granule density of β-cells was analyzed in transmission electron microscopic images.

Transmission electron microscopy revealed a reduced density of dark granules in β-cells of WT mice after glucose stimulation, whereas density of dark granules in β-cells of D1KO mice was unaffected by glucose stimulation (Fig. 23A). After glucose stimulation the density of dark granules was significantly higher in D1KO β-cells, when compared to WT β-cells. At the same time also the density of pale granules was significantly higher in D1KO β-cells, when compared to WT β-cells after glucose stimulation (Fig. 23B). These data reflect the situation 60 minutes after the respective glucose condition, which reflects also the same conditions as the GSIS results. It has been shown early that glucose stimulates the trafficking of insulin vesicles [230, 231]. It is also accepted that the density of dark granules decreases to various extents after different times of glucose stimulation [232, 233]. In one report 40 minutes of rat pancreas perfusion with 27 mM glucose resulted in a decrease of approx. 7 % in the dark granules compared to control conditions with 3.9 mM glucose. Apparently, the time of pancreas perfusion was insufficient to induce glucose-stimulated insulin synthesis [232]. In this thesis, the reduction of dark granules 60 minutes after 25 mM glucose stimulation of isolated wildtype mouse islets was approx. 21 %. The fact, that this decrease was not observed in islets of D1KO mice suggests that islets of D1KO mice might have an increased synthesis of insulin throughout the glucose stimulation period, compared to WT mice. This is supported by the finding of increased pale granules in D1KO β-cells after glucose stimulation, as these granules represent newcomer granules, containing both, proinsulin and insulin [232, 234-236]. The mobility of newly formed insulin granules is higher than that of older ones and new granules are preferred for translocation to secrete insulin [237]. If β-cells of D1KO mice exhibit accelerated insulin synthesis, accompanied with increased pale granule generation they can deplete the newly synthesized granules, while β-cells of WT mice need to deplete more of the old granules to maintain insulin release. This assumption would be in line with the observed differences in granule densities. The pictures represent the situation 60 minutes after basal or stimulated glucose concentration, thus it rather shows the events belonging to the second phase of insulin secretion, than the first phase. Second phase insulin secretion seems to be more important with regard to insulin vesicle translocation, than first phase. “Previous studies have demonstrated that glucose-stimulated insulin release utilizes Rab-GTPases that regulated a highly dynamic interplay of insulin granule formation, granule storage and granule trafficking and fusion with the plasma membrane [88, 132, 133, 238].”

Those are Rab3A, Rab27A and Rab37 [88, 132, 133, 238]. “In earlier studies, only Rab27A has been shown to be a relevant substrate for the RabGAP domain of TBC1D1 *in vitro* [111]. However, other Rabs might be additionally involved in the regulation of insulin granule mobility” or, as mentioned earlier, the secondary structure of the short isoform of TBC1D1 might be altered and with this also substrate specificity for Rabs.

SORCS1 as a protein belonging to the vacuolar protein sorting-10 family was described as a crucial component in the promotion of secretory granule biogenesis in pancreatic β-cells [239]. It is also involved in vesicle trafficking and overexpression was associated with an increase in the secretory granule content, whereas SORCS1 deletion led to severely decreased insulin secretory granules. Since no scientific publication links the expression of TBC1D1 or any other RabGAP with the expression or activity of SORCS1 it is speculative, whether SORCS1 is involved in the elevated insulin granule density after glucose stimulation. However, the described SORCS1-related phenotype of insulin granule biogenesis seemed to be independent of glucose [239], whereas *Tbc1d1*-deficiency revealed its phenotype only after glucose stimulation. The maturation of insulin inside the granules was reported to strongly depend on the expression of zink transporter ZnT8. Deletion of this transporter in mice led to a defective maturation and crystallization of insulin, accompanied with a switched ratio of dark to pale granules in the β-cells [240]. An increased number of both, dark and pale insulin granules might also imply an increase in the total pancreatic insulin content, as already discussed in 5.3. However, total pancreatic insulin content was unchanged between WT and D1KO mice. This might be due to the fact that mice, where the pancreata were taken from, were not stimulated with glucose, prior to pancreas dissection.

Tbc1d1-knockout in islets showed for the first time an increased density of both, dark and pale granules 60 minutes after glucose stimulation compared to wildtype littermates, where the density of dark granules decreased by 21 % compared to non-stimulatory conditions. Thus, insulin vesicle dynamics or insulin synthesis seems to be altered in D1KO mice during glucose stimulation that is also represented by the increased second phase insulin secretion in the perifusion experiment.

5.6 Role of *Tbc1d1* in secretagogue-induced insulin secretion

Isolated islets of *Tbc1d1*-deficient mice secrete more insulin in both phases upon glucose stimulation compared to islets of the respective wildtype mice. Increased second phase insulin secretion in D1KO β-cells might be due to altered vesicle dynamics represented by an increased or at least maintained insulin granule density after glucose stimulation compared

to WT β-cells, as analyzed by electron microscopy. To analyze the impact of *Tbc1d1*-deficiency on the triggering insulin secretion pathway, representing first phase insulin secretion (Fig. 3), a mechanistic and pharmacologic approach was initiated. “Glibenclamide and tolbutamide as substances belonging to the group of sulfonylureas positively affect insulin secretion at low glucose concentrations by blocking ATP-sensitive K^+-channels [70, 71].” In the Rustenbeck-Lab tolbutamide-induced insulin secretion was investigated in the isolated islets of D1KO mice in a perifusion experiment. The glibenclamide-induced insulin secretion was investigated in a static approach. “The increase in both, glibenclamide- and tolbutamide-stimulated insulin secretion at basal glucose concentrations (2 mM and 5 mM) was potentiated in isolated islets of D1KO mice” (glibenclamide: Fig. 27, tolbutamide: Fig. 30), while addition of KCl showed no changes in insulin secretion between the genotypes. This suggests mechanistic differences at the site of the K^+-ATP channel. “Interestingly, the K^+-ATP channels have been reported to not only localize to the plasma membrane of β-cells, but also were shown to be present on insulin secretory granules [88, 241]. Moreover, glibenclamide and other sulfonylureas were found to stimulate insulin secretion via granule-localized channel inhibition without binding to plasma membrane K^+-ATP channels [242]. Since sulfonylurea-potentiated secretion at low glucose concentration was increased in D1KO islets, it is possible that *Tbc1d1*-deficiency may increase K^+-ATP channel trafficking and surface expression [243-247].” This trafficking was reported to be mainly dependent on AMPK activation [200, 201, 248]. TBC1D1 is a known downstream target of AMPK and thus likely to be involved in this pathway. However, K^+-ATP channel surface expression is not only controlled by exocytotic trafficking, but also by endocytotic recycling and degradation [249]. The respective regulatory Rabs and RabGAPs or RabGEFs have not been described, yet. It is possible that insulin and K^+-ATP channels undergo concerted trafficking mediated by Rab27A, controlled by TBC1D1.

AMPK activity is involved in K^+-ATP channel trafficking that might be regulated by TBC1D1. The AMPK activator AICAR was shown to potentiate insulin secretion from isolated mouse islets at stimulatory glucose conditions [59]. Activated AMPK is able to phosphorylate and thereby inactivate TBC1D1 [158], thus it is possible that TBC1D1 knockout influences AICAR-mediated insulin secretion. Knockout of TBC1D1 reflects a situation of hyperphosphorylation and inactivation of TBC1D1 therefore it would mimic also AMPK phosphorylation. We could not find a different insulin secretion effect of AICAR on D1KO islets with 11 mM glucose stimulation (Fig. 32) than on WT islets. It is possible that 25 mM glucose stimulation would lead to different results but these conditions were not sufficiently tested. To date it is still controversial how activated AMPK affects insulin secretion in islets [250]. The presence of AMP and the AMP-mediated AMPK phosphorylation and activation is usually linked to a low cellular energy status [61], although insulin secretion physiologically appears at high

ATP and thereby low AMP levels. Since TBC1D1 knockout already mimics effects of AMPK phosphorylation it is possible, that further AMPK phosphorylation has no additional effect. This would suggest that AICAR potentiated GSIS could still be mediated by TBC1D1 in wildtype islets. Notably, the active metabolite of AICAR, ZMP, is able to also activate other AMP-activated enzymes, for instance glycogen phosphorylase [251] and fructose-1,6-bisphosphatase [252]. The latter is an essential enzyme in the gluconeogenesis, and therefore unlikely to be relevant in pancreatic islets. However, glycogen phosphorylase as a necessary enzyme in glycogen breakdown is expressed and active in rat pancreatic islets [253].

“A previous study reported that knockdown of *Tbc1d1* prevents insulin secretion induced by depolarizing concentrations of KCl in sorted rat β-cells [174]. Conversely, the present data show that genetic ablation of *Tbc1d1* does not result in altered response of islets to KCl (Fig. 28). This might be attributed to the difference between incubation times for KCl between both studies and again the fact that *Tbc1d1* knockdown in rat β-cells led to just 70 % reduction of TBC1D1 protein. When bypassing the further downstream Ca^{2+}-channel with the Ca^{2+}-ionophore A23187 [73, 199], insulin secretion was the same in both, wildtype and D1KO islets (Fig. 29).” This suggests that the TBC1D1 contribution to first phase insulin secretion in isolated mouse islets is localized around the K^{+}-ATP channel. The depolarization that is induced by closing or blocking the K^{+}-ATP channel is not directly committed to the voltage-gated L-type Ca^{2+}-channel. In between there are also transient receptor potential (TRP) channels, Na^{+}-channels and T-type Ca^{2+}-channels, all of them increasing the initial membrane depolarization to the required threshold to open the voltage-gated L-type Ca^{2+}-channel [35]. The TRP channels of the pancreatic β-cells are reported to be mostly activated by certain steroids [254, 255] to contribute to insulin secretion [256]. However, a recent study demonstrated that also GLP-1 stimulates insulin secretion in part by activation of TRP channels [257]. Compared to the prominent participants of the insulin secretion pathway the contribution of the other mentioned receptors in the transmission and enhancement of the depolarization is mostly neglected. Nevertheless, it cannot be excluded that TBC1D1 might play a role in the regulation of surface expression of these receptors and channels.

Notably, there is an existing bypassing pathway of insulin secretion that is also often neglected in the consideration of the different secretion pathways. This pathway is initiated by the glucose-induced generation of cAMP [258, 259]. cAMP is well known as a cellular second messenger that transmits signals inside the cell [260], i.e. after activation of certain GPCRs. The precise mechanism, how glucose increases cellular cAMP levels in β-cells is unknown, but is suggested to be due to activation of adenylyl cyclase [258]. cAMP, if not inactivated by phosphodiesterases, activates the cAMP-dependent protein kinase A (PKA) [261]. A limited number of publications link the activity of cAMP and PKA to mechanisms of

insulin secretion [262] and exocytosis either via crosstalk with AMPK [263] or activation of the cAMP-dependent RabGEF Epac2 [264] or activation of β-catenin [258]. Besides the PKA-mediated effects, cAMP was also shown to amplify insulin secretion by Epac2 independent of PKA activation [265]. *Tbc1d1*-deficiency may also impact this described pathway, especially when considering the role of Epac2 as RabGEF. It was described as the specific GEF for Rap1 [266], which was also found to localize to the insulin granule next to Rab3A, Rab27A and Rab37 [88]. Thus, it is possible that due to *Tbc1d1*-deficiency, Epac2 activity predominates to over-activate granule trafficking via Rap1.

5.7 Gene expression in islets of WT and D1KO mice

To analyze, whether the above described changes in insulin secretion, are accompanied with changes in gene expression, relative mRNA quantification was measured by real time PCR. Isolated islets of D1KO mice showed reduced expression of the transcription factor *Mafa* compared to islets of WT littermates (Fig. 24). Although MafA regulates insulin gene expression and is itself regulated by glucose [185] mRNA of the *insulin 2* gene in islets of D1KO mice was not different compared to wildtype littermates. It is not clear, whether the reduced *Mafa* expression is causative for the insulin secretion effect in D1KO islets, although the presence of MafA was reported to be relevant for functional GSIS in postnatal islets [267]. It might indicate a reduced number of β-cells in the islets, although this was not represented by *Ins2* or *Pdx1* gene expression or total pancreatic insulin content (Fig. 20). In addition *Mafb* mRNA as a surrogate for the number of α-cells [268, 269] as well as *Ngn3* mRNA as a marker for β-cell dedifferentiation [188] was unchanged. A feasible antibody to clearly detect and quantify MafA in mouse protein lysates by western blot was commercially not available.

In addition a number of other genes that are relevant for insulin secretion in general and especially exocytosis were analyzed. The only gene that showed significantly different expression in D1KO islets compared to WT islets was *Dnajc5* (Fig. 25A). This gene showed elevated transcripts in D1KO islets. *Dnajc5* encodes the cysteine-string protein α (CSPα). This is a DnaJ homologue that shows guanine nucleotide exchange activity for G_α proteins [190] and has been shown to regulate insulin exocytosis via interaction with syntaxin-1a [89, 191]. In contrast to *Dnajc5*, *Stx1a* as the gene encoding syntaxin-1a was unchanged in mRNA expression (Fig. 25A). Moreover, gene expression of *Dnajc5* did not correlate with the CSPα protein expression (Fig. 25B). Since protein is the more executive molecule in the regulation of cellular processes the significant increase in mRNA might not be relevant for the observed insulin exocytosis effect. *Rab27a* mRNA as well as the reported RabGAP for Rab27A,

TBC1D10A was expressed in mouse islets but was unchanged between the genotypes (Fig. 25A). Thus, expression differences of *Rab27a* or *Tbc1d10a* between the genotypes can be likely excluded to contribute to the insulin secretion effect upon *Tbc1d1*-deficiency. This does not mean that maybe activation states of both components may be different in the *Tbc1d1*-deficient state, although this has not been reported in the literature, yet. Expression of *Irs1* and *Irs2* was measured. Both are components of the insulin signaling pathway in β-cells that have been described for their role in insulin secretion and synthesis [195, 270]. While *Irs1* was unchanged between WT and D1KO, *Irs2* expression was significantly increased by approx. 30 % in islets if D1KO mice. As overexpression of *Irs2* in isolated rat islets was associated with increased second phase and total insulin secretion [196], this suggests a role for TBC1D1 in insulin synthesis and secretion, which would be in line with the findings of the ultrastructural analysis and the perifusion experiment. However, IRS2 protein abundance was not different between WT and D1KO islets.

The observation that sulfonylurea-induced insulin secretion at low glucose levels is elevated in D1KO islets suggest, that K^+-ATP channel surface expression might be increased. To have an idea about the total expression of the subunits of the channel the relative gene expression of *Kcnj11* und *Abcc8* was measured. Total expression of both subunits was not significantly different between D1KO and WT islets, although *Abcc8* showed slightly elevated mRNA levels in D1KO islets. Due to the lack of appropriate antibodies that detect both protein subunits by western blot in mouse protein lysates there is no information on protein expression. Moreover, total gene or even protein expression does not reflect the surface expression of the subunits. Nevertheless, leptin-induced increase in K^+-ATP channel surface expression had been proposed to regulate insulin secretion [271], as well as increased surface expression that is induced by downregulated syntaxin-1a [244].

However, since RNA and also protein were taken from islets that were cultured overnight in islet medium and not stimulated with 25 mM glucose concentration, the results might not represent the situation after glucose stimulation.

5.8 Impact of *Tbc1d1*-deficiency *in vivo*

Previous studies investigated *in vivo* glucose- and insulin tolerance and also plasma insulin levels of *Tbc1d1*-deficient mice [155, 167]. Young mice that globally lack *Tbc1d1* showed neither alteration in glucose tolerance, nor insulin tolerance or gross differences in plasma insulin levels throughout the test period. These observations were in large part reproduced in the present study. Young D1KO mice exhibited the same glucose tolerance as young WT

mice (Fig. 17A). However, plasma insulin levels in the basal state were significantly lower in D1KO mice compared to WT littermates but with no differences in the progression of the test (Fig. 17B). In contrast, previous observations reported significantly increased fasting plasma insulin levels in D1KO mice [167]. It cannot be completely excluded that this difference is due to a clustering of insulin values in the mice, although no such clustering of the plasma insulin values were observed with the used animals in the present study. The fasting period of the mice in the mentioned study was just two hours less compared to the period in the present study. However, this difference is unlikely to be the cause for this opposed finding. Although housing conditions of the mice were similar the animal facility for the breeding of the mice was different. Even if the mice were genetically identical it was shown that the composition of the gut microbiota of mice in different laboratories can influence metabolic parameters [272, 273]. This difference in the gut microbiome can be caused by diet but also by other parameters [274, 275].

For a small subset of mice the glucose tolerance test was repeated when the mice were at the age around 50 weeks. In contrast to the results with young mice the genotype seemed to affect glucose tolerance at higher ages. Interestingly, fasting blood glucose levels were not different in old mice when compared to young mice independent of the genotype. However, glucose tolerance of old D1KO mice was improved compared to old WT mice (Fig. 18). The overall plasma insulin levels were markedly higher in the old animals but D1KO mice achieved to improve glucose tolerance with only moderate insulin secretion. In contrast, WT mice with impaired glucose tolerance had a pronounced increase in insulin secretion. This indicates a higher degree of insulin resistance in the WT mice at higher ages compared to D1KO mice. The used mouse model represents a whole-body knockout for TBC1D1. For the accurate assessment of insulin resistance a hyperinsulinemic-euglycemic clamp experiment is the gold standard method [276]. With this procedure the participation of the liver and the skeletal muscle in glucose uptake and glucose production can be evaluated. Whole-body *Tbc1d1*-knockout in mice was shown to be associated with a substantially reduced expression of GLUT4 protein in *EDL*, *TA* and quadriceps muscle with a severely impaired insulin- and AICAR-stimulated glucose uptake in isolated *EDL* muscle. However, insulin- and AICAR-stimulated glucose uptake in the soleus muscle and insulin-stimulated glucose uptake in WAT was unchanged in D1KO mice, compared to wildtype littermates, as they showed equal GLUT4 abundance [155]. Furthermore, the unchanged glucose tolerance in *Tbc1d1*-deficient mice has been demonstrated also by other groups [160, 167, 202]. That an increased insulin secretion was not directly observed in D1KO mice *in vivo* could be due to inter-organ signals acting on the repression of insulin secretion which would not be present in the *ex vivo* assay. It was shown that factors released from exercised mouse muscles reduce insulin secretion from INS1 cells, although this effect was not seen in isolated rat islets [277]. Likewise secret-

ed factors of human myotubes treated with TNF-α repressed GSIS in primary rat- and human β-cells [278]. However, the young D1KO mice did not exhibit any signs of insulin resistance or glucose intolerance. Nevertheless, endurance training in rats was associated with decreased plasma insulin levels but an improved glucose tolerance [279] as these effects were present in the old D1KO mice. This indicates that signals from other organs than the pancreas can indeed influence insulin secretion *in vivo* and that this might cause unaltered insulin secretion in the young D1KO mice *in vivo*. In addition the mice were fasted 6 hours prior to the glucose tolerance test, whereas islet isolation was carried out from random fed mice and isolated islets were starved in the GSIS assay just one hour with 2 mM glucose. Thus a direct comparison between *in vivo* and *ex vivo* approaches is not feasible.

5.8.1 Repetitive glucose stimulation

In a physiological context, insulin secretion is not only triggered by a single glucose stimulation, as assessed in the GSIS assays and also in the *in vivo* GTTs, but rather by maintained or repetitive stimulation. To simulate these conditions, isolated islets of D1KO mice were subjected to a GSIS assay with three repetitive glucose stimulations, each with 25 mM, interrupted by phases of 60 minutes with 2 mM glucose. As shown in Figure 33, islets of D1KO mice are still able to secrete more insulin compared to islets of WT mice, even after the third glucose stimulation. Unfortunately a significant increase in insulin secretion after the first two stimulations was not observed. More importantly, insulin secretion after the third stimulation was approx. twice as high compared to the first two stimulations in both genotypes. “This indicates that the mechanism, leading to increased GSIS upon *Tbc1d1*-deficiency is continuously working with repetitive glucose stimulations. This effect is therefore highly relevant in a physiological context.” The concept of insulin secretion after repetitive glucose stimulations is not well described and characterized in the literature. Islets of leptin-deficient *ob/ob* mice with a deletion of SORCS1 fail to maintain insulin secretion after three repetitive glucose stimulations, compared to their respective *ob/ob* controls [239]. In contrast to this thesis, the stimulations were only for 15 minutes and the interrupting phases with basal glucose were only for five minutes. These conditions might have abrogated the propagation of second phase insulin secretion, which was shown to be highly relevant for the effect upon *Tbc1d1*-deficiency. However, islets of D1KO mice are able to increase insulin secretion even after three repetitive glucose stimulations compared to islets of WT mice, which promotes physiological relevance.

5.8.2 High-fat diet

Tbc1d1-deficiency increases GSIS from isolated mouse islets but was unchanged in islets overexpressing *Tbc1d1* under the control of the RIP2 promoter (Fig. 9, 14). In isolated islets of wildtype mice on standard diet 25 mM glucose stimulation potentiates insulin secretion by approx. 12-fold compared to basal glucose concentrations with 2 mM under non-challenging diet conditions. It is long known that mouse islets are capable of storing and utilizing triacylglycerols [280]. The effects of chronic and acute fatty acid exposure on insulin secretion is also well known [55]. Challenging the mice with feeding a high-fat diet for four weeks severely impaired the glucose-induced insulin secretion index to only approx. 2.5-fold in wildtype islets (Fig. 34B). Upon *Tbc1d1* deficiency the secretion index is 4-fold but this is a result of a slightly lower basal and slightly higher stimulated insulin secretion. However, none of the differences between wildtype and D1KO islets were statistically significant.

Chronic exposure of islets to fatty acids should decrease insulin secretion performance due to the development of lipotoxicity and due to inhibition of insulin gene expression [53, 55, 281]. This decrease in insulin secretion performance was also demonstrated in the present study. Obviously the lack of *Tbc1d1* does not change the insulin secretion performance after chronic exposure of the mice to high-fat diet, compared to mice on standard diet. *Tbc1d1*-deficiency was reported to increase fatty acid uptake and oxidation in isolated skeletal muscle. At the same time glucose uptake and oxidation was reduced [156]. Isolated islets of D1KO mice also exhibited an increased uptake of radioactively labelled palmitic acid compared to islets of wildtype littermates (PhD thesis Franziska Menzel). *Tbc1d1* was therefore believed to act as a molecular switch for nutrient preference to use for energy production [156]. This fat-challenging approach should show if islets of mice fed a high-fat diet can beneficially compensate for lipotoxicity upon *Tbc1d1*-deficiency by maintaining the ability to secrete insulin after glucose stimulation appropriately. Apparently, this was neither the case for the chronic exposure to high-fat diet, nor for acute exposure of isolated islets to palmitate (Fig. 34).

In contrast to long-term exposure of islets to fatty acids acute exposure potentiates glucose-induced insulin secretion without affecting insulin secretion at basal glucose concentrations [53, 56, 57]. Most of the acute effect on fatty acid potentiation of insulin secretion is mediated by the free fatty acid receptor 1 (FFAR1, also known as GPR40) [282-284] but other signals are still necessary for the entire effect *in vivo* [285]. Potentiation of insulin secretion by acutely applied free fatty acids is mediated by the amplifying pathway of insulin secretion [48, 117, 286, 287]. This secondary pathway is strongly dependent on glucose metabolism, thus at basal glucose concentrations the amplifying pathway is mostly inactive [222, 288, 289].

Therefore palmitate was only added to 25 mM glucose. The potentiating effect of palmitate to insulin secretion was shown in Figure 34A. In this experimental setup the effect of *Tbc1d1*-deficiency on increasing insulin secretion was unfortunately neither seen without nor with palmitate supplementation to 25 mM glucose. However, gene expression analyses showed no differences of various receptors, transporters and key enzymes in lipid metabolism of pancreatic islets of WT and D1KO mice (*Ffar1*, *Ffar2*, *Ffar3*, *Gpr119*, *Gpr120*, *Cd36*, *Fatp1*, *Fabp3*, *Fabp5*, *Acadl*, *Pgc1a*, *Cpt1a*) [290-296] (Fig. 35) suggesting no changes in functional lipid metabolism upon *Tbc1d1*-deficiency. At this point it is not feasible to imply that *Tbc1d1*-deficiency has no impact on palmitate potentiation of insulin secretion since the genotype effect at 25 mM glucose alone failed to show significant differences compared to the WT islets, although gene expression suggest no functional changes in lipid metabolism.

5.9 Conclusions

The present thesis aimed to investigate the role of the signaling protein TBC1D1 in pancreatic islets and especially in the mechanism of insulin secretion from β-cells. For the first time this thesis demonstrates that loss of TBC1D1 increased glucose-induced insulin secretion in isolated islets. Additional knockout of the close homologue *Tbc1d4* has no further impact on GSIS and results in the same increase in glucose-stimulated insulin secretion as the single *Tbc1d1*-knockout. TBC1D1 is expressed as short isoform in pancreatic islets of C57BL/6J origin and is predominant over TBC1D4. This clearly indicates a more relevant role of TBC1D1 in the regulation of insulin secretion. In contrast, overexpression of the physiologically relevant short *Tbc1d1* isoform under the control of the RIP2-promoter had no influence on GSIS, indicating, that TBC1D1 is not rate-limiting in this process. Due to potential compensatory mechanisms in whole-body physiology and signals from other organs absolute insulin secretion after glucose stimulation is not significantly different in young D1KO mice compared to WT mice *in vivo*. In contrast, one year old mice show some interesting differences in glucose homeostasis with regard to *Tbc1d1*-deficiency as measured by i.p. GTT and plasma insulin concentrations. *Tbc1d1*-deficiency increases glucose-induced insulin granule density in islet β-cells that indicates a role in the generation and trafficking of insulin granules. Furthermore, *Tbc1d1*-deficiency increases glibenclamide-induced insulin secretion in isolated islets at low glucose concentrations, suggesting a regulatory role for TBC1D1 in also trafficking and surface expression of K^+-ATP channels. These suggestions are in line with increased first and second phase of GSIS as well as the increased tolbutamide-induced insulin secretion in D1KO islets that was observed in perifusion experiments performed in

Braunschweig. Manipulation of more downstream steps in the triggering pathway from isolated islets show no alterations in insulin secretion due to the loss of TBC1D1.

Taken together, the present data strongly suggest TBC1D1 as a novel component in the regulation of insulin secretion in mouse pancreatic β-cells by modulating insulin granule dynamics and presumably K^+-ATP channel trafficking (Fig. 36).

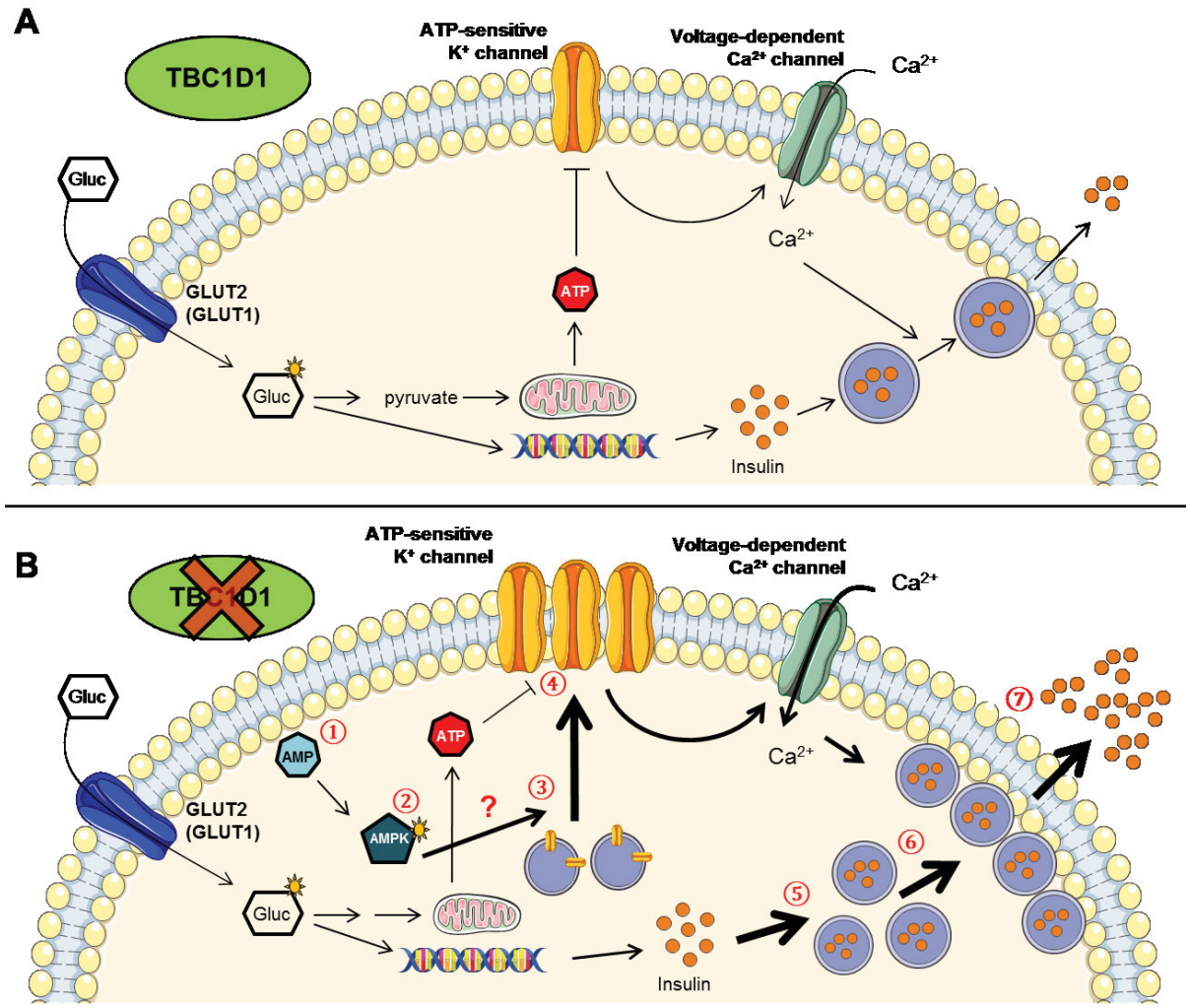

Figure 36: Proposed mechanism of action of *Tbc1d1*-deficiency on glucose- and sulfonylurea-induced insulin secretion. (A) The triggering pathway of insulin secretion as already described in 1.3.1 in the normal situation under normal TBC1D1 expression. **(B)** According to the presented results, *Tbc1d1*-deficiency indicates changes in the β-cell physiology by modifying vesicle trafficking at least at two different locations. On the one hand, translocation of K^+-ATP channel containing vesicles to the plasma membrane (3) and a subsequent increase in the surface expression of the channels (4) might lead to increased sulfonylurea-induced insulin secretion at basal glucose concentrations. The literature suggests that this process is regulated upstream by AMP-mediated (1) AMPK phosphorylation (2) at low glucose levels. On the other hand, the generation (5) and the dynamics of insulin containing vesicles (6) under stimulated glucose concentrations are altered towards an increased vesicle density leading to an increased secretion of insulin (7).

6 SUMMARIES

6.1 Summary (English)

Background and aims:

The Rab-GTPase activating protein (RabGAP) TBC1D1 has been described for its role in both glucose and lipid metabolism in skeletal muscle. TBC1D1 is also expressed in pancreatic β-cells but its role in glucose-stimulated insulin secretion (GSIS) remains to be determined. Recently TBC1D1 was shown to contribute to insulin secretion in sorted rat β-cells but with no detailed insights into a potential mechanism. To specify the role of TBC1D1 in insulin secretion its function in secretagogue-induced insulin secretion in isolated islets from *Tbc1d1*-deficient mice, transgenic mice overexpressing *Tbc1d1* under the control of a RIP2 promoter and *Tbc1d1/Tbc1d4*-double-deficient mice, respectively was investigated.

Materials and methods:

Mouse pancreatic islets were isolated by ductal collagenase perfusion and subsequent pancreas digestion. The isolated islets were applied to static and dynamic secretagogue-induced insulin secretion measurements. Whole-body glucose tolerance was measured by intraperitoneal glucose tolerance test and dissected pancreases were used for histologic and morphometric analysis of islets. Isolated islets were also used for ultrastructural insulin granule determination and quantification as well as quantification of protein and gene expression in lysates by western blot and quantitative Real time PCR, respectively. Statistics were calculated with appropriate tests.

Results:

GSIS at 25 mM glucose stimulation was substantially increased in islets from *Tbc1d1*-deficient mice, whereas the overexpression of *Tbc1d1* had no effect on GSIS. In both cases insulin secretion at basal glucose (2 mM) was unchanged. Moreover, the additional knockout of the close TBC1D1 homologue TBC1D4 had no additive effect on GSIS compared to the single knockout of *Tbc1d1*. Pancreatic islets of normal C57BL/6J mice exclusively express the short variant of *Tbc1d1* which was used for the generation of transgenic mice on a C57BL/6J background (RIP2-TG). *Tbc1d1* mRNA in islets was predominant over *Tbc1d4*. TBC1D1 protein expression in RIP2-TG islets was 2.6-fold higher compared to RIP2-WT controls, whereas TBC1D1 was undetected in islets of D1KO mice. Dynamic perifusion of D1KO islets showed that the increased GSIS was attributed to both, first and second phase of insulin secretion. The *Tbc1d1*-related *ex vivo* effect on insulin secretion could not be

shown *in vivo*. Although no differences were found in general islet morphometry between D1KO and WT mice, transmission electron microscopy revealed an increased density of both, pale and dark insulin granules in β-cells of D1KO mice after glucose stimulation. Stimulation of islets with 1 µM of the K^+-ATP channel inhibitor glibenclamide with 2 mM glucose as well as 500 µM tolbutamide with 5 mM glucose, resulted in an increased insulin secretion in D1KO islets. In addition, glibenclamide potentiated GSIS at 25 mM glucose in WT islets, but not in D1KO islets. In contrast, exposure of isolated islets to 30-40 mM KCl or to 5 µM calcium ionophore A23187, respectively, had no effect on genotype-dependent insulin secretion at basal glucose levels. Protein and gene expression only showed an increase in *Irs2* in D1KO islets as relevant target for insulin secretion and synthesis.

Conclusion:

Loss of TBC1D1 increased glucose- and sulfonylurea-induced insulin secretion in isolated islets due to increased first and second phase, but β-cell specific overexpression of the physiologic relevant short *Tbc1d1* isoform does not. Due to potential compensatory mechanisms insulin secretion after glucose stimulation is not pronounced in D1KO mice *in vivo*. Loss of TBC1D1 increases glucose-induced insulin granule density in islet β-cells. The present data suggest that TBC1D1 is a novel component in the regulation of insulin secretion in mouse pancreatic β-cells and modulates insulin granule dynamics and presumably K^+-ATP channel trafficking.

6.2 Zusammenfassung (Deutsch)

Fragestellung:

Die Rolle des Rab-GTPase aktivierenden Proteins (RabGAP) TBC1D1 wurde bereits sowohl für den Glukose- als auch den Lipidmetabolismus des Skelettmuskels beschrieben. TBC1D1 ist ebenfalls in pankreatischen β-Zellen exprimiert, seine Rolle in der glukose-stimulierten Insulinsekretion (GSIS) muss jedoch noch ermittelt werden. Kürzlich wurde gezeigt, dass TBC1D1 zur Insulinsekretion in isolierten β-Zellen der Ratte beiträgt, jedoch ohne detaillierte Einblicke in einen möglichen Mechanismus. Um die Rolle von TBC1D1 in der Insulinsekretion zu spezifizieren, wird seine Funktion im Zusammenhang mit verschiedenen sekretionsanregenden Substanzen in isolierten Inseln untersucht. Dazu werden Inseln von *Tbc1d1*-defizienten Mäusen, transgenen Mäusen, die *Tbc1d1* unter der Kontrolle des RIP2 Promotors exprimieren und *Tbc1d1*/*Tbc1d4*-doppel-defizienten Mäusen verwendet.

Material und Methoden:

Inseln der Maus wurden durch Collagenase-Perfusion des Pankreas durch den Pankreasgang und anschließendem Verdau des Pankreas isoliert. Die Inseln wurden für die Analyse der statischen und dynamischen Insulinsekretion nach Applikation verschiedener sekretionsanregender Substanzen verwendet. Ganz-Körper Glukosetoleranz wurde durch einen intraperitonealen Glukosetoleranztest in Mäusen ermittelt. Das präparierte Maus-Pankreas wurde für die histologische und morphometrische Analyse der Inseln verwendet sowie isolierte Inseln für die ultrastrukturelle Detektion und Quantifizierung der Insulingranula. Die zusätzliche Quantifizierung der Protein- und Genexpression mittels *Western Blot* und quantitativer *Real time PCR* wurde mit entsprechenden Lysaten isolierter Inseln durchgeführt. Die statistische Auswertung erfolgte durch angemessene Tests.

Ergebnisse:

Insulinsekretion nach 25 mM Glukosestimulation war in Inseln der D1KO Mäuse deutlich erhöht, während die Überexpression von *Tbc1d1* keinen Einfluss auf die GSIS hatte. In beiden Fällen war die Insulinsekretion bei 2 mM Glukose ähnlich. Darüber hinaus hatte der zusätzliche Verlust des TBC1D1 Homologs TBC1D4 keinen additiven Effekt auf die GSIS im Vergleich zur einzelnen *Tbc1d1*-Defizienz. Langerhans Inseln von normalen C57BL/6J Mäusen exprimieren ausschließlich die kurze Isoform von *Tbc1d1*, welches für die Generierung der transgenen Mäuse auf dem C57BL/6J Hintergrund (RIP2-TG) verwendet wurde. *Tbc1d1* mRNA war in Inseln deutlich stärker gegenüber *Tbc1d4* exprimiert. TBC1D1 wurde in den RIP2-TG Inseln 2,6-fach stärker exprimiert, als in den RIP2-WT Inseln, wohingegen TBC1D1

in D1KO Inseln nicht detektiert wurde. Die Perifusion von D1KO Inseln zeigte, dass die erhöhte GSIS auf eine Erhöhung beider Insulinsekretionsphasen zurückzuführen war. Der *Tbc1d1*-abhängige Effekt auf die Insulinsekretion *ex vivo* konnte *in vivo* nicht gezeigt werden. Obwohl keine Unterschiede in der generellen Inselmorphologie zwischen D1KO und WT Mäusen gefunden wurden, enthüllte die Transmissionselektronenmikroskopie eine erhöhte Dichte von sowohl blassen als auch dunklen Insulingranula in β-Zellen der D1KO Inseln nach Stimulation mit Glukose. Stimulation isolierter Inseln mit sowohl 1 µM des K^+-ATP Kanal-Inhibitors Glibenclamid bei 2 mM Glukose, als auch 500 µM Tolbutamid bei 5 mM Glukose, führte zu einer erhöhten Insulinsekretion in D1KO Inseln. Zusätzlich potenzierte Glibenclamid die GSIS mit 25 mM zwar in WT Inseln, jedoch nicht in D1KO Inseln. Im Gegensatz dazu wurde die Insulinsekretion bei basalen Glukosekonzentrationen weder durch 30-40 mM KCl, noch durch 5 µM des Kalzium-Ionophors A23187 genotyp-spezifisch verändert. Die Protein- und Genexpression einer Vielzahl von Genen, zeigte nur bei *Irs2* als relevantes Gen für Insulinsekretion und –synthese eine erhöhte Expression in D1KO Inseln.

Schlussfolgerungen:

Der Ausfall von TBC1D1 verändert die Glukose- und Sulfonylharnstoff-induzierte Insulinsekretion in isolierten Inseln durch die Erhöhung beider Insulinsekretionsphasen. Die β-Zell spezifische Überexpression der physiologisch relevanten kurzen *Tbc1d1* Isoform hat dagegen keinen Effekt auf die GSIS. Aufgrund potentieller Kompensationsmechanismen ist die erhöhte Insulinsekretion nach Glukosestimulation in D1KO Mäusen nicht ausgeprägt. Der Ausfall von TBC1D1 erhöht die glukose-induzierte Insulingranuladichte in β-Zellen. Die vorliegenden Daten weisen darauf hin, dass TBC1D1 ein neuer Bestandteil in der Regulation der Insulinsekretion der Mausinsel ist und die Dynamik der Insulingranula und möglicherweise die Translokation von K^+-ATP-Kanälen moduliert.

7 FURTHER QUESTIONS AND PERSPECTIVES

The presented thesis does not provide enough experimental information to draw a final conclusion about the mechanism by which TBC1D1 regulates insulin secretion from pancreatic β-cells. For this purpose additional experiments are necessary.

Obviously insulin granule dynamics are different in islets of D1KO mice. Although this thesis reports and increase in granule density after 60 minutes of glucose stimulation this represents just a snapshot of a highly dynamic process. Visualization of granule movement for example by TIRF microscopy would give a deeper insight into the dynamic processes as described in the literature [46, 237, 297]. In this regard it might be a relevant issue to also identify the responsible Rab-GTPases that are involved in the insulin vesicle translocation, regulated by TBC1D1.

One important experiment might be the measurement of K^+-ATP channel surface expression and maybe AICAR-stimulated insulin secretion at 25 mM glucose. Most available data on surface expression of $K_{ir}6.2$ and SUR1 subunits in islets were generated with biotinylation of surface proteins or HA-tagged constructs in rat pancreatic tissue or cell lines [200, 201, 248, 249, 298]. No relevant data were generated with mouse tissue. This might be due to a lack of good antibodies for mouse channel subunits. Moreover, for biotinylation of surface proteins lysine residues in the extracellular domains of the proteins are required to covalently link the biotin to the protein. Literature search (www.uniprot.org) revealed two extracellular domains in the $K_{ir}6.2$ protein in mouse and rat, but interestingly in both animals none of the two domains contains a lysine residue. In contrast rat SUR1 subunits contains more than one lysine residue in their multiple extracellular domains but the database has no information about the respective mouse sequence. The measurement of glucose- and sulfonylurea-induced changes in membrane potential and calcium flux in the islets of D1KO and WT mice would give a deeper insight into the role of TBC1D1 in the events of the triggering insulin secretion pathway.

The influence of the islet energy metabolism in D1KO mice on the changes in insulin secretion would give some more information about the events in insulin secretion. Mitochondrial activity and ATP production likely modulate the triggering pathway in an early state of the cell metabolism but also the amplifying pathway. Thus, the measurement of mitochondrial activity in D1KO islets by a flux analyzer (Seahorse Bioscience) will help to understand a potential role of the mitochondria in insulin secretion. That mitochondrial activity and mitochondrial metabolites have an influence on insulin secretion has been shown in recent publications [223, 299]. Another interesting question is, whether Rab27A is indeed a relevant substrate

for the native full length TBC1D1 in its short isoform. If this is the case the subcellular localization of TBC1D1 in the β-cells would be interesting to know, since this is also a yet unaddressed issue. The initial steps to answer this question were already taken, although they are not described in the present thesis. All commercially available antibodies against TBC1D1 are unable to work appropriately in immunohistochemistry approaches. With the use of the 3xFLAG-tagged *Tbc1d1* construct in the generation of the transgenic mice there is an available tool to use the FLAG-tag for the detection of TBC1D1 in histologic samples. The subcellular localization of TBC1D1 could be determined by transmission electron microscopy via labelling the FLAG-tag and use an immunogold-labelled secondary antibody to visualize the FLAG-tagged TBC1D1.

To investigate, whether TBC1D1 might also play a role in the cAMP-PKA-mediated pathway of insulin secretion the GAP activity of TBC1D1 towards the Rap1 protein would be something to evaluate.

One question that has not been addressed within this thesis is the impact of α-cell function on the described insulin secretion effects upon *Tbc1d1*-deficiency. Since it has been shown previously that α-cell to β-cell communication also affects insulin secretion [300, 301] it would be interesting to investigate also glucagon secretion or α-cell function in general.

It would also be interesting to know, whether the GTPase activity of TBC1D1 is necessary for the observed effects described in this thesis. Therefore an amino acid exchange from arginine to lysine (RK mutant) in the GAP domain of TBC1D1 [111] would lead to the expression of the protein but with an inactive GTPase activity. Such a construct could be used for the overexpression in β-cells.

Ultimately, it is possible that TBC1D1 has not only a single site of action and therefore a single mechanism in the regulation of insulin secretion, but multiple sites that act in concert are imaginable. Since TBC1D1 is a regulatory protein for cellular vesicle sorting, its functions in this regard are most likely.

8 REFERENCES AND LITERATURE

8.1 Scientific publications

1. Ryle, A.P., et al., *The disulphide bonds of insulin.* Biochem J, 1955. **60**(4): p. 541-56.
2. Nicol, D.S. and L.F. Smith, *Amino-acid sequence of human insulin.* Nature, 1960. **187**: p. 483-5.
3. Hanahan, D., *Heritable formation of pancreatic beta-cell tumours in transgenic mice expressing recombinant insulin/simian virus 40 oncogenes.* Nature, 1985. **315**(6015): p. 115-22.
4. Klip, A. and M.R. Paquet, *Glucose transport and glucose transporters in muscle and their metabolic regulation.* Diabetes Care, 1990. **13**(3): p. 228-43.
5. Levy, J., et al., *The stimulus-secretion coupling of glucose-induced insulin release. XX. fasting: a model for altered glucose recognition by the B-cell.* Metabolism, 1976. **25**(5): p. 583-91.
6. Maechler, P. and C.B. Wollheim, *Mitochondrial function in normal and diabetic beta-cells.* Nature, 2001. **414**(6865): p. 807-12.
7. Hedeskov, C.J. and K. Capito, *The effect of starvation on insulin secretion and glucose metabolism in mouse pancreatic islets.* Biochem J, 1974. **140**(3): p. 423-33.
8. Lammert, E., O. Cleaver, and D. Melton, *Induction of pancreatic differentiation by signals from blood vessels.* Science, 2001. **294**(5542): p. 564-7.
9. Thomsen, J., et al., *The amino acid sequence of human glucagon.* FEBS Lett, 1972. **21**(3): p. 315-319.
10. Barg, S., *Mechanisms of exocytosis in insulin-secreting B-cells and glucagon-secreting A-cells.* Pharmacol Toxicol, 2003. **92**(1): p. 3-13.
11. Liljenquist, J.E., et al., *Evidence for an important role of glucagon in the regulation of hepatic glucose production in normal man.* J Clin Invest, 1977. **59**(2): p. 369-74.
12. Cherrington, A.D., et al., *Differential time course of glucagon's effect on glycogenolysis and gluconeogenesis in the conscious dog.* Diabetes, 1981. **30**(3): p. 180-7.
13. Brubaker, P.L. and D.J. Drucker, *Structure-function of the glucagon receptor family of G protein-coupled receptors: the glucagon, GIP, GLP-1, and GLP-2 receptors.* Receptors Channels, 2002. **8**(3-4): p. 179-88.
14. Gerich, J.E., *Somatostatin and the endocrine pancreas.* Curr Top Mol Endocrinol, 1976. **3**: p. 127-43.
15. Konturek, S.J., et al., *Brain-gut axis in pancreatic secretion and appetite control.* J Physiol Pharmacol, 2003. **54**(3): p. 293-317.
16. Granata, R., et al., *Unraveling the role of the ghrelin gene peptides in the endocrine pancreas.* J Mol Endocrinol, 2010. **45**(3): p. 107-18.
17. Wittingen, J. and C.F. Frey, *Islet concentration in the head, body, tail and uncinate process of the pancreas.* Ann Surg, 1974. **179**(4): p. 412-4.
18. Henderson, J.R. and M.C. Moss, *A morphometric study of the endocrine and exocrine capillaries of the pancreas.* Q J Exp Physiol, 1985. **70**(3): p. 347-56.
19. Hellman, B., *The frequency distribution of the number and volume of the islets Langerhans in man. I. Studies on non-diabetic adults.* Acta Soc Med Ups, 1959. **64**: p. 432-60.
20. Kim, A., et al., *Islet architecture: A comparative study.* Islets, 2009. **1**(2): p. 129-36.
21. Huang, H.H., et al., *Low insulin content of large islet population is present in situ and in isolated islets.* Islets, 2011. **3**(1): p. 6-13.
22. Malaisse, W.J., *Regulation, perturbation, and correction of metabolic events in pancreatic islets.* Acta Diabetol, 1996. **33**(3): p. 173-9.
23. De Vos, A., et al., *Human and rat beta cells differ in glucose transporter but not in glucokinase gene expression.* J Clin Invest, 1995. **96**(5): p. 2489-95.

24. Johnson, J.H., et al., *The high Km glucose transporter of islets of Langerhans is functionally similar to the low affinity transporter of liver and has an identical primary sequence.* J Biol Chem, 1990. **265**(12): p. 6548-51.
25. Ashcroft, S.J. and P.J. Randle, *Glucose phosphorylation in mouse pancreatic islets.* Biochem J, 1968. **107**(4): p. 599-600.
26. Niemeyer, H., T. Ureta, and L. Clark-Turri, *Adaptive character of liver glucokinase.* Mol Cell Biochem, 1975. **6**(2): p. 109-26.
27. Iynedjian, P.B., *Molecular physiology of mammalian glucokinase.* Cell Mol Life Sci, 2009. **66**(1): p. 27-42.
28. Ashcroft, S.J. and P.J. Randle, *Enzymes of glucose metabolism in normal mouse pancreatic islets.* Biochem J, 1970. **119**(1): p. 5-15.
29. Matschinsky, F.M., *Banting Lecture 1995. A lesson in metabolic regulation inspired by the glucokinase glucose sensor paradigm.* Diabetes, 1996. **45**(2): p. 223-41.
30. Ashcroft, F.M., D.E. Harrison, and S.J. Ashcroft, *Glucose induces closure of single potassium channels in isolated rat pancreatic beta-cells.* Nature, 1984. **312**(5993): p. 446-8.
31. Ashcroft, F.M. and P. Rorsman, *Electrophysiology of the pancreatic beta-cell.* Prog Biophys Mol Biol, 1989. **54**(2): p. 87-143.
32. Cook, D.L. and C.N. Hales, *Intracellular ATP directly blocks K+ channels in pancreatic B-cells.* Nature, 1984. **311**(5983): p. 271-3.
33. Henquin, J.C., *D-glucose inhibits potassium efflux from pancreatic islet cells.* Nature, 1978. **271**(5642): p. 271-3.
34. Sturgess, N.C., et al., *The sulphonylurea receptor may be an ATP-sensitive potassium channel.* Lancet, 1985. **2**(8453): p. 474-5.
35. Hiriart, M. and L. Aguilar-Bryan, *Channel regulation of glucose sensing in the pancreatic beta-cell.* Am J Physiol Endocrinol Metab, 2008. **295**(6): p. E1298-306.
36. Gilon, P., R.M. Shepherd, and J.C. Henquin, *Oscillations of secretion driven by oscillations of cytoplasmic Ca2+ as evidences in single pancreatic islets.* J Biol Chem, 1993. **268**(30): p. 22265-8.
37. Tomas, A., et al., *Regulation of pancreatic beta-cell insulin secretion by actin cytoskeleton remodelling: role of gelsolin and cooperation with the MAPK signalling pathway.* J Cell Sci, 2006. **119**(Pt 10): p. 2156-67.
38. Llanos, P., et al., *Glucose-Dependent Insulin Secretion in Pancreatic beta-Cell Islets from Male Rats Requires Ca2+ Release via ROS-Stimulated Ryanodine Receptors.* PLoS One, 2015. **10**(6): p. e0129238.
39. Santulli, G., et al., *Calcium release channel RyR2 regulates insulin release and glucose homeostasis.* J Clin Invest, 2015. **125**(5): p. 1968-78.
40. Daniel, S., et al., *Identification of the docked granule pool responsible for the first phase of glucose-stimulated insulin secretion.* Diabetes, 1999. **48**(9): p. 1686-90.
41. Ohara-Imaizumi, M., et al., *Imaging analysis reveals mechanistic differences between first- and second-phase insulin exocytosis.* J Cell Biol, 2007. **177**(4): p. 695-705.
42. Ohara-Imaizumi, M., et al., *Imaging exocytosis of single insulin secretory granules with evanescent wave microscopy: distinct behavior of granule motion in biphasic insulin release.* J Biol Chem, 2002. **277**(6): p. 3805-8.
43. Ohara-Imaizumi, M., et al., *TIRF imaging of docking and fusion of single insulin granule motion in primary rat pancreatic beta-cells: different behaviour of granule motion between normal and Goto-Kakizaki diabetic rat beta-cells.* Biochem J, 2004. **381**(Pt 1): p. 13-8.
44. Olofsson, C.S., et al., *Fast insulin secretion reflects exocytosis of docked granules in mouse pancreatic B-cells.* Pflugers Arch, 2002. **444**(1-2): p. 43-51.
45. Seino, S., T. Shibasaki, and K. Minami, *Dynamics of insulin secretion and the clinical implications for obesity and diabetes.* J Clin Invest, 2011. **121**(6): p. 2118-25.
46. Dehghany, J., et al., *A Spatial Model of Insulin-Granule Dynamics in Pancreatic beta-Cells.* Traffic, 2015. **16**(8): p. 797-813.

47. Ullrich, S., *Glucose-induced insulin secretion: is the small G-protein Rab27A the mediator of the K(ATP) channel-independent effect?* J Physiol, 2008. **586**(22): p. 5291.
48. Dunne, M.J., et al., *Hyperinsulinism in infancy: from basic science to clinical disease.* Physiol Rev, 2004. **84**(1): p. 239-75.
49. Efendic, S. and N. Portwood, *Overview of incretin hormones.* Horm Metab Res, 2004. **36**(11-12): p. 742-6.
50. Meier, J.J. and M.A. Nauck, *Glucagon-like peptide 1(GLP-1) in biology and pathology.* Diabetes Metab Res Rev, 2005. **21**(2): p. 91-117.
51. Thorens, B., *Glucagon-like peptide-1 and control of insulin secretion.* Diabete Metab, 1995. **21**(5): p. 311-8.
52. Thorens, B., *Expression cloning of the pancreatic beta cell receptor for the gluco-incretin hormone glucagon-like peptide 1.* Proc Natl Acad Sci U S A, 1992. **89**(18): p. 8641-5.
53. Crespin, S.R., W.B. Greenough, 3rd, and D. Steinberg, *Stimulation of insulin secretion by infusion of free fatty acids.* J Clin Invest, 1969. **48**(10): p. 1934-43.
54. Haber, E.P., et al., *Palmitate modulates the early steps of insulin signalling pathway in pancreatic islets.* FEBS Lett, 2003. **544**(1-3): p. 185-8.
55. Haber, E.P., et al., *Pleiotropic effects of fatty acids on pancreatic beta-cells.* J Cell Physiol, 2003. **194**(1): p. 1-12.
56. Parker, S.M., et al., *Palmitate potentiation of glucose-induced insulin release: a study using 2-bromopalmitate.* Metabolism, 2003. **52**(10): p. 1367-71.
57. Itoh, Y., et al., *Free fatty acids regulate insulin secretion from pancreatic beta cells through GPR40.* Nature, 2003. **422**(6928): p. 173-6.
58. Liu, Z., et al., *Dose- and Glucose-Dependent Effects of Amino Acids on Insulin Secretion from Isolated Mouse Islets and Clonal INS-1E Beta-Cells.* Rev Diabet Stud, 2008. **5**(4): p. 232-44.
59. Dufer, M., et al., *Activation of the AMP-activated protein kinase enhances glucose-stimulated insulin secretion in mouse beta-cells.* Islets, 2010. **2**(3): p. 156-63.
60. Corton, J.M., et al., *5-aminoimidazole-4-carboxamide ribonucleoside. A specific method for activating AMP-activated protein kinase in intact cells?* Eur J Biochem, 1995. **229**(2): p. 558-65.
61. Winder, W.W., *Energy-sensing and signaling by AMP-activated protein kinase in skeletal muscle.* J Appl Physiol (1985), 2001. **91**(3): p. 1017-28.
62. Halban, P.A., et al., *The possible importance of contact between pancreatic islet cells for the control of insulin release.* Endocrinology, 1982. **111**(1): p. 86-94.
63. Hopcroft, D.W., D.R. Mason, and R.S. Scott, *Structure-function relationships in pancreatic islets: support for intraislet modulation of insulin secretion.* Endocrinology, 1985. **117**(5): p. 2073-80.
64. Konstantinova, I., et al., *EphA-Ephrin-A-mediated beta cell communication regulates insulin secretion from pancreatic islets.* Cell, 2007. **129**(2): p. 359-70.
65. Luther, M.J., et al., *MIN6 beta-cell-beta-cell interactions influence insulin secretory responses to nutrients and non-nutrients.* Biochem Biophys Res Commun, 2006. **343**(1): p. 99-104.
66. Pipeleers, D., et al., *Glucose-induced insulin release depends on functional cooperation between islet cells.* Proc Natl Acad Sci U S A, 1982. **79**(23): p. 7322-5.
67. Jain, R., et al., *Pharmacological inhibition of Eph receptors enhances glucose-stimulated insulin secretion from mouse and human pancreatic islets.* Diabetologia, 2013. **56**(6): p. 1350-5.
68. Anderson, E. and F.E. Wherry, *Studies on the effect of tolbutamide on insulin secretion.* Proc Soc Exp Biol Med, 1962. **111**: p. 446-50.
69. Loubatieres, A., et al., *[Experimental study of a new especially active hypoglycemic sulfonamide, HB-419 or Glibenclamide].* Diabetologia, 1969. **5**(1): p. 1-10.
70. Pfeiffer, E.F., et al., *Clinical and experimental studies of insulin secretion following tolbutamide and metahexamide administration.* Ann N Y Acad Sci, 1959. **82**: p. 479-95.

71. Schmid-Antomarchi, H., et al., *The antidiabetic sulfonylurea glibenclamide is a potent blocker of the ATP-modulated K+ channel in insulin secreting cells.* Biochem Biophys Res Commun, 1987. **146**(1): p. 21-5.
72. Howell, S.L. and K.W. Taylor, *Potassium ions and the secretion of insulin by islets of Langerhans incubated in vitro.* Biochem J, 1968. **108**(1): p. 17-24.
73. Wollheim, C.B., et al., *Calcium-induced insulin release in monolayer culture of the endocrine pancreas. Studies with ionophore A23187.* J Biol Chem, 1975. **250**(4): p. 1354-60.
74. Cantley, J., *The control of insulin secretion by adipokines: current evidence for adipocyte-beta cell endocrine signalling in metabolic homeostasis.* Mamm Genome, 2014. **25**(9-10): p. 442-54.
75. Goberna, R., et al., *Action of B-hydroxy butyrate, acetoacetate and palmitate on the insulin release in the perfused isolated rat pancreas.* Horm Metab Res, 1974. **6**(4): p. 256-60.
76. Gromada, J., et al., *Neuronal calcium sensor-1 potentiates glucose-dependent exocytosis in pancreatic beta cells through activation of phosphatidylinositol 4-kinase beta.* Proc Natl Acad Sci U S A, 2005. **102**(29): p. 10303-8.
77. Gurgul-Convey, E., K. Hanzelka, and S. Lenzen, *Mechanism of prostacyclin-induced potentiation of glucose-induced insulin secretion.* Endocrinology, 2012. **153**(6): p. 2612-22.
78. Jitrapakdee, S., et al., *Regulation of insulin secretion: role of mitochondrial signalling.* Diabetologia, 2010. **53**(6): p. 1019-32.
79. Marquard, J., et al., *Effects of dextromethorphan as add-on to sitagliptin on blood glucose and serum insulin concentrations in individuals with type 2 diabetes mellitus: a randomized, placebo-controlled, double-blinded, multiple crossover, single-dose clinical trial.* Diabetes Obes Metab, 2016. **18**(1): p. 100-3.
80. Ohara-Imaizumi, M., et al., *Serotonin regulates glucose-stimulated insulin secretion from pancreatic beta cells during pregnancy.* Proc Natl Acad Sci U S A, 2013. **110**(48): p. 19420-5.
81. Patane, G., et al., *Adiponectin increases glucose-induced insulin secretion through the activation of lipid oxidation.* Acta Diabetol, 2013. **50**(6): p. 851-7.
82. Paulmann, N., et al., *Intracellular serotonin modulates insulin secretion from pancreatic beta-cells by protein serotonylation.* PLoS Biol, 2009. **7**(10): p. e1000229.
83. Vetterli, L., et al., *Resveratrol potentiates glucose-stimulated insulin secretion in INS-1E beta-cells and human islets through a SIRT1-dependent mechanism.* J Biol Chem, 2011. **286**(8): p. 6049-60.
84. Lang, J., *Molecular mechanisms and regulation of insulin exocytosis as a paradigm of endocrine secretion.* Eur J Biochem, 1999. **259**(1-2): p. 3-17.
85. Sollner, T., et al., *SNAP receptors implicated in vesicle targeting and fusion.* Nature, 1993. **362**(6418): p. 318-24.
86. Burgoyne, R.D. and A. Morgan, *Secretory granule exocytosis.* Physiol Rev, 2003. **83**(2): p. 581-632.
87. Schvartz, D., et al., *Improved characterization of the insulin secretory granule proteomes.* J Proteomics, 2012. **75**(15): p. 4620-31.
88. Suckale, J. and M. Solimena, *The insulin secretory granule as a signaling hub.* Trends Endocrinol Metab, 2010. **21**(10): p. 599-609.
89. Brown, H., et al., *Cysteine string protein (CSP) is an insulin secretory granule-associated protein regulating beta-cell exocytosis.* EMBO J, 1998. **17**(17): p. 5048-58.
90. Latreille, M., et al., *MicroRNA-7a regulates pancreatic beta cell function.* J Clin Invest, 2014. **124**(6): p. 2722-35.
91. Sharma, M., J. Burre, and T.C. Sudhof, *CSPalpha promotes SNARE-complex assembly by chaperoning SNAP-25 during synaptic activity.* Nat Cell Biol, 2011. **13**(1): p. 30-9.
92. Zhang, H., et al., *Mutational analysis of cysteine-string protein function in insulin exocytosis.* J Cell Sci, 1999. **112 (Pt 9)**: p. 1345-51.

93. Zhang, H., et al., *Cysteine-string proteins regulate exocytosis of insulin independent from transmembrane ion fluxes.* FEBS Lett, 1998. **437**(3): p. 267-72.
94. Jewell, J.L., E. Oh, and D.C. Thurmond, *Exocytosis mechanisms underlying insulin release and glucose uptake: conserved roles for Munc18c and syntaxin 4.* Am J Physiol Regul Integr Comp Physiol, 2010. **298**(3): p. R517-31.
95. Patti, M.E. and C.R. Kahn, *The insulin receptor--a critical link in glucose homeostasis and insulin action.* J Basic Clin Physiol Pharmacol, 1998. **9**(2-4): p. 89-109.
96. Lee, J. and P.F. Pilch, *The insulin receptor: structure, function, and signaling.* Am J Physiol, 1994. **266**(2 Pt 1): p. C319-34.
97. Rosen, O.M., et al., *Phosphorylation activates the insulin receptor tyrosine protein kinase.* Proc Natl Acad Sci U S A, 1983. **80**(11): p. 3237-40.
98. Eck, M.J., et al., *Structure of the IRS-1 PTB domain bound to the juxtamembrane region of the insulin receptor.* Cell, 1996. **85**(5): p. 695-705.
99. Kaburagi, Y., et al., *The role of the NPXY motif in the insulin receptor in tyrosine phosphorylation of insulin receptor substrate-1 and Shc.* Endocrinology, 1995. **136**(8): p. 3437-43.
100. Sun, X.J., et al., *Structure of the insulin receptor substrate IRS-1 defines a unique signal transduction protein.* Nature, 1991. **352**(6330): p. 73-7.
101. Endemann, G., K. Yonezawa, and R.A. Roth, *Phosphatidylinositol kinase or an associated protein is a substrate for the insulin receptor tyrosine kinase.* J Biol Chem, 1990. **265**(1): p. 396-400.
102. Ruderman, N.B., et al., *Activation of phosphatidylinositol 3-kinase by insulin.* Proc Natl Acad Sci U S A, 1990. **87**(4): p. 1411-5.
103. Wardzala, L.J., S.W. Cushman, and L.B. Salans, *Mechanism of insulin action on glucose transport in the isolated rat adipose cell. Enhancement of the number of functional transport systems.* J Biol Chem, 1978. **253**(22): p. 8002-5.
104. Hawkins, P.T., et al., *Signalling through Class I PI3Ks in mammalian cells.* Biochem Soc Trans, 2006. **34**(Pt 5): p. 647-62.
105. Franke, T.F., et al., *Direct regulation of the Akt proto-oncogene product by phosphatidylinositol-3,4-bisphosphate.* Science, 1997. **275**(5300): p. 665-8.
106. Currie, R.A., et al., *Role of phosphatidylinositol 3,4,5-trisphosphate in regulating the activity and localization of 3-phosphoinositide-dependent protein kinase-1.* Biochem J, 1999. **337 (Pt 3)**: p. 575-83.
107. Alessi, D.R., et al., *Characterization of a 3-phosphoinositide-dependent protein kinase which phosphorylates and activates protein kinase Balpha.* Curr Biol, 1997. **7**(4): p. 261-9.
108. Sarbassov, D.D., et al., *Phosphorylation and regulation of Akt/PKB by the rictor-mTOR complex.* Science, 2005. **307**(5712): p. 1098-101.
109. Gonzalez, E. and T.E. McGraw, *Insulin signaling diverges into Akt-dependent and -independent signals to regulate the recruitment/docking and the fusion of GLUT4 vesicles to the plasma membrane.* Mol Biol Cell, 2006. **17**(10): p. 4484-93.
110. Kane, S., et al., *A method to identify serine kinase substrates. Akt phosphorylates a novel adipocyte protein with a Rab GTPase-activating protein (GAP) domain.* J Biol Chem, 2002. **277**(25): p. 22115-8.
111. Roach, W.G., et al., *Substrate specificity and effect on GLUT4 translocation of the Rab GTPase-activating protein Tbc1d1.* Biochem J, 2007. **403**(2): p. 353-8.
112. Sano, H., et al., *Insulin-stimulated phosphorylation of a Rab GTPase-activating protein regulates GLUT4 translocation.* J Biol Chem, 2003. **278**(17): p. 14599-602.
113. Bottazzo, G.F., A. Florin-Christensen, and D. Doniach, *Islet-cell antibodies in diabetes mellitus with autoimmune polyendocrine deficiencies.* Lancet, 1974. **2**(7892): p. 1279-83.
114. Knip, M., et al., *Environmental triggers and determinants of type 1 diabetes.* Diabetes, 2005. **54 Suppl 2**: p. S125-36.
115. Craighead, J.E., *Current views on the etiology of insulin-dependent diabetes mellitus.* N Engl J Med, 1978. **299**(26): p. 1439-45.

116. Ionescu-Tirgoviste, C., P.A. Gagniuc, and C. Guja, *Structural Properties of Gene Promoters Highlight More than Two Phenotypes of Diabetes.* PLoS One, 2015. **10**(9): p. e0137950.
117. Nolan, C.J., P. Damm, and M. Prentki, *Type 2 diabetes across generations: from pathophysiology to prevention and management.* Lancet, 2011. **378**(9786): p. 169-81.
118. Rett, K., M. Wicklmayr, and E. Standl, *[The metabolic syndrome. Pathophysiologic causes, diagnosis, therapy].* Wien Klin Wochenschr, 1994. **106**(24): p. 750-7.
119. Kasuga, M., *Insulin resistance and pancreatic beta cell failure.* J Clin Invest, 2006. **116**(7): p. 1756-60.
120. Seino, S., *Cell signalling in insulin secretion: the molecular targets of ATP, cAMP and sulfonylurea.* Diabetologia, 2012. **55**(8): p. 2096-108.
121. Hutagalung, A.H. and P.J. Novick, *Role of Rab GTPases in membrane traffic and cell physiology.* Physiol Rev, 2011. **91**(1): p. 119-49.
122. Ishikura, S., A. Koshkina, and A. Klip, *Small G proteins in insulin action: Rab and Rho families at the crossroads of signal transduction and GLUT4 vesicle traffic.* Acta Physiol (Oxf), 2008. **192**(1): p. 61-74.
123. Stenmark, H., *Rab GTPases as coordinators of vesicle traffic.* Nat Rev Mol Cell Biol, 2009. **10**(8): p. 513-25.
124. Araki, S., et al., *Regulation of reversible binding of smg p25A, a ras p21-like GTP-binding protein, to synaptic plasma membranes and vesicles by its specific regulatory protein, GDP dissociation inhibitor.* J Biol Chem, 1990. **265**(22): p. 13007-15.
125. Pereira-Leal, J.B., A.N. Hume, and M.C. Seabra, *Prenylation of Rab GTPases: molecular mechanisms and involvement in genetic disease.* FEBS Lett, 2001. **498**(2-3): p. 197-200.
126. Pereira-Leal, J.B. and M.C. Seabra, *The mammalian Rab family of small GTPases: definition of family and subfamily sequence motifs suggests a mechanism for functional specificity in the Ras superfamily.* J Mol Biol, 2000. **301**(4): p. 1077-87.
127. Rak, A., et al., *Crystal structure of the GAP domain of Gyp1p: first insights into interaction with Ypt/Rab proteins.* EMBO J, 2000. **19**(19): p. 5105-13.
128. West, M., H.F. Kung, and T. Kamata, *A novel membrane factor stimulates guanine nucleotide exchange reaction of ras proteins.* FEBS Lett, 1990. **259**(2): p. 245-8.
129. Trahey, M. and F. McCormick, *A cytoplasmic protein stimulates normal N-ras p21 GTPase, but does not affect oncogenic mutants.* Science, 1987. **238**(4826): p. 542-5.
130. Chen, D., et al., *Molecular cloning and characterization of rab27a and rab27b, novel human rab proteins shared by melanocytes and platelets.* Biochem Mol Med, 1997. **60**(1): p. 27-37.
131. Stinchcombe, J.C., et al., *Rab27a is required for regulated secretion in cytotoxic T lymphocytes.* J Cell Biol, 2001. **152**(4): p. 825-34.
132. Yi, Z., et al., *The Rab27a/granuphilin complex regulates the exocytosis of insulin-containing dense-core granules.* Mol Cell Biol, 2002. **22**(6): p. 1858-67.
133. Kasai, K., et al., *Rab27a mediates the tight docking of insulin granules onto the plasma membrane during glucose stimulation.* J Clin Invest, 2005. **115**(2): p. 388-96.
134. Cheviet, S., et al., *The Rab-binding protein Noc2 is associated with insulin-containing secretory granules and is essential for pancreatic beta-cell exocytosis.* Mol Endocrinol, 2004. **18**(1): p. 117-26.
135. Kimura, T., et al., *The GDP-dependent Rab27a effector coronin 3 controls endocytosis of secretory membrane in insulin-secreting cell lines.* J Cell Sci, 2008. **121**(Pt 18): p. 3092-8.
136. Yamaoka, M., T. Ishizaki, and T. Kimura, *Interplay between Rab27a effectors in pancreatic beta-cells.* World J Diabetes, 2015. **6**(3): p. 508-16.
137. Itoh, T. and M. Fukuda, *Identification of EPI64 as a GTPase-activating protein specific for Rab27A.* J Biol Chem, 2006. **281**(42): p. 31823-31.
138. Hou, Y., et al., *EPI64B acts as a GTPase-activating protein for Rab27B in pancreatic acinar cells.* J Biol Chem, 2013. **288**(27): p. 19548-57.

139. Imai, A., et al., *EPI64 protein functions as a physiological GTPase-activating protein for Rab27 protein and regulates amylase release in rat parotid acinar cells.* J Biol Chem, 2011. **286**(39): p. 33854-62.
140. Marat, A.L., H. Dokainish, and P.S. McPherson, *DENN domain proteins: regulators of Rab GTPases.* J Biol Chem, 2011. **286**(16): p. 13791-800.
141. Strom, M., et al., *A yeast GTPase-activating protein that interacts specifically with a member of the Ypt/Rab family.* Nature, 1993. **361**(6414): p. 736-9.
142. Richardson, P.M. and L.I. Zon, *Molecular cloning of a cDNA with a novel domain present in the tre-2 oncogene and the yeast cell cycle regulators BUB2 and cdc16.* Oncogene, 1995. **11**(6): p. 1139-48.
143. Fukuda, M., et al., *Large scale screening for novel rab effectors reveals unexpected broad Rab binding specificity.* Mol Cell Proteomics, 2008. **7**(6): p. 1031-42.
144. Kanno, E., et al., *Comprehensive screening for novel rab-binding proteins by GST pull-down assay using 60 different mammalian Rabs.* Traffic, 2010. **11**(4): p. 491-507.
145. Gao, X.D., et al., *The GAP activity of Msb3p and Msb4p for the Rab GTPase Sec4p is required for efficient exocytosis and actin organization.* J Cell Biol, 2003. **162**(4): p. 635-46.
146. Pan, X., et al., *TBC-domain GAPs for Rab GTPases accelerate GTP hydrolysis by a dual-finger mechanism.* Nature, 2006. **442**(7100): p. 303-6.
147. Frasa, M.A., et al., *Illuminating the functional and structural repertoire of human TBC/RABGAPs.* Nat Rev Mol Cell Biol, 2012. **13**(2): p. 67-73.
148. Haas, A.K., et al., *A GTPase-activating protein controls Rab5 function in endocytic trafficking.* Nat Cell Biol, 2005. **7**(9): p. 887-93.
149. Itoh, T., et al., *Screening for target Rabs of TBC (Tre-2/Bub2/Cdc16) domain-containing proteins based on their Rab-binding activity.* Genes Cells, 2006. **11**(9): p. 1023-37.
150. Fukuda, M., *TBC proteins: GAPs for mammalian small GTPase Rab?* Biosci Rep, 2011. **31**(3): p. 159-68.
151. Miinea, C.P., et al., *AS160, the Akt substrate regulating GLUT4 translocation, has a functional Rab GTPase-activating protein domain.* Biochem J, 2005. **391**(Pt 1): p. 87-93.
152. An, D., et al., *TBC1D1 regulates insulin- and contraction-induced glucose transport in mouse skeletal muscle.* Diabetes, 2010. **59**(6): p. 1358-65.
153. Baus, D., et al., *Identification of a novel AS160 splice variant that regulates GLUT4 translocation and glucose-uptake in rat muscle cells.* Cell Signal, 2008. **20**(12): p. 2237-46.
154. Brewer, P.D., et al., *Loss of AS160 Akt substrate causes Glut4 protein to accumulate in compartments that are primed for fusion in basal adipocytes.* J Biol Chem, 2011. **286**(30): p. 26287-97.
155. Chadt, A., et al., *"Deletion of both Rab-GTPase-activating proteins TBC1D1 and TBC1D4 in mice eliminates insulin- and AICAR-stimulated glucose transport [corrected].* Diabetes, 2015. **64**(3): p. 746-59.
156. Chadt, A., et al., *Tbc1d1 mutation in lean mouse strain confers leanness and protects from diet-induced obesity.* Nat Genet, 2008. **40**(11): p. 1354-9.
157. Chavez, J.A., et al., *Inhibition of GLUT4 translocation by Tbc1d1, a Rab GTPase-activating protein abundant in skeletal muscle, is partially relieved by AMP-activated protein kinase activation.* J Biol Chem, 2008. **283**(14): p. 9187-95.
158. Chen, S., et al., *Complementary regulation of TBC1D1 and AS160 by growth factors, insulin and AMPK activators.* Biochem J, 2008. **409**(2): p. 449-59.
159. Dokas, J., et al., *Conventional knockout of Tbc1d1 in mice impairs insulin- and AICAR-stimulated glucose uptake in skeletal muscle.* Endocrinology, 2013. **154**(10): p. 3502-14.
160. Hargett, S.R., N.N. Walker, and S.R. Keller, *Rab GAPs AS160 and Tbc1d1 play non-redundant roles in the regulation of glucose and energy homeostasis in mice.* Am J Physiol Endocrinol Metab, 2015: p. ajpendo 00342 2015.

161. Jessen, N., et al., *Exercise increases TBC1D1 phosphorylation in human skeletal muscle.* Am J Physiol Endocrinol Metab, 2011. **301**(1): p. E164-71.
162. Kane, S. and G.E. Lienhard, *Calmodulin binds to the Rab GTPase activating protein required for insulin-stimulated GLUT4 translocation.* Biochem Biophys Res Commun, 2005. **335**(1): p. 175-80.
163. Lansey, M.N., et al., *Deletion of Rab GAP AS160 modifies glucose uptake and GLUT4 translocation in primary skeletal muscles and adipocytes and impairs glucose homeostasis.* Am J Physiol Endocrinol Metab, 2012. **303**(10): p. E1273-86.
164. Sakamoto, K. and G.D. Holman, *Emerging role for AS160/TBC1D4 and TBC1D1 in the regulation of GLUT4 traffic.* Am J Physiol Endocrinol Metab, 2008. **295**(1): p. E29-37.
165. Slot, J.W., et al., *Translocation of the glucose transporter GLUT4 in cardiac myocytes of the rat.* Proc Natl Acad Sci U S A, 1991. **88**(17): p. 7815-9.
166. Stone, S., et al., *TBC1D1 is a candidate for a severe obesity gene and evidence for a gene/gene interaction in obesity predisposition.* Hum Mol Genet, 2006. **15**(18): p. 2709-20.
167. Szekeres, F., et al., *The Rab-GTPase-activating protein TBC1D1 regulates skeletal muscle glucose metabolism.* Am J Physiol Endocrinol Metab, 2012. **303**(4): p. E524-33.
168. Taylor, E.B., et al., *Discovery of TBC1D1 as an insulin-, AICAR-, and contraction-stimulated signaling nexus in mouse skeletal muscle.* J Biol Chem, 2008. **283**(15): p. 9787-96.
169. Vichaiwong, K., et al., *Contraction regulates site-specific phosphorylation of TBC1D1 in skeletal muscle.* Biochem J, 2010. **431**(2): p. 311-20.
170. Wilson, C.M. and S.W. Cushman, *Insulin stimulation of glucose transport activity in rat skeletal muscle: increase in cell surface GLUT4 as assessed by photolabelling.* Biochem J, 1994. **299 (Pt 3)**: p. 755-9.
171. Treebak, J.T., et al., *Identification of a novel phosphorylation site on TBC1D4 regulated by AMP-activated protein kinase in skeletal muscle.* Am J Physiol Cell Physiol, 2010. **298**(2): p. C377-85.
172. Dash, S., et al., *A truncation mutation in TBC1D4 in a family with acanthosis nigricans and postprandial hyperinsulinemia.* Proc Natl Acad Sci U S A, 2009. **106**(23): p. 9350-5.
173. Bouzakri, K., et al., *Rab GTPase-activating protein AS160 is a major downstream effector of protein kinase B/Akt signaling in pancreatic beta-cells.* Diabetes, 2008. **57**(5): p. 1195-204.
174. Rutti, S., et al., *Expression, phosphorylation and function of the Rab-GTPase activating protein TBC1D1 in pancreatic beta-cells.* FEBS Lett, 2014. **588**(1): p. 15-20.
175. Protzek, A.O., et al., *Augmented beta-Cell Function and Mass in Glucocorticoid-Treated Rodents Are Associated with Increased Islet Ir-beta /AKT/mTOR and Decreased AMPK/ACC and AS160 Signaling.* Int J Endocrinol, 2014. **2014**: p. 983453.
176. Burnette, W.N., *"Western blotting": electrophoretic transfer of proteins from sodium dodecyl sulfate--polyacrylamide gels to unmodified nitrocellulose and radiographic detection with antibody and radioiodinated protein A.* Anal Biochem, 1981. **112**(2): p. 195-203.
177. Hashimoto, F., et al., *An improved method for separation of low-molecular-weight polypeptides by electrophoresis in sodium dodecyl sulfate-polyacrylamide gel.* Anal Biochem, 1983. **129**(1): p. 192-9.
178. Gultekin, H. and K.H. Heermann, *The use of polyvinylidenedifluoride membranes as a general blotting matrix.* Anal Biochem, 1988. **172**(2): p. 320-9.
179. Belz, M., et al., *Insulinotropic effect of high potassium concentration beyond plasma membrane depolarization.* Am J Physiol Endocrinol Metab, 2014. **306**(6): p. E697-706.

180. Sutherland, B.W., J. Toews, and J. Kast, *Utility of formaldehyde cross-linking and mass spectrometry in the study of protein-protein interactions.* J Mass Spectrom, 2008. **43**(6): p. 699-715.
181. Llewellyn, B.D., *Nuclear staining with alum hematoxylin.* Biotech Histochem, 2009. **84**(4): p. 159-77.
182. Weibel, E.R., *Stereological principles for morphometry in electron microscopic cytology.* Int Rev Cytol, 1969. **26**: p. 235-302.
183. Spurr, A.R., *A low-viscosity epoxy resin embedding medium for electron microscopy.* J Ultrastruct Res, 1969. **26**(1): p. 31-43.
184. Livak, K.J. and T.D. Schmittgen, *Analysis of relative gene expression data using real-time quantitative PCR and the 2(-Delta Delta C(T)) Method.* Methods, 2001. **25**(4): p. 402-8.
185. Kataoka, K., et al., *MafA is a glucose-regulated and pancreatic beta-cell-specific transcriptional activator for the insulin gene.* J Biol Chem, 2002. **277**(51): p. 49903-10.
186. Madsen, O.D., et al., *Transcription factors contributing to the pancreatic beta-cell phenotype.* Horm Metab Res, 1997. **29**(6): p. 265-70.
187. Raum, J.C., et al., *FoxA2, Nkx2.2, and PDX-1 regulate islet beta-cell-specific mafA expression through conserved sequences located between base pairs -8118 and -7750 upstream from the transcription start site.* Mol Cell Biol, 2006. **26**(15): p. 5735-43.
188. Talchai, C., et al., *Pancreatic beta cell dedifferentiation as a mechanism of diabetic beta cell failure.* Cell, 2012. **150**(6): p. 1223-34.
189. Poirier, M.A., et al., *Protease resistance of syntaxin.SNAP-25.VAMP complexes. Implications for assembly and structure.* J Biol Chem, 1998. **273**(18): p. 11370-7.
190. Bai, L., L.A. Swayne, and J.E. Braun, *The CSPalpha/G protein complex in PC12 cells.* Biochem Biophys Res Commun, 2007. **352**(1): p. 123-9.
191. Nie, Z., et al., *Overexpression of cysteine-string proteins in Drosophila reveals interactions with syntaxin.* J Neurosci, 1999. **19**(23): p. 10270-9.
192. Efanov, A.M., S.V. Zaitsev, and P.O. Berggren, *Inositol hexakisphosphate stimulates non-Ca2+-mediated and primes Ca2+-mediated exocytosis of insulin by activation of protein kinase C.* Proc Natl Acad Sci U S A, 1997. **94**(9): p. 4435-9.
193. Eliasson, L., et al., *PKC-dependent stimulation of exocytosis by sulfonylureas in pancreatic beta cells.* Science, 1996. **271**(5250): p. 813-5.
194. Geng, X., et al., *alpha-Synuclein binds the K(ATP) channel at insulin-secretory granules and inhibits insulin secretion.* Am J Physiol Endocrinol Metab, 2011. **300**(2): p. E276-86.
195. Hribal, M.L., F. Oriente, and D. Accili, *Mouse models of insulin resistance.* Am J Physiol Endocrinol Metab, 2002. **282**(5): p. E977-81.
196. Mohanty, S., et al., *Overexpression of IRS2 in isolated pancreatic islets causes proliferation and protects human beta-cells from hyperglycemia-induced apoptosis.* Exp Cell Res, 2005. **303**(1): p. 68-78.
197. Martina, M., G. Kilic, and E. Cherubini, *The effect of intracellular Ca2+ on GABA-activated currents in cerebellar granule cells in culture.* J Membr Biol, 1994. **142**(2): p. 209-16.
198. Wang, X., et al., *Intracellular calcium dependent activation of p72syk in platelets.* J Biochem, 1994. **116**(4): p. 858-61.
199. Cui, X., et al., *Akt signals upstream of L-type calcium channels to optimize insulin secretion.* Pancreas, 2012. **41**(1): p. 15-21.
200. Park, S.H., W.K. Ho, and J.H. Jeon, *AMPK regulates K(ATP) channel trafficking via PTEN inhibition in leptin-treated pancreatic beta-cells.* Biochem Biophys Res Commun, 2013. **440**(4): p. 539-44.
201. Park, S.H., et al., *Leptin promotes K(ATP) channel trafficking by AMPK signaling in pancreatic beta-cells.* Proc Natl Acad Sci U S A, 2013. **110**(31): p. 12673-8.
202. Stockli, J., et al., *The RabGAP TBC1D1 plays a central role in exercise-regulated glucose metabolism in skeletal muscle.* Diabetes, 2015. **64**(6): p. 1914-22.

203. Bahr, I., et al., *GLUT4 in the endocrine pancreas--indicating an impact in pancreatic islet cell physiology?* Horm Metab Res, 2012. **44**(6): p. 442-50.
204. Cushman, S.W., et al., *Molecular mechanisms involved in GLUT4 translocation in muscle during insulin and contraction stimulation.* Adv Exp Med Biol, 1998. **441**: p. 63-71.
205. Klip, A. and A. Marette, *Acute and chronic signals controlling glucose transport in skeletal muscle.* J Cell Biochem, 1992. **48**(1): p. 51-60.
206. Leibiger, I.B., B. Leibiger, and P.O. Berggren, *Insulin signaling in the pancreatic beta-cell.* Annu Rev Nutr, 2008. **28**: p. 233-51.
207. Cheng, K.K., et al., *APPL1 potentiates insulin secretion in pancreatic beta cells by enhancing protein kinase Akt-dependent expression of SNARE proteins in mice.* Proc Natl Acad Sci U S A, 2012. **109**(23): p. 8919-24.
208. Saito, T., et al., *The interaction of Akt with APPL1 is required for insulin-stimulated Glut4 translocation.* J Biol Chem, 2007. **282**(44): p. 32280-7.
209. Cheng, K.K., et al., *The adaptor protein APPL2 inhibits insulin-stimulated glucose uptake by interacting with TBC1D1 in skeletal muscle.* Diabetes, 2014. **63**(11): p. 3748-58.
210. Yamaoka, M., et al., *PI3K regulates endocytosis after insulin secretion by mediating signaling crosstalk between Arf6 and Rab27a.* J Cell Sci, 2016. **129**(3): p. 637-49.
211. Baker, K.E. and R. Parker, *Nonsense-mediated mRNA decay: terminating erroneous gene expression.* Curr Opin Cell Biol, 2004. **16**(3): p. 293-9.
212. Conti, E. and E. Izaurralde, *Nonsense-mediated mRNA decay: molecular insights and mechanistic variations across species.* Curr Opin Cell Biol, 2005. **17**(3): p. 316-25.
213. Fasken, M.B. and A.H. Corbett, *Process or perish: quality control in mRNA biogenesis.* Nat Struct Mol Biol, 2005. **12**(6): p. 482-8.
214. Lejeune, F. and L.E. Maquat, *Mechanistic links between nonsense-mediated mRNA decay and pre-mRNA splicing in mammalian cells.* Curr Opin Cell Biol, 2005. **17**(3): p. 309-15.
215. Rehwinkel, J., J. Raes, and E. Izaurralde, *Nonsense-mediated mRNA decay: Target genes and functional diversification of effectors.* Trends Biochem Sci, 2006. **31**(11): p. 639-46.
216. Andrikopoulos, S., et al., *Differential effect of inbred mouse strain (C57BL/6, DBA/2, 129T2) on insulin secretory function in response to a high fat diet.* J Endocrinol, 2005. **187**(1): p. 45-53.
217. Berglund, E.D., et al., *Glucose metabolism in vivo in four commonly used inbred mouse strains.* Diabetes, 2008. **57**(7): p. 1790-9.
218. Fergusson, G., et al., *Defective insulin secretory response to intravenous glucose in C57Bl/6J compared to C57Bl/6N mice.* Mol Metab, 2014. **3**(9): p. 848-54.
219. Funkat, A., et al., *Metabolic adaptations of three inbred strains of mice (C57BL/6, DBA/2, and 129T2) in response to a high-fat diet.* J Nutr, 2004. **134**(12): p. 3264-9.
220. Siegel, E.G., et al., *Dependency of cyclic AMP-induced insulin release on intra- and extracellular calcium in rat islets of Langerhans.* J Clin Invest, 1980. **65**(2): p. 233-41.
221. Wong, N., et al., *The deletion variant of nicotinamide nucleotide transhydrogenase (Nnt) does not affect insulin secretion or glucose tolerance.* Endocrinology, 2010. **151**(1): p. 96-102.
222. Henquin, J.C., *Triggering and amplifying pathways of regulation of insulin secretion by glucose.* Diabetes, 2000. **49**(11): p. 1751-60.
223. Ferdaoussi, M., et al., *Isocitrate-to-SENP1 signaling amplifies insulin secretion and rescues dysfunctional beta cells.* J Clin Invest, 2015. **125**(10): p. 3847-60.
224. Henquin, J.C., et al., *In vivo and in vitro glucose-induced biphasic insulin secretion in the mouse: pattern and role of cytoplasmic Ca2+ and amplification signals in beta-cells.* Diabetes, 2006. **55**(2): p. 441-51.
225. Rustenbeck, I., C. Herrmann, and T. Grimmsmann, *Energetic requirement of insulin secretion distal to calcium influx.* Diabetes, 1997. **46**(8): p. 1305-11.

226. Xie, L., et al., *Syntaxin-4 mediates exocytosis of pre-docked and newcomer insulin granules underlying biphasic glucose-stimulated insulin secretion in human pancreatic beta cells.* Diabetologia, 2015. **58**(6): p. 1250-9.
227. Xie, L., et al., *Exocyst sec5 regulates exocytosis of newcomer insulin granules underlying biphasic insulin secretion.* PLoS One, 2013. **8**(7): p. e67561.
228. Zhu, D., et al., *Munc18c mediates exocytosis of pre-docked and newcomer insulin granules underlying biphasic glucose stimulated insulin secretion in human pancreatic beta-cells.* Mol Metab, 2015. **4**(5): p. 418-26.
229. Aoyagi, K., et al., *Glinide, but not sulfonylurea, can evoke insulin exocytosis by repetitive stimulation: imaging analysis of insulin exocytosis by secretagogue-induced repetitive stimulations.* Exp Diabetes Res, 2009. **2009**: p. 278762.
230. Lacy, P.E., E.H. Finke, and R.C. Codilla, *Cinemicrographic studies on beta granule movement in monolayer culture of islet cells.* Lab Invest, 1975. **33**(5): p. 570-6.
231. Somers, G., et al., *Motile events in pancreatic endocrine cells.* Endocrinology, 1979. **104**(1): p. 255-64.
232. Borg, L.A., M. Westberg, and V. Grill, *The priming effect of glucose on insulin release does not involve redistribution of secretory granules within the pancreatic B-cell.* Mol Cell Endocrinol, 1988. **56**(3): p. 219-25.
233. Norlund, R., L. Norlund, and I.B. Taljedal, *Morphometry of Rambourg-positive and Rambourg-negative beta-cell granules after culture with low and high glucose concentrations.* Diabetes, 1988. **37**(2): p. 194-9.
234. Orci, L., et al., *A clathrin-coated, Golgi-related compartment of the insulin secreting cell accumulates proinsulin in the presence of monensin.* Cell, 1984. **39**(1): p. 39-47.
235. Orci, L., et al., *Nonconverted, amino acid analog-modified proinsulin stays in a Golgi-derived clathrin-coated membrane compartment.* J Cell Biol, 1984. **99**(6): p. 2187-92.
236. Orci, L., et al., *Direct identification of prohormone conversion site in insulin-secreting cells.* Cell, 1985. **42**(2): p. 671-81.
237. Hoboth, P., et al., *Aged insulin granules display reduced microtubule-dependent mobility and are disposed within actin-positive multigranular bodies.* Proc Natl Acad Sci U S A, 2015. **112**(7): p. E667-76.
238. Ljubicic, S., et al., *The GTPase Rab37 Participates in the Control of Insulin Exocytosis.* PLoS One, 2013. **8**(6): p. e68255.
239. Kebede, M.A., et al., *SORCS1 is necessary for normal insulin secretory granule biogenesis in metabolically stressed beta cells.* J Clin Invest, 2014. **124**(10): p. 4240-56.
240. Lemaire, K., et al., *Insulin crystallization depends on zinc transporter ZnT8 expression, but is not required for normal glucose homeostasis in mice.* Proc Natl Acad Sci U S A, 2009. **106**(35): p. 14872-7.
241. Geng, X., et al., *The insulin secretory granule is the major site of K(ATP) channels of the endocrine pancreas.* Diabetes, 2003. **52**(3): p. 767-76.
242. Geng, X., et al., *Antidiabetic sulfonylurea stimulates insulin secretion independently of plasma membrane KATP channels.* Am J Physiol Endocrinol Metab, 2007. **293**(1): p. E293-301.
243. Bruederle, C.E., J. Gay, and S.L. Shyng, *A role of the sulfonylurea receptor 1 in endocytic trafficking of ATP-sensitive potassium channels.* Traffic, 2011. **12**(9): p. 1242-56.
244. Chen, P.C., et al., *Syntaxin 1A regulates surface expression of beta-cell ATP-sensitive potassium channels.* Am J Physiol Cell Physiol, 2011. **300**(3): p. C506-16.
245. Kozlowski, R.Z. and M.L. Ashford, *ATP-sensitive K(+)-channel run-down is Mg2+ dependent.* Proc R Soc Lond B Biol Sci, 1990. **240**(1298): p. 397-410.
246. Sivaprasadarao, A., et al., *Trafficking of ATP-sensitive potassium channels in health and disease.* Biochem Soc Trans, 2007. **35**(Pt 5): p. 1055-9.
247. Speier, S., et al., *KATP-channels in beta-cells in tissue slices are directly modulated by millimolar ATP.* Mol Cell Endocrinol, 2005. **230**(1-2): p. 51-8.
248. Lim, A., et al., *Glucose deprivation regulates KATP channel trafficking via AMP-activated protein kinase in pancreatic beta-cells.* Diabetes, 2009. **58**(12): p. 2813-9.

249. Manna, P.T., et al., *Constitutive endocytic recycling and protein kinase C-mediated lysosomal degradation control K(ATP) channel surface density.* J Biol Chem, 2010. **285**(8): p. 5963-73.
250. Fu, A., C.E. Eberhard, and R.A. Screaton, *Role of AMPK in pancreatic beta cell function.* Mol Cell Endocrinol, 2013. **366**(2): p. 127-34.
251. Longnus, S.L., et al., *5-Aminoimidazole-4-carboxamide 1-beta -D-ribofuranoside (AICAR) stimulates myocardial glycogenolysis by allosteric mechanisms.* Am J Physiol Regul Integr Comp Physiol, 2003. **284**(4): p. R936-44.
252. Vincent, M.F., et al., *Inhibition by AICA riboside of gluconeogenesis in isolated rat hepatocytes.* Diabetes, 1991. **40**(10): p. 1259-66.
253. Zhang, T.M., C.G. Ostenson, and W.J. Malaisse, *Glycogen synthase, glycogen phosphorylase and alpha-amylase activity in homogenates of islets of GK rats: comparison with hepatic and pancreatic extracts.* Cell Biochem Funct, 1994. **12**(3): p. 185-9.
254. Wagner, T.F., et al., *Transient receptor potential M3 channels are ionotropic steroid receptors in pancreatic beta cells.* Nat Cell Biol, 2008. **10**(12): p. 1421-30.
255. Nilius, B. and T. Voets, *A TRP channel-steroid marriage.* Nat Cell Biol, 2008. **10**(12): p. 1383-4.
256. Guinamard, R., M. Demion, and P. Launay, *Physiological roles of the TRPM4 channel extracted from background currents.* Physiology (Bethesda), 2010. **25**(3): p. 155-64.
257. Shigeto, M., et al., *GLP-1 stimulates insulin secretion by PKC-dependent TRPM4 and TRPM5 activation.* J Clin Invest, 2015. **125**(12): p. 4714-28.
258. Cognard, E., et al., *Identification of a pathway by which glucose regulates beta-catenin signalling via the cAMP/protein kinase A pathway in beta-cell models.* Biochem J, 2013. **449**(3): p. 803-11.
259. Abou-Sabe, M.A., *Stimulation of cAMP synthesis by glucose in a mutant of E. coli B-r.* Nat New Biol, 1973. **243**(127): p. 182-5.
260. Farese, R.V., *The phosphatidate-phosphoinositide cycle: an intracellular messenger system in the action of hormones and neurotransmitters.* Metabolism, 1983. **32**(6): p. 628-41.
261. Conti, M. and S.L. Jin, *The molecular biology of cyclic nucleotide phosphodiesterases.* Prog Nucleic Acid Res Mol Biol, 1999. **63**: p. 1-38.
262. Kaihara, K.A., et al., *beta-Cell-specific protein kinase A activation enhances the efficiency of glucose control by increasing acute-phase insulin secretion.* Diabetes, 2013. **62**(5): p. 1527-36.
263. Hurley, R.L., et al., *Regulation of AMP-activated protein kinase by multisite phosphorylation in response to agents that elevate cellular cAMP.* J Biol Chem, 2006. **281**(48): p. 36662-72.
264. Idevall-Hagren, O., et al., *Spatial control of Epac2 activity by cAMP and Ca2+-mediated activation of Ras in pancreatic beta cells.* Sci Signal, 2013. **6**(273): p. ra29 1-11, S1-6.
265. Idevall-Hagren, O., et al., *cAMP mediators of pulsatile insulin secretion from glucose-stimulated single beta-cells.* J Biol Chem, 2010. **285**(30): p. 23007-18.
266. Leech, C.A., O.G. Chepurny, and G.G. Holz, *Epac2-dependent rap1 activation and the control of islet insulin secretion by glucagon-like peptide-1.* Vitam Horm, 2010. **84**: p. 279-302.
267. Tweedie, E., et al., *Maintenance of hepatic nuclear factor 6 in postnatal islets impairs terminal differentiation and function of beta-cells.* Diabetes, 2006. **55**(12): p. 3264-70.
268. Artner, I., et al., *MafA and MafB regulate genes critical to beta-cells in a unique temporal manner.* Diabetes, 2010. **59**(10): p. 2530-9.
269. Hang, Y. and R. Stein, *MafA and MafB activity in pancreatic beta cells.* Trends Endocrinol Metab, 2011. **22**(9): p. 364-73.
270. Withers, D.J., et al., *Disruption of IRS-2 causes type 2 diabetes in mice.* Nature, 1998. **391**(6670): p. 900-4.
271. Chen, P.C., Y.N. Kryukova, and S.L. Shyng, *Leptin regulates KATP channel trafficking in pancreatic beta-cells by a signaling mechanism involving AMP-activated*

protein kinase (AMPK) and cAMP-dependent protein kinase (PKA). J Biol Chem, 2013. **288**(47): p. 34098-109.
272. de Waard, R., et al., *Comparison of faecal Lactobacillus populations in experimental animals from different breeding facilities and possible consequences for probiotic studies.* Lett Appl Microbiol, 2002. **34**(2): p. 105-9.
273. Hufeldt, M.R., et al., *Variation in the gut microbiota of laboratory mice is related to both genetic and environmental factors.* Comp Med, 2010. **60**(5): p. 336-47.
274. Campbell, S.C., et al., *The Effect of Diet and Exercise on Intestinal Integrity and Microbial Diversity in Mice.* PLoS One, 2016. **11**(3): p. e0150502.
275. Reardon, S., *A mouse's house may ruin experiments.* Nature, 2016. **530**(7590): p. 264.
276. Deems, R.O., et al., *Insulin action on whole body glucose utilization and on muscle glucose transporter translocation in mice.* Biochem Biophys Res Commun, 1994. **199**(2): p. 662-70.
277. Christensen, C.S., et al., *Skeletal Muscle to Pancreatic beta-Cell Cross-talk: The Effect of Humoral Mediators Liberated by Muscle Contraction and Acute Exercise on beta-Cell Apoptosis.* J Clin Endocrinol Metab, 2015. **100**(10): p. E1289-98.
278. Bouzakri, K., et al., *Bimodal effect on pancreatic beta-cells of secretory products from normal or insulin-resistant human skeletal muscle.* Diabetes, 2011. **60**(4): p. 1111-21.
279. Calegari, V.C., et al., *Endurance training activates AMP-activated protein kinase, increases expression of uncoupling protein 2 and reduces insulin secretion from rat pancreatic islets.* J Endocrinol, 2011. **208**(3): p. 257-64.
280. Berne, C., *The metabolism of lipids in mouse pancreatic islets. The biosynthesis of triacylglycerols and phospholipids.* Biochem J, 1975. **152**(3): p. 667-73.
281. Guo, J., et al., *Palmitate-induced inhibition of insulin gene expression in rat islet beta-cells involves the ceramide transport protein.* Cell Physiol Biochem, 2010. **26**(4-5): p. 717-28.
282. Alquier, T., et al., *Deletion of GPR40 impairs glucose-induced insulin secretion in vivo in mice without affecting intracellular fuel metabolism in islets.* Diabetes, 2009. **58**(11): p. 2607-15.
283. Kebede, M., et al., *The fatty acid receptor GPR40 plays a role in insulin secretion in vivo after high-fat feeding.* Diabetes, 2008. **57**(9): p. 2432-7.
284. Ferdaoussi, M., et al., *G protein-coupled receptor (GPR)40-dependent potentiation of insulin secretion in mouse islets is mediated by protein kinase D1.* Diabetologia, 2012. **55**(10): p. 2682-92.
285. Latour, M.G., et al., *GPR40 is necessary but not sufficient for fatty acid stimulation of insulin secretion in vivo.* Diabetes, 2007. **56**(4): p. 1087-94.
286. Tiano, J.P. and F. Mauvais-Jarvis, *Importance of oestrogen receptors to preserve functional beta-cell mass in diabetes.* Nat Rev Endocrinol, 2012. **8**(6): p. 342-51.
287. Zhao, S., et al., *alpha/beta-Hydrolase domain-6 and saturated long chain monoacylglycerol regulate insulin secretion promoted by both fuel and non-fuel stimuli.* Mol Metab, 2015. **4**(12): p. 940-50.
288. Aizawa, T., et al., *ATP-sensitive K+ channel-independent glucose action in rat pancreatic beta-cell.* Am J Physiol, 1994. **266**(3 Pt 1): p. C622-7.
289. Sato, Y., et al., *Dual functional role of membrane depolarization/Ca2+ influx in rat pancreatic B-cell.* Diabetes, 1992. **41**(4): p. 438-43.
290. Glatz, J.F., J.J. Luiken, and A. Bonen, *Membrane fatty acid transporters as regulators of lipid metabolism: implications for metabolic disease.* Physiol Rev, 2010. **90**(1): p. 367-417.
291. Hyder, A., et al., *Expression of fatty acid binding proteins 3 and 5 genes in rat pancreatic islets and INS-1E cells: regulation by fatty acids and glucose.* Islets, 2010. **2**(3): p. 174-84.
292. Kebede, M.A., et al., *Lipid receptors and islet function: therapeutic implications?* Diabetes Obes Metab, 2009. **11 Suppl 4**: p. 10-20.

293. Kim, Y.W., et al., *Inhibition of fatty acid translocase cluster determinant 36 (CD36), stimulated by hyperglycemia, prevents glucotoxicity in INS-1 cells.* Biochem Biophys Res Commun, 2012. **420**(2): p. 462-6.
294. Layden, B.T., et al., *Short chain fatty acids and their receptors: new metabolic targets.* Transl Res, 2013. **161**(3): p. 131-40.
295. Noushmehr, H., et al., *Fatty acid translocase (FAT/CD36) is localized on insulin-containing granules in human pancreatic beta-cells and mediates fatty acid effects on insulin secretion.* Diabetes, 2005. **54**(2): p. 472-81.
296. Odori, S., et al., *GPR119 expression in normal human tissues and islet cell tumors: evidence for its islet-gastrointestinal distribution, expression in pancreatic beta and alpha cells, and involvement in islet function.* Metabolism, 2013. **62**(1): p. 70-8.
297. Ivanova, A., et al., *Age-dependent labeling and imaging of insulin secretory granules.* Diabetes, 2013. **62**(11): p. 3687-96.
298. Wu, Y., S.L. Shyng, and P.C. Chen, *Concerted Trafficking Regulation of Kv2.1 and KATP Channels by Leptin in Pancreatic beta-Cells.* J Biol Chem, 2015. **290**(50): p. 29676-90.
299. Panten, U., et al., *Acute metabolic amplification of insulin secretion in mouse islets is mediated by mitochondrial export of metabolites, but not by mitochondrial energy generation.* Metabolism, 2013. **62**(10): p. 1375-86.
300. Ellingsgaard, H., et al., *Interleukin-6 enhances insulin secretion by increasing glucagon-like peptide-1 secretion from L cells and alpha cells.* Nat Med, 2011. **17**(11): p. 1481-9.
301. Kawai, K., et al., *Evidence that glucagon stimulates insulin secretion through its own receptor in rats.* Diabetologia, 1995. **38**(3): p. 274-6.
302. Miele, C., et al., *PED/PEA-15 regulates glucose-induced insulin secretion by restraining potassium channel expression in pancreatic beta-cells.* Diabetes, 2007. **56**(3): p. 622-33.
303. Dhawan, S., et al., *Pancreatic beta cell identity is maintained by DNA methylation-mediated repression of Arx.* Dev Cell, 2011. **20**(4): p. 419-29.
304. Gao, N., et al., *Foxa2 controls vesicle docking and insulin secretion in mature Beta cells.* Cell Metab, 2007. **6**(4): p. 267-79.
305. Wu, X., et al., *Transplantation of human menstrual blood progenitor cells improves hyperglycemia by promoting endogenous progenitor differentiation in type 1 diabetic mice.* Stem Cells Dev, 2014. **23**(11): p. 1245-57.
306. Kubo, A., et al., *Pdx1 and Ngn3 overexpression enhances pancreatic differentiation of mouse ES cell-derived endoderm population.* PLoS One, 2011. **6**(9): p. e24058.

8.2 Other literature sources

Position statement: Screening for Type 2 Diabetes, Clinical Diabetes, Vol 18. No 2 Spring 2000, ADA

Pancreapedia.org: Longnecker 2014, DOI: 10.3998/panc.2014.3

Diabetes mellitus a guide to patient care.

Philadelphia: Lippincott Williams & Wilkins. 2007. p. 15. ISBN 978-1-58255-732-8

Animal Models in Diabetes Research, Methods in Molecular Biology

Hans-Georg Joost et al. (eds.), vol. 933, DOI 10.1007/978-1-62703-068-7_12, © Springer Science+Business Media, LLC 2012

9 APPENDIX

9.1 Manuscripts used as a reference

Torben Stermann, Franziska Menzel, Carmen Weidlich, Kay Jeruschke, Jürgen Weiß, Anna Pujol, Fatima Bosch, Ingo Rustenbeck, Christian de Wendt, Sandra Lebek, Tanja Schallschmidt, Martin Kragl, Eckhard Lammert, Alexandra Chadt, Hadi Al-Hasani: „The RabGAP TBC1D1 regulates glucose- and sulfonylurea-induced insulin secretion in isolated mouse islets“. ***Cell Reports***. Submitted August 29th 2016

Parts of the discussion section of this thesis are written in quotation marks. These parts have been adopted either word by word or with modifications from the above mentioned manuscript that has been submitted for publication to the journal Cell Reports.

The manuscript was in large parts written by myself and complemented with parts from Prof. Dr. Ingo Rustenbeck, Alexandra Chadt, Eckhard Lammert and Hadi Al-Hasani (all co-authors). The figures that are presented in this manuscript have been generated and prepared mostly by myself. Figure 3C of the manuscript was prepared by Dr. Jürgen Weiß (co-author), and the experiments that led to the figures 4A and 4C were done by Verena Lier-Glaubitz from the lab of Prof. Dr. Rustenbeck (co-author).

9.2 Abbreviations

A23187	Calcium ionophore
ADP	adenosine diphosphate
AICAR	5-aminoimidazol-4-carboxamid 1-β-D-ribo-furanoside
AKT	refers to PKB
a.m.	latin: *ante meridiem* – before noon
AMP	adenosine monophosphate
AMPK	AMP-activated protein kinase
approx.	approximately
APS	ammoniumpersulfat
AS160	AKT substrate of 160 kDa
ATP	adenosine triphosphate
B6	C57BL/6J
BAT	brown adipose tissue
BCA	bicinchonic acid
bp	base pair
BSA	bovine serum albumin
cAMP	cyclic adenosine monophosphate
CBD	calmodulin binding domain
CD36	cluster of differentiation 36
cDNA	complementary DNA
CMRL	Connaught Medical Research Laboratories
CO_2	carbon dioxide
Cpt	Carnitin palmitoyl transferase
CSP	Cystine string protein
Ct	cycle threshold
D1KO	TBC1D1 knockout
D1/4KO	TBC1D1/TBC1D4 knockout

DBA	Dilute Brown Non-Agouti
DENN	differentially expressed in neoplastic versus normal cells
DIfE	German Institute for Human Nutrition
DMEM	Dulbecco's Modified Eagles Medium
DMSO	dimethylsulfoxide
DNA	desoxyribo nucleic acid
dNTP	desoxyribo nucleotide triphosphate
DTT	dithiothreitol
ECL	Enhanced chemoluminescence
EDL	*Extensor digitorum longus*
EDTA	ethylene diamine tetra acetate
e.g.	latin: *exempli gratia* – for example
EGTA	ethylene glycol-bis(aminoethylether)-N,N,N',N'-tetra acetate
ELISA	enzyme-linked immuno sorbent assay
et al.	latin: *et alia* – and others
FABP	fatty acid binding protein
FATP	fatty acid transport protein
FBS	fetal bovine serum
FLAG™	FLAG is a registered trademark of Sigma-Aldrich Co. LLC
FFAR	Free fatty acid receptor
FFPE	Formalin-fixed, paraffin embedded
FVB	Friend Leukemia Virus B
GADA	glutamic acid-decarboxylase
GAP	GTPase activating protein
GAPDH	glyceraldehyde-3-phosphate dehydrogenase
GDP	guanosine diphosphate
GEF	guanine nucleotide exchange factor
GIP	gastric inhibitory polypeptide / glucose-dependent insulinotropic polypeptide
GLP-1	glucagon-like peptide-1

GLUT	glucose transporter
GP(C)R	G-protein coupled receptor
GSIS	glucose-stimulated insulin secretion
GTP	guanosine triphosphate
GTT	glucose tolerance test
HA	hemagglutinin
HDL	high-density lipoprotein
HE	hematoxylin and eosin
HEPES	2-(4-(2-hydroxyethyl)-1-piperazinyl)-ethane sulfonic acid
HFD	high-fat diet
HRP	horseradish peroxidase
IA-2	islet antigen-2
IAA	insulin autoantibody
IBMX	isobutylmethylxanthine
ICA	islet cell antibody
IgG	immunoglobulin G
i.p.	intraperitoneal
IRS	insulin receptor substrate
kb	kilo base
kcal	kilo calories
kDa	kilo dalton
KHB	Krebs-Henseleit-Buffer
K_{ir}	potassium inward rectifier
K_M	Michaelis constant
KO	knockout
KRH	Krebs-Ringer-HEPES
LSB	Lämmli sample buffer
Mb	mega base
MIN6	mouse insulinoma cell line

MQ	ultrapure (*Milli-Q*)
mRNA	messenger RNA
mTOR	mammalian target of rapamycin
NADPH	nicotinamide adenine dinucleotide phosphate
Noc2	Rabphilin-3A-like protein
PAGE	polyacrylamide gel electrophoresis
PCR	polymerase chain reaction
PDK1	phosphoinositide-dependent kinase-1
PFA	paraformaldehyde
PI3	phosphatidylinositol-4,5-bisphosphate 3
PIP2	phosphatidylinositol (3,4)-bisphosphate
PIP3	phosphatidylinositol (3,4,5)-trisphosphate
PKB	protein kinase B (AKT)
PPAR	peroxisome-proliferator-activated receptor
PTB	phospho-tyrosine-binding
PVDF	polyvinylidene difluoride
Rab	Ras-related in brain
rcf	relative centrifugal force
RCS	recombinant congenic strain
RIP2	rat insulin promoter 2
RNA	ribonucleic acid
rRNA	ribosomal RNA
RRP	readily releasable pool
RT	reverse transcriptase
RyR	ryanodine receptor
SD	standard deviation
SDS	sodium dodecylsulfate
SEM	standard error of the mean
siRNA	small interfering RNA

SJL	Swiss Jim Lambert
SM	smooth muscle
SNAP	synaptosomal-associated protein
SNARE	Soluble N-ethylmaleimide-sensitive factor attachment protein receptor
SUR	sulfonylurea receptor
TA	*Tibialis anterior*
TAE	tris-acetate-EDTA
Taq	*Thermophilus aquaticus*
TBC1D1	***T**RE2, **B**ub2, **C**DC16 **1** **d**omain family member **1***
TBS-T	tris-buffered saline – Tween 20
TEMED	N,N,N',N'-tetramethyl ethylene diamine
TG	transgene
TIRF	total internal reflection fluorescence
TMB	3,3',5,5'-tetramethylbenzidine
TL	Thermolysin low
TRP	transient receptor potential
VAMP	vesicle associated membrane protein
VDCC	voltage-dependent L-type Ca^{2+}-channel
vs.	versus
WAT	white adipose tissue
WT	wildtype
ZMP	5-amino-1-β-D-ribofuranosylimidazole-4-carboxamide-5′-monophosphate

9.3 Additional Tables

Table 18: Oligonucleotide primer sequences for cDNA amplification

Target Gene		Sequence 5' → 3'	Product	Reference
Tbc1d1	For Rev	ACAGTGTGGGAAAAGATGCT AGGTGGAACTGCTCAGCTAG	143 bp	
Tbc1d4	For Rev	CCAACAGTCTTGCCTCAGAG GAATGTGTGAGCCCGTCTTC	146 bp	
Kcnj11	For Rev	TCCACCAGGTAGACATCCC TAGGAGCCAGGTCGTAGAG	120 bp	[302]
Abcc8	For Rev	CTAACTTCCCCAAGCTGCTG CCCGTAGAGGATCACCAGAA	152 bp	
Rab27a	For Rev	ACCACAGTGGGCATTGATTT CCCATAACTGCAGGTGGATT	103 bp	
Tbc1d10a	For Rev	TCTGTGAGAAGTACCTGCCTG TCAATCTTCTGGCGGCTGAG	133 bp	
Sytl4	For Rev	AGGTCCACATGGACTCTTGG TGGAGGCTGGGATGTATTTC	144 bp	
Snap25	For Rev	ATGGAGAAGGCTGATTCCAAC CCATGAGAGAAGCATGAAGGA	148 bp	[207]
Vamp2	For Rev	CCCACACACCAGGTTTTCTGT GCAGGGGACACTGGGATAATA	130 bp	[207]
Stx1a	For Rev	GTGAGGAATTGGAAGACATGC GCCTTGCTCTGGTACTTGACG	298 bp	[207]
Snca	For Rev	AAGAAGAGTCTGTTCGCTGGA AAAGATGTATTTTTGCTCCACACTT	69 bp	[90]
Dnajc5	For Rev	CTGCTGTGGGAAATGCAAG GCTGTATGACGATCGGTGTG	131 bp	[90]
Prkcb	For Rev	GAAACTCGAACGCAAGGAGA ACCGGTCGAAGTTTTCAGC	77 bp	[90]
Pdx1	For Rev	GAAATCCACCAAAGCTCACG CGGGTTCCGCTGTGTAAG	65 bp	[303]
Ins2	For Rev	CCCTGCTGGCCCTGCTCTT AGGTCTGAAGGTCACCTGCT	102 bp	
Mafa	For Rev	GAGGAGGTCATCCGACTGAAA GCACTTCTCGCTCTCCAGAAT	114 bp	[304]
Mafb	For Rev	CTGCGCCCCTAGCCCTGGACTC GGCGGCCCTGGCACTCACAAA	319 bp	[305]
Ngn3	For Rev	CTGCGCATAGCGGACCACAGCTTC CTTCACAAGAAGTCTGAGAACACCAG	233 bp	[306]
Ffar1	For Rev	GGCCCTATAATGCCTCCAAT CCAGGACCTGTTCCCAAGTA	139 bp	
Ffar2	For Rev	GATCATGTCCTTTGGCCACT GCTCTTGGGTGAAGTTCTCG	113 bp	
Ffar3	For Rev	GCAGCAGAGTGCCAGTTGT CACCAACAGGTAGACGGAAAA	101 bp	
Gpr119	For Rev	ACCAGAGAAAGCGCCTATCA CAACCTGCCTTTACCAGTTG	147 bp	

Target Gene		Sequence 5' → 3'	Product	Reference
Gpr120	For	CCCCTCTGCATCTTGTTCC	102 bp	
	Rev	GATTTCTCCTATGCGGTTGG		
Cd36	For	GATGTGCAAAACCCAGATGA	122 bp	
	Rev	TCCTCGGGGTCCTGAGTTAT		
Fabp3	For	CGGTACCTGGAAGCTAGTGG	128 bp	
	Rev	TATCCCCGTTCTTCTCGATG		
Fabp5	For	ATGGGAAGATGATCGTGGAG	109 bp	
	Rev	CTGGCAGCTAACTCCTGTCC		
Fatp1	For	TGCTTTGGTTTCTGGGACTT	149 bp	
	Rev	CCGAACACGAATCAGAACAG		
Acadl	For	ATTGCTGAGTTGGCGATTTC	112 bp	
	Rev	GCTGCACCGTCTGTATGTGT		
Pgc1a	For	GAGTCTGAAAGGGCCAAACA	148 bp	
	Rev	TGCATTCCTCAATTTCACCA		
Cpt1a	For	CTCAGTGGGAGCGACTCTTCA	105 bp	
	Rev	GGCCTCTGTGGTACACGACAA		
Irs1	For	CAATGAGGGCAACTCCCCAA	122 bp	
	Rev	GGTCTTCATTCTGCTGTGATGT		
Irs2	For	GCCTGGGGATAATGGTGACTA	141 bp	
	Rev	TCCATGAGACTTAGCCGCTTC		
36b4	For	GCCGTGATGCCCAGGGAAGACA	126 bp	[90]
	Rev	CATCTGCTTGGAGCCCACGTTG		

Table 19: Oligonucleotide primers for genotyping and *Tbc1d1* isoforms

Primer	Sequence 5' → 3'	Annealing temperature
Tbc1d1-WT for	GGACAAGCAGCTTTCTTGTTT	60 °C
Tbc1d1-WT rev	TCCTGGTCCAGAAGCGAG	58 °C
Tbc1d1-KO for	CAACATTCTGAAGGCCTTCTG	62 °C
Tbc1d1-KO rev	TCCCTGGCTACAAGCTGAGT	62 °C
FLAG for	CCATGGATTACAAGGATGACG	47,3 °C
FLAG rev	AGGCTTGCACTCAAAGATGC	60 °C
AS160 for	AGTAGACTCAGAGTGGTCTTGG	49,7 °C
AS160 WT rev	GTCTTCCGACTCCATATTTGC	47,3 °C
AS160 KO rev	GCAGCGCATCGCCTTCTATC	64 °C
Tbc1d1-Iso for	AAGAGTCTGCCCTGTTGTCA	60 °C
Tbc1d1-Iso rev	ACACCGGTTCTAAAGGGGAG	62 °C

Table 20: Thermocycler settings to amplify the target region of *Tbc1d1* cDNA for isoform discrimination

Stage	Temperature	Duration	Repeats
Lid heating	105 °C	∞	Throughout the entire cycling
Hot Start	95 °C	2:00 min	-
Denaturation	95 °C	0:30 min	30 x
Annealing	60 / 62 / 65 °C	0:30 min	
Elongation	72 °C	1:00 min	
Final elongation	72 °C	7:00 min	-
	4 °C	∞	-

Table 21: Thermocycler settings for the different genotyping PCRs

Stage	*Tbc1d1*		FLAG		*Tbc1d4*		Repeats
	Temp.	Duration	Temp.	Duration	Temp.	Duration	
Lid heating	105 °C	∞	105 °C	∞	105 °C	∞	entire cycling
Hot Start	98 °C	0:30 min	95 °C	3:00 min	95 °C	2:00 min	-
Denaturation	98 °C	0:10 min	95 °C	0:30 min	95 °C	0:30 min	30 x
Annealing	65 °C	0:30 min	57 °C	0:30 min	60 °C	0:30 min	
Elongation	72 °C	0:05 min	72 °C	1:00 min	72 °C	1:00 min	
	72 °C	7:00 min	72 °C	10:00 min	72 °C	5:00 min	-
	4 °C	∞	4 °C	∞	4 °C	∞	-

9.4 Additional Figures

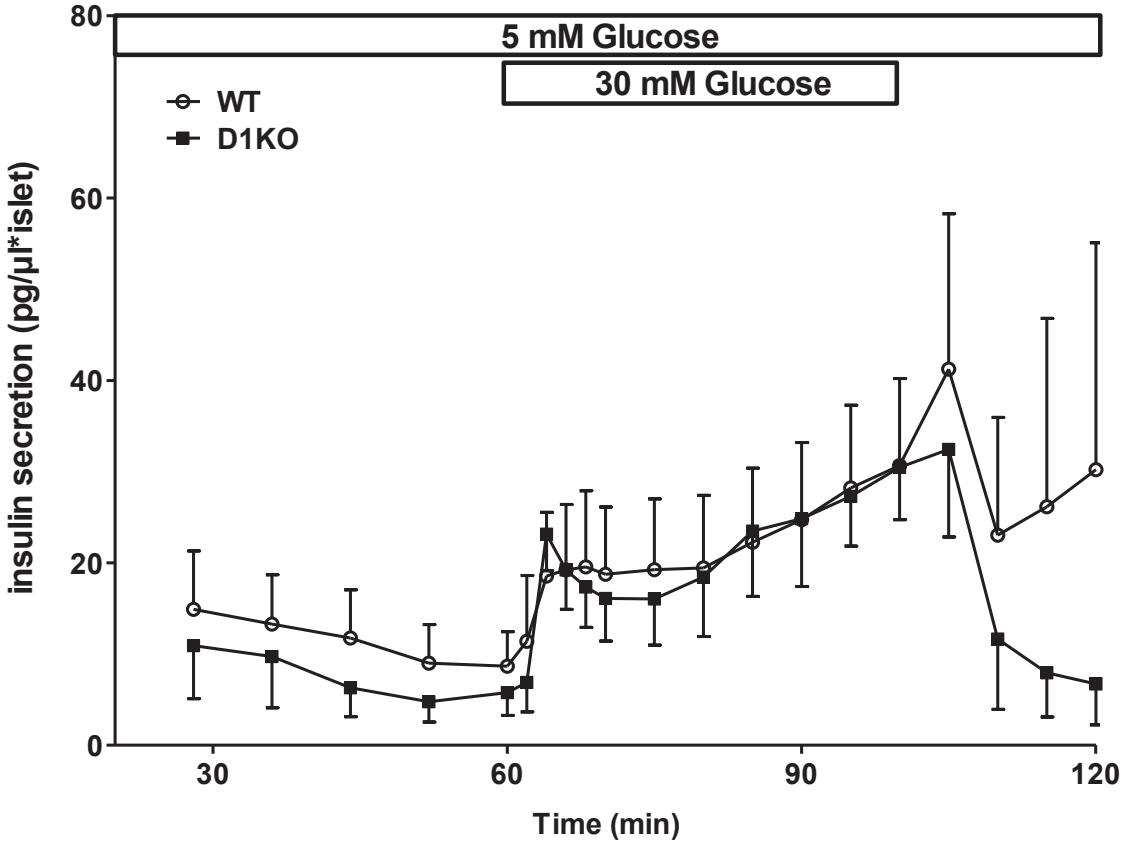

Figure 37: Absolute data for dynamic GSIS in isolated islets of D1KO mice. 50 islets per genotype were perifused in a custom-made perifusion chamber with 5 mM glucose and 30 mM glucose for the designated time points. Insulin from the eluate fractions was measured with ELISA and the values are expressed as pg insulin per µL and islet. Data are mean values ± SEM (n = 5).

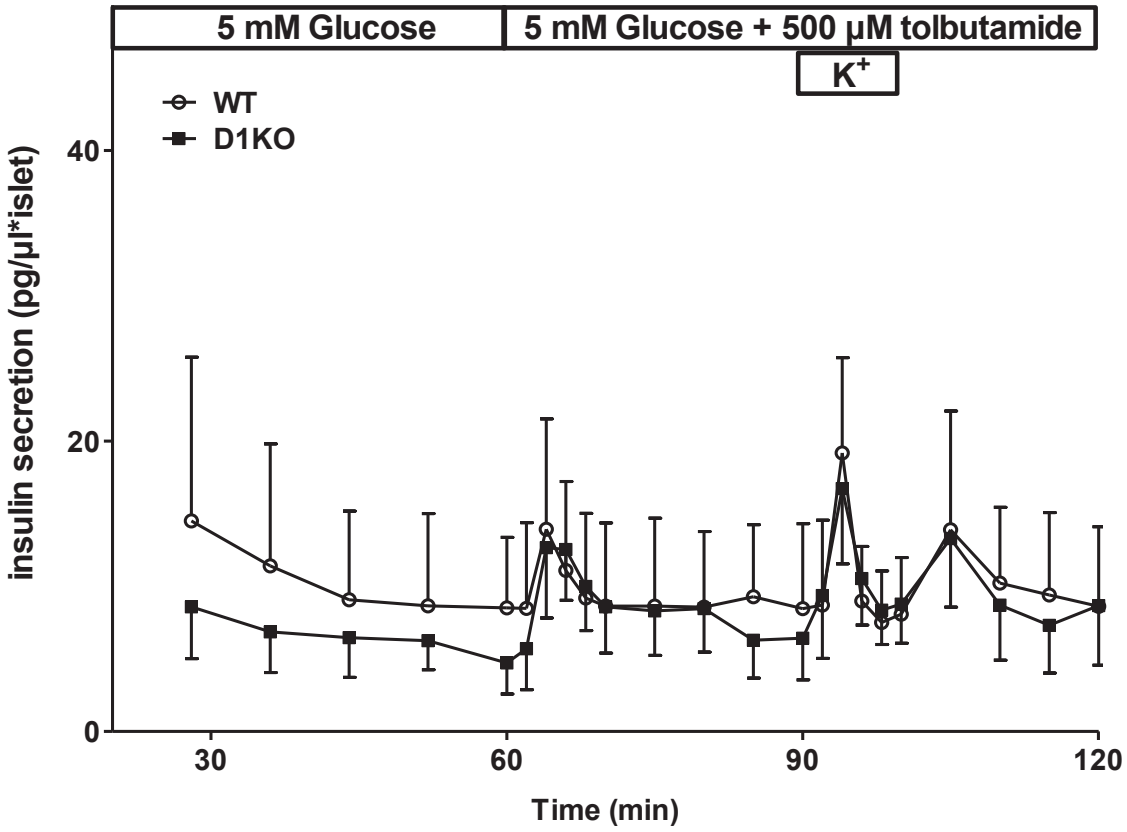

Figure 38: Absolute data for dynamic secretagogue-stimulated insulin secretion in isolated islets of D1KO mice. 50 islets per genotype were perifused in a custom-made perifusion chamber with 5 mM glucose and together with 500 µM tolbutamide and 40 mM KCl for the designated time points. Insulin from the eluate fractions was measured with ELISA and the values are expressed as pg insulin per µL and islet. Data are mean values ± SEM (n = 5).

9.5 List of figures

All figures were generated by myself either with graphical material (http://www.servier.com/Powerpoint-image-bank) under a free-to-use Creative Commons Attribution 3.0 Unported License (Figures 1, 2, 7 and 36) or with the GraphPad Prism 5 software.

9.6 List of tables

10 ACKNOWLEDGEMENTS

The first appreciation is directed towards my thesis supervisor Prof. Dr. Hadi Al-Hasani. I would like to thank you for the opportunity to work on such an interesting and also promising research project. Thank you for the trust in me and for all the valuable input and suggestions to always improve the research performance. Thank you also for the possibilities to share and present my work on national and international conferences and workshops and to get in touch with researchers from all over the world for a stimulating exchange. Thank you for the opportunity to get involved into the research training group of “vivid” that comprised great individual researchers and that strengthened my personal skills apart from the lab. An equivalent appreciation goes to my second supervisor Prof. Dr. Eckhard Lammert, who already was my supervisor for my bachelor thesis. Thank you for conducting my scientific development throughout the past years and for always encouraging me to go one step further. Likewise I would like to thank Dr. Martin Kragl and Barbara Bartosinska from your lab, who always helped me in dealing with problems throughout the thesis.

A very special gratitude is for my lab supervisor Dr. Alexandra Chadt. From the very beginning you were a cooperative, productive and well organized supervisor. Although you had no methodological experience yourself in working with islets you always had valuable suggestions for improvements. Thank you for investing your time in my personal and professional development by reading, correcting, commenting, communicating, motivating and many other things. Thank you also for sharing your office in the last months of my thesis that also made some private conversations possible in between. I appreciate your patience and sympathy, but also that you never lost the focus of my project. This made me feel that you believe in me and my performance. Thank you very much!

I would like to thank Carmen Weidlich, who did her bachelor thesis under my supervision and who markedly supported my work with doing most of the histological methods. You did a great job. I enjoyed the time with you and I am especially happy that you finally got a position in the histology unit. Likewise I would like to thank Kay Jeruschke and Dr. Jürgen Weiß from the histology unit. Without your participation in conducting experiments and doing the electron microscopy, the results of this thesis would not be that strong as they are. Kay, the EM pictures that you produced are really awesome and are probably the best in the world! Thank you.

Prof. Dr. Ingo Rustenbeck as well as Verena Lier-Glaubitz from the TU Braunschweig deserved special thanks for performing and analyzing the dynamic perifusion experiments.

Likewise I would like to thank you for the opportunity to visit your lab to conduct the experiments and to get an insight into the special requirements for such an experiment.

I would like to thank the PhD students, supervisors and coordinators that were involved in the "vivid" graduate school. Thank you for maintaining a very good relationship to each other and for the evenings and social events in "Scotties", "Siam Bar" or "Stier Royal" ☺. I wish you all the best for your personal and professional futures.

A very special gratitude is for my numerous colleagues in the lab. Jennifer Schwettmann, thank you for taking good care of my mice and to deliver them accurately on time. Annette Schober, Angelika Horrighs, Anette Kurowski, Antonia Osmers and Ilka Römer: thank you for your kind introductions into the general lab techniques and for always supporting in various organizational and experimental issues. And of course I will not forget the rest of the crew, Sabrina Müller-Lühlhoff (Dr. MüLü), Christian de Wendt, Tim Benninghoff, Christian Springer, Sandra Lebek, Tanja Schallschmidt, Matthias Dille, Christian Binsch, Delsi Altenhofen, Dr. Sven Görgens, Simon Göddeke, David Barbosa. Thank you for creating such an incredible atmosphere and for the time outside the lab. Thank you for being friends and to share your private time. I am sure that "Gentlemen's Coffee Club" and "Ilf güldene Zwölf" will persist ☺.

I would also like to remember some persons, who unfortunately passed away within the last 4.5 years. Thank you for being part of my life and make yourselves a good time in heaven.

Grete Peter	**†**	**28.03.2013**
Peter Wellnitz	**†**	**27.02.2014**
Stephan Lauber	**†**	**28.02.2013**
Uwe Rosenthal	**†**	**30.01.2014**
Detlef Baumeister	**†**	**22.09.2013**
Marc Kauffeld	**†**	**02.08.2016**

Finally I would like to end my acknowledgements with a deep gratitude to my family. Thank you Hedi and Till for your unconditional support on every possible level throughout the last 34.5 years. I would not be at that point without you. Thank you Erik, Gabi and Shorty, for nice barbecues, beers and coffees and the time you were at my side. Thank you Tante Ruth for your loyal, but also financial support throughout the last years. Special thanks are dedicated to my wife Anika. You always stood at my side and encouraged me to even decide for that interesting research project. You are a precious person in my life and made the time that passed for the thesis spin away. With you I gained another family which I also would like to thank. Thank you Sigrid, Karl-Heinz, Klaus, Melanie, Liana, Jakob and Merle. You enriched my life and I don't want to miss the time that I had with you.